

AFIT/DS/ENY/96-8

SIMULTANEOUS COMPOSITE TAILORING AND
BENDING CONTROL OPTIMIZATION FOR DAMPING
THE TORSIONAL VIBRATION OF A PLATE

DISSERTATION

Douglas W. DeHart, Captain, USAF
AFIT/DS/ENY/96-8

DTIC QUALITY INSPECTED 2

Approved for public release; distributed unlimited

19960718 121

SIMULTANEOUS COMPOSITE TAILORING AND BENDING CONTROL
OPTIMIZATION FOR DAMPING THE TORSIONAL VIBRATION OF A PLATE

DISSERTATION

Presented to the Faculty of the School of Engineering
of the Air Force Institute of Technology
Air University In Partial Fulfillment of the
Requirements for the Degree of
Doctor of Philosophy

Douglas W. DeHart, B.S., M.S.
Captain, USAF

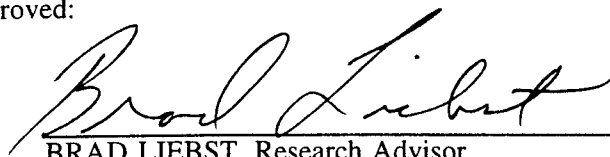
June 1996

Approved for public release; distributed unlimited

SIMULTANEOUS COMPOSITE TAILORING AND BENDING CONTROL
OPTIMIZATION FOR DAMPING THE TORSIONAL VIBRATION OF A PLATE

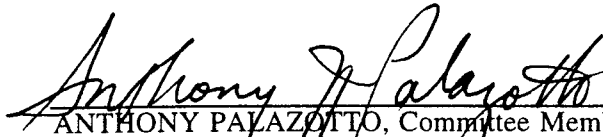
Douglas W. DeHart, B.S., M.S.
Captain, USAF

Approved:



BRAD LIEBST, Research Advisor
Associate Professor of Aerospace Engineering
Department of Aeronautics and Astronautics

17 May 1996



ANTHONY PALAZOTTO, Committee Member
Professor of Aerospace Engineering
Department of Aeronautics and Astronautics

17 May 1996



ALAN LAIR, Committee Member
Professor of Mathematics
Department of Mathematics and Statistics

20 May 1996



ROBERT CANFIELD, Dean's Representative
Major USAF
Assistant Professor of Aerospace Engineering
Department of Aeronautics and Astronautics

17 May 96

Accepted:



Robert A. Calico, Jr.
Dean, Graduate School of Engineering

Acknowledgments

I am indebted to my thesis advisor, Dr. Brad Liebst, and the rest of my committee, Dr. Palazatto, Dr. Lair, and Maj Canfield for their assistance and guidance during this research effort. They helped me stay on track and motivated me to complete this dissertation.

This research would not have been possible without the support from the Structures and Controls Division of the Phillips Laboratory. The monetary support given to me made this research possible through the purchase of a workstation. Also, the experimental results would not have occurred without the use of their world class facilities such as the Applied Composites Laboratory. Specifically, I would like to thank Mr. Kevin Slimak, Dr. Alok Das, Maj Jay Galbraith, Lt John Paul, Mr. Jason Lasely, Capt Jeanie Sullivan, Dr. Moon Kwak, Mr. Robert Acree, and Dr. Mark Mimovich.

Finally, I would like to thank my family who supported me every step of the way, including leaving town for three weeks while I studied for my qualifiers. My wife Sue has carried the responsibility of raising a family and has sheltered me from this responsibility while I completed this research. During this time, my children, Sara and Amber, have tried to show me what life is outside of doing research. Now that the research is over, I will learn from them what life is really about.

TABLE OF CONTENTS

<i>Acknowledgments</i>	iii
<i>Symbol List</i>	v
<i>List of Figures</i>	viii
<i>List of Tables</i>	x
<i>Abstract</i>	xii
<i>I. Introduction</i>	1
<i>II. Historical Development</i>	5
<i>Composite Material</i>	5
<i>Composite Tailoring</i>	13
<i>III. Theory</i>	24
<i>Composite Plate Theory</i>	24
<i>Active Control Derivation</i>	36
<i>Discretization of the Equations of Motion</i>	40
<i>Control Theory and Optimization</i>	55
<i>Control Theory</i>	55
<i>Performance Index and Sensitivity Equations</i>	61
<i>IV. Optimization Results</i>	69
<i>V. Experimental Apparatus and Procedure</i>	80
<i>VI. Comparisons Between Baseline, Modified Plate and Theory</i>	93
<i>VII. Summary</i>	103
<i>Bibliography</i>	106
<i>Appendix A</i>	111
<i>Appendix B</i>	113
<i>Appendix C</i>	141
<i>Vita</i>	149

Symbol List

The following is a list of symbols used in this dissertation:

a	Plate length
$[A]$	Plant matrix determined from the stiffness matrix and the inverse of the mass matrix
A_{cl}	Closed loop system matrix
A_{MN}	Eigenvectors of the plate
b	Plate width
$[B]$	Control matrix determined from the actuator coupling coefficients, location matrix and the inverse of the mass matrix
$[C]$	Sensor matrix determined from the sensor and dynamic coupling coefficients
C_{ij}	Composite compliance Matrix Term
c_1	1st element of the constraint matrix
c_2	2nd element of the constrain matrix
C_r	Location matrix for the difference between the left corner and the center of the plate tip
C_b	Location matrix for center of the plate tip
C_N	Constants
c_{11}^E	Elastic modulus of the sensor material
d	Torsional disturbance amplitude at free end of plate
δ	First variation with respect to the dependent variables
d_{31}	Piezoelectric constant
D_{ij}	Stiffness matrix
ϵ_x	Normal strain in x direction
ϵ_y	Normal strain in y direction
$E()$	Expectation operator
E_1	Elastic modulus - 1 direction
E_2	Elastic modulus - 2 direction
E_v	Elastic modulus
F_i	Force
$[G]$	Constant control gains
G	Actuator gain matrix
G_{12}	Shear modulus in 12 direction
G_v	Shear modulus
h	Thickness of the plate
$[H]$	Disturbance matrix determined from the disturbance location matrix and the inverse of the mass matrix
$h/2$	One half plate thickness
I	Moment of Inertia
I_1	Simplifying Parameter
I_2	Simplifying Parameter
J	Performance index/objective function
$[K]$	Stiffness Matrix
γ_{xy}	Shear strain in xy direction

K_s	Sensor coefficient
K_v	Actuator coefficient
κ_x	X - axis curvature
κ_y	Y - axis curvature
κ_{xy}	XY curvature
λ	Relates to the natural frequencies of the plate
$[M]$	Mass matrix
M_x	Bending moment in x direction per unit length
M_y	Bending moment in y direction per unit length
M_{xy}	Twisting moment in xy direction per unit length
N	Number of sensor and actuators
ν_{12}	Possion's Ratio 12 direction
ν_{21}	Possion's Ratio 21 direction
p	Frequency
p_i	Design parameters
ρ	Density
q	State variables
Q	Covariance matrix from Lyapunov equation
Q_i	Nonconservative work term in La Grange equations
Q_{ij}	Stiffness parameter in ij direction
r	Position vector
R_F	Resistor associated with an ideal op amp used to acquire the signal
σ_x	Normal stress in x direction
σ_y	Normal stress in y direction
S_{11}	Strain
t	Time
T	Kinetic energy
θ	Ply angle
τ_{xy}	Shear stress in xy direction
U	Potential/strain energy
u	Control vector {actuator voltages}
$u(x,z,t)$	Displacement in x direction
V	Work done by external forces
V_D	Voltage across the piezoceramic actuator
V_0	Measured voltage from the sensor
$v(x,z,t)$	Displacement in y direction
$w(x,z,t)$	Displacement in z direction
w_d	Sensor width
w_0	Midplane displacement in z direction
$w_{0,xx}$	2nd partial derivative with respect to x
$w_{0,xy}$	2nd partial derivative with respect to x and y
$w_{0,yy}$	2nd partial derivative with respect to y
w_r	Difference of the corner displacement vector and the center displacement vector of the plate tip
w_b	Center displacement vector of the plate tip
X	X - direction component of solution to equations of motion - trigonometric functions

X	X component of buckling equation of motion
x_i	Endpoint of sensor
$\Psi(t)$	Time component of solution to equations of motion
y	Sensor voltage signal (strain rate of the plate) collocated at actuator position
Y	Y - direction component of solution to equations of motion - trigonometric functions
Y	Y component of buckling equation of motion
ζ	Parameter to vary the weight on a torsional versus bending motion
Ξ	Fixed mean square control energy
ξ_1	Fixed mean square control energy for actuator one
ξ_2	Fixed mean square control energy for actuator two

List of Figures

Figure 1	Spacecraft Bus and Solar Array Panels for IntelSat Satellite [1]	2
Figure 2	Composite Lamina	7
Figure 3	Stacking of Composite Lamina	7
Figure 4	Design Versatility using Composite Materials	8
Figure 5	Plane Stress	11
Figure 6	Transformation Angle	11
Figure 7	Coordinate System	14
Figure 8	Ply Angle Varied Along X-Axis	20
Figure 9	Outline of Research	25
Figure 10	Dimensions of Composite Plate	25
Figure 11	Combining Equations Of Motion with Control Theory	38
Figure 12	Actuator and Sensor Attached to Structure	38
Figure 13	New Plate Coordinate System	45
Figure 14	D_{16} Coefficient versus Ply Angle	64
Figure 15	Outline of Optimization	70
Figure 16	Test for Convexity	70
Figure 17	Bagging the Composite Layup	82
Figure 18	Standard Cure Cycle of Graphic Epoxy Materials	82
Figure 19	Location of Sensor and Actuator on Plate	89
Figure 20	Strain Rate Feedback Circuit	89
Figure 21	Response - Strain Rate Feedback Circuit 1	90

Figure 22 Response - Strain Rate Feedback Circuit 2	90
Figure 23 Schematic of Control Electronics	92
Figure 24 Optimal Location of Actuators from [24] [25] [26]	95
Figure 25 1st Bending Mode of the Plate	98
Figure 26 2nd Bending Mode of the Plate	98
Figure 27 1st Torsional Mode of the Plate	98
Figure 28 2nd Torsional Mode of the Plate	98
Figure 29 Open Loop Frequency Response of Isotropic Plate	100
Figure 30 Open and Closed Loop Response of Optimized Plate	101
Figure 31 Optimization Program Flow Chart	113

List of Tables

TABLE 1 TYPICAL COMPOSITE PROPERTIES	49
TABLE 2 FREQUENCIES FOR THE TEST CASES FOR THE ONE MODE APPROXIMATION	50
TABLE 3 FREQUENCIES AND MODE SHAPES FOR THE TEST CASES FOR THE FOUR MODE APPROXIMATION	50
TABLE 4 TEST CASE 1 FREQUENCIES FOR THE NINE MODE APPROXIMATION	52
TABLE 5 TEST CASE 1 FREQUENCIES FOR THE ONE, FOUR, AND NINE MODE APPROXIMATION	53
TABLE 6 EXPERIMENTALLY DETERMINED COMPOSITE PROPERTIES	71
TABLE 7 DEFINITION OF OPTIMIZATION PARAMETERS	74
TABLE 8 SUMMARY OF "GLOBAL MINIMUM" SOLUTIONS FROM STARTING POSITIONS	75
TABLE 9 EFFECTS OF ζ ON THE PLY ANGLE, ACTUATOR LOCATION AND OBJECTIVE FUNCTION	77
TABLE 10 RESULTS FOR THE 0 DEGREE COMPOSITE MATERIAL TESTS	84
TABLE 11 RESULTS FOR THE 45 DEGREE COMPOSITE MATERIAL TESTS	85
TABLE 12 RESULTS FOR THE 90 DEGREE COMPOSITE MATERIAL TESTS	85
TABLE 13 OPTIMAL PLY ANGLE FROM [24] [25] [26]	96
TABLE 14 COMPARISON BETWEEN REFERENCED PAPER AND DISSERTATION PARAMETERS	96

TABLE 15	FREQUENCY COMPARISON OF THEORETICAL CALCULATIONS	
	AND EXPERIMENTAL MEASUREMENTS OF THE 21 DEGREE PLATE . . .	97
TABLE 16	THEORETICAL DAMPING FACTORS FOR ISOTROPIC AND 21	
	DEGREE	102

Abstract

A method for the simultaneous structural and control optimization for torsional vibration of a composite plate which simulates a spacecraft solar array structure was developed in this study. Included in the optimization of the plate are the location of the piezoceramic actuators and sensors that provide bending/torsion actuation, the control gains, and the orientation of the graphite fibers in the composite plies. This research included the effects of using composite tailoring to promote the coupling of the twisting-bending mode to enhance the damping system. The plate was modeled by classical lamination plate theory using a linear elastic strain-displacement theory. This theory was then incorporated into a performance index which contains both structural and control parameters that minimizes torsional and bending motion at the tip of the plate due to a torsional force at the tip. Along with the performance index, there are inequality constraints on the amount of power to the actuators. This performance index and constraints, along with upper and lower bounds on the design variables, were incorporated into an optimization subroutine which then produced an optimal design for controlling both torsional and bending vibration. This optimal plate was fabricated and tested with a torsional load to decide the validity of the theory in improving damping. A comparison was made between the results of the theory and the experimental results of testing the optimized plate and a baseline plate made up of a quasi-isotropic lay-up. The frequencies of the experimental and the theoretical results were within 15% of each other. Also the damping factor for the 1st torsional and 2nd torsional modes of vibration increased significantly for the optimized plate versus the baseline plate which verifies the basic premise of the theory.

SIMULTANEOUS COMPOSITE TAILORING AND BENDING CONTROL OPTIMIZATION FOR DAMPING THE TORSIONAL VIBRATION OF A PLATE

I. Introduction

Background

Spacecraft have always been subjected to some form of disturbances. Some of these disturbances can be classified as either random or persistent. The random disturbances are caused by such things as micrometeorite impacts, increased solar activity, material degradation, etc. The persistent disturbances can be caused by such things as cryo-cooling elements, vibrations from flexible elements, momentum wheel mass imbalance or bearing noise, etc. Some of these disturbances do not degrade the performance of the satellite due to their small amplitude and the robustness of the control system. However these disturbances will degrade the performance if they are large enough or if the pointing requirements of the satellite are stringent enough. The twisting-bending motion of a solar array panel caused by either internal or external forces can induce large vibrations on the main spacecraft structure called the satellite bus.

Statement of the Problem

The flexible vibration of the solar arrays, that are connected to the satellite bus, are the cause of one such disturbance source as shown on the IntelSat satellite in figure 1 which is found in reference [1] and on the IntelSat WWW Home page. As satellites require more power, the size of the solar

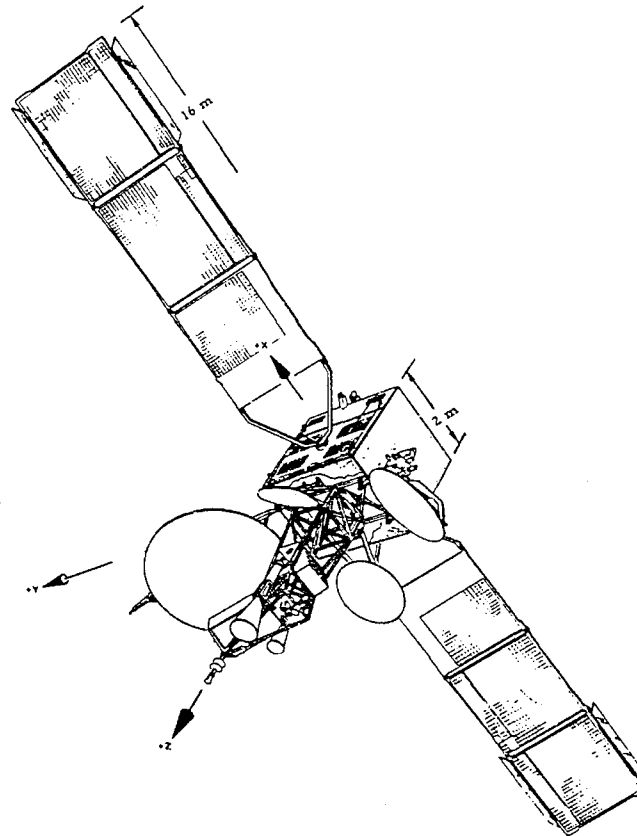


Figure 1 Spacecraft Bus and Solar Array Panels for IntelSat Satellite [1]

array increases tremendously. These solar arrays are prone to vibrations due to their large size and light weight. The solar arrays can be subjected to a multitude of loading conditions such as bending, torsion, combined loading, etc. The bending vibration of a solar array can be controlled by attaching bending force actuators and sensors to the array at various locations. The sensors are able to detect mechanical motion and produce an electrical voltage. The actuators receive an electrical signal and convert it to a mechanical motion. However, the torsional vibrations are not easily controlled. There are very few ways to damp out torsional vibrations in a flat panel and the ones that are available are very costly in terms of weight and power requirements. This research centers on damping out these unwanted torsional vibrations in the structure using a combination of bending force actuators and the structural bending-torsion phenomenon exhibited by unbalanced composite plate layups.

Solution

This dissertation looks at controlling the vibrations which could occur in the solar array by modeling it as a plate which will minimize both torsional and bending vibrations. This plate is modeled by classical laminated plate theory using a linear elastic strain-displacement theory for combined loading. The plate is then simultaneously optimized with respect to both the structural and control system to isolate the satellite bus from the disturbance source by improving the damping of the plate. Improving the damping of the plate results in suppressing its motion caused by the external disturbance. If the motion of the plate is suppressed, then the satellite bus is isolated from that external disturbance. The control system performance is improved by enhancing the coupling of the twisting and bending modes by altering the ply layup. Since this plate is made up of composite material, the stiffness is optimized by varying the orientation of the composite fibers of each ply. The

twisting-bending coupling due to an unbalanced ply-layup is designed to provide the maximum energy to those vibratory modes which the control system can damp. Very few active damping systems work well in damping out the torsional motion of spacecraft structures. If the energy from the torsion mode can be transferred into a bending mode by ply coupling, then the disturbance will be damped out by the active control system. In short, the entire system consisting of the stiffness of the plate, location, and power requirements of the actuators and sensors is optimized for maximized performance for torsional loading. A comparison is then made experimentally between the modified structure versus the unmodified structure for improved performance. The root mean squared (RMS) motion and damping factors of the optimized structure are also compared to the theoretical results of this research to determine if the modelling of the plate is accurate.

In this dissertation, the historical background will first be discussed along with the formation of the theory. Once the theory is complete, the optimization is performed and from this output an optimized plate is fabricated and tested. Finally comparisons are made between the theoretical predictions and the experimental results.

II. Historical Development

Introduction

In this chapter, the work accomplished by previous researchers is discussed as it directly relates to this dissertation. Also, the development of the fundamental composite equations of the theory are discussed. The historic development is divided into two different sections. The composite material theoretical equations are provided in the first section. Instead of dealing with the historic development of composite material, the elasticity equations are formulated which will be used later in the theoretical development. These elasticity equations are derived from Hooke's Law for three dimensional stress-strain relationships.

The second section provides a background look at the theory of composite tailoring and coupling. This section will present historical work in this area about aeroelasticity and current work which deals with the problem defined in this research. Aeroelasticity predominately deals with aircraft, but the same principles can also be applied to parts of the spacecraft such as the solar arrays. The solar arrays sometimes act as large wings on a spacecraft when in the presence of the low Earth orbit environment. Through the use of aeroelastic tailoring, better control can be accomplished of the solar array structures.

Composite Material

A composite material consists of a reinforcement to provide strength and stiffness and a matrix material that acts as a glue to hold the structure together. Early examples of composite material include the clay/straw mixture used to make adobe structures to steel reinforced concrete used to support very large structures such as bridges, dams, etc. When one speaks of advanced composites, one usually means composites that use stiffening agents such

as glass, graphite, carbon, boron, and metal fibers; and matrix materials such as epoxy, metal, and carbon versus the previously mentioned materials and glass composites. Composite materials usually have very good stiffness and strength characteristics when compared to conventional materials especially when weight is a factor. The specific stiffness, or stiffness to weight ratio, and the specific strength, or strength to weight ratio, of composites are vastly superior to conventional materials like aluminum, steel and even titanium.

All composite materials whether they are hand layed-up, filament wound, woven, or pultruded are made up by stacking individual layers, called laminae, together to form the structure. Each lamina consists of fibers oriented in the same direction held together by the matrix material. (See figure 2.) The laminae are then stacked together, allowing the fiber orientation to vary from one to another to form the laminate or structure. One of the principal advantages of composite materials is that each individual lamina can have varying fiber orientations with respect to one another. By stacking laminae with varying fiber orientations, the properties of the structure will change. For example, to obtain maximum longitudinal and bending stiffness, all of the fibers in each lamina need to be oriented in the axial direction. The fiber orientation will decide the strength, stiffness, and almost every other property of the structure. Figure 3 shows how each ply can be different from the preceding ply by changing the orientation of the fibers. This allows the structure made out of composite material to be tailored to meet any designers requirements. The plot in figure 4, made by an engineer at the Phillips Laboratory using in-house composite test data, shows the design versatility of using composite material with respect to aluminum. The properties of aluminum are set to unity and the relative composite properties are shown. At least in the aerospace industry, the trend is to fabricate almost everything out of composite materials due to their

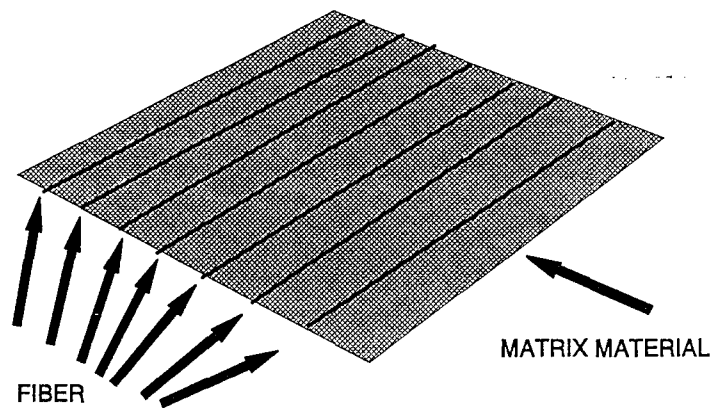


Figure 2 Composite Lamina

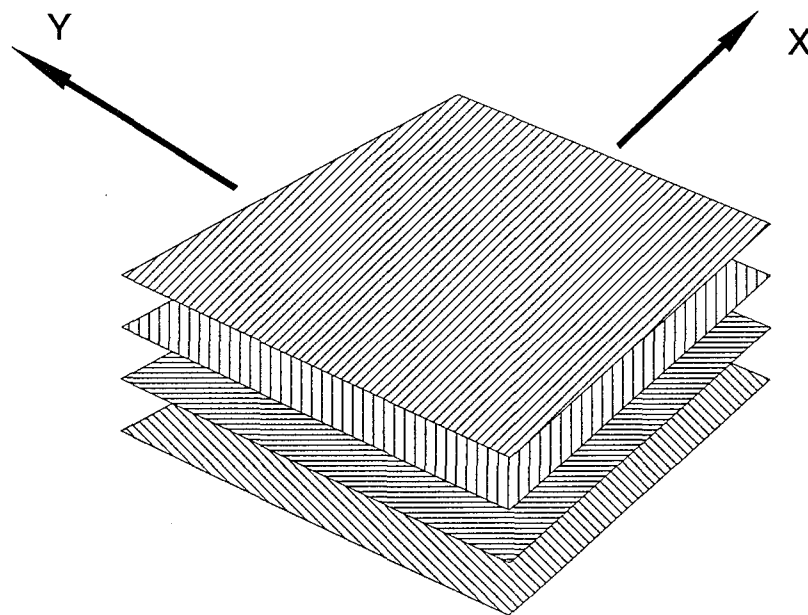


Figure 3 Stacking of Composite Lamina

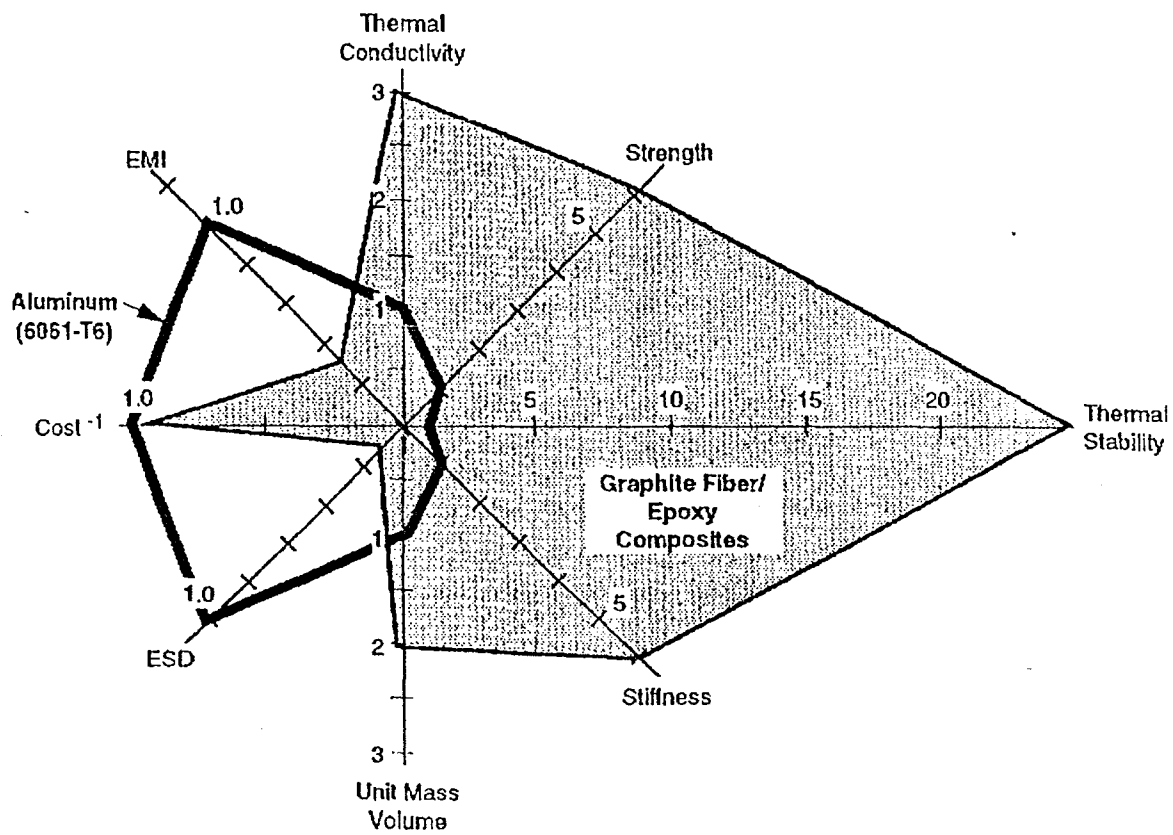


Figure 4 Design Versatility using Composite Materials

tailorability and superior properties.

Several assumptions are made to analyze composite laminae: [2]

- (a) The fibers are homogeneous, linearly elastic and isotropic. They are equally spaced and perfectly aligned.
- (b) The matrix is homogeneous, linearly elastic and isotropic. Hooke's Law governs the mechanical behavior of a composite lamina.

Jones [3] and Murray [4] provide a very good description of the macromechanical behavior of a lamina and a laminate. The generalized Hooke's Law for an anisotropic material can be written in matrix form as:

$$\begin{Bmatrix} \sigma_1 \\ \sigma_2 \\ \sigma_3 \\ \tau_{23} \\ \tau_{31} \\ \tau_{12} \end{Bmatrix} = \begin{bmatrix} C_{11} & C_{12} & C_{13} & C_{14} & C_{15} & C_{16} \\ C_{12} & C_{22} & C_{23} & C_{24} & C_{25} & C_{26} \\ C_{13} & C_{23} & C_{33} & C_{34} & C_{35} & C_{36} \\ C_{14} & C_{24} & C_{34} & C_{44} & C_{45} & C_{46} \\ C_{15} & C_{25} & C_{35} & C_{45} & C_{55} & C_{56} \\ C_{16} & C_{26} & C_{36} & C_{46} & C_{56} & C_{66} \end{bmatrix} \begin{Bmatrix} \epsilon_1 \\ \epsilon_2 \\ \epsilon_3 \\ \gamma_{23} \\ \gamma_{31} \\ \gamma_{12} \end{Bmatrix} \quad (1)$$

where σ_i are the stress components, $[C]$ is the stiffness matrix, and ϵ_i are the strain components. The stiffness matrix can be related to standard engineering constants such as Young's Modulus E , Poisson's Ratio ν , and the shear modulus G for each direction. In anisotropic materials there are no planes of symmetry, since none of the axes of the lamina line up with the principal axes of material symmetry.

In most composites, two axes of the lamina line up with the principal axes of the material which form two planes of symmetry. The 1 direction consists of fiber dominated properties while the 2 direction consists of matrix dominated properties. This material is

defined to be an orthotropic material. The stress-strain relationship for this material is:

$$\begin{Bmatrix} \sigma_1 \\ \sigma_2 \\ \sigma_3 \\ \tau_{23} \\ \tau_{31} \\ \tau_{12} \end{Bmatrix} = \begin{bmatrix} C_{11} & C_{12} & C_{13} & 0 & 0 & 0 \\ C_{12} & C_{22} & C_{23} & 0 & 0 & 0 \\ C_{13} & C_{23} & C_{33} & 0 & 0 & 0 \\ 0 & 0 & 0 & C_{44} & 0 & 0 \\ 0 & 0 & 0 & 0 & C_{55} & 0 \\ 0 & 0 & 0 & 0 & 0 & C_{66} \end{bmatrix} \begin{Bmatrix} \epsilon_1 \\ \epsilon_2 \\ \epsilon_3 \\ \gamma_{23} \\ \gamma_{31} \\ \gamma_{12} \end{Bmatrix} \quad (2)$$

If a laminate is thin enough, a state of plane stress exists and is characterized by:

$$\sigma_3 = \tau_{23} = \tau_{31} = 0 \quad (3)$$

This is shown in figure 5 which also shows the principle directions of the structure. The stress-strain relationship expressed in equation 2 is now reduced to:

$$\begin{Bmatrix} \sigma_1 \\ \sigma_2 \\ \tau_{12} \end{Bmatrix} = \begin{bmatrix} Q_{11} & Q_{12} & 0 \\ Q_{12} & Q_{22} & 0 \\ 0 & 0 & Q_{66} \end{bmatrix} \begin{Bmatrix} \epsilon_1 \\ \epsilon_2 \\ \gamma_{12} \end{Bmatrix} \quad (4)$$

where:

$$Q_{11} = C_{11} - \frac{C_{13}^2}{C_{33}} = \frac{E_1}{1 - \nu_{12}\nu_{21}} \quad (5)$$

$$Q_{12} = C_{12} - \frac{C_{23}C_{13}}{C_{33}} = \frac{\nu_{21}E_1}{1 - \nu_{12}\nu_{21}} \quad (6)$$

$$Q_{22} = C_{22} - \frac{C_{23}^2}{C_{33}} = \frac{E_2}{1 - \nu_{12}\nu_{21}} \quad (7)$$

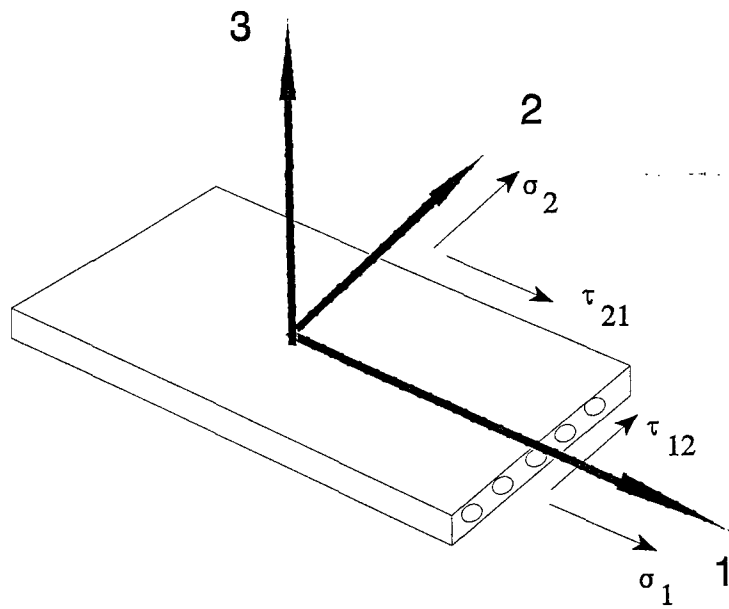


Figure 5 Plane Stress

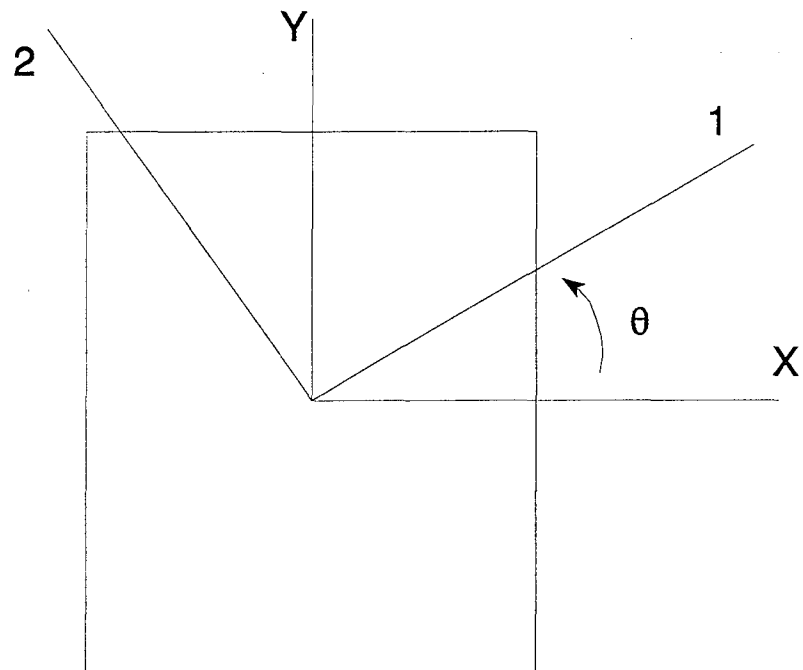


Figure 6 Transformation Angle

$$Q_{66} = C_{66} = G_{12} \quad (8)$$

When the principle material directions move to a different coordinate system and differ from the principle directions of the structure as in the case of angle ply layups, the stresses and strains need to undergo a coordinate transformation. (See figure 6). The angle θ is the angle from the x-axis to the 1-axis. The transformation from the 1-2-3 coordinate system to the x-y-z system is:

$$\{\sigma\}_{xyz} = [T]^{-1} \{\sigma\}_{123} \quad (9)$$

where $[T]^{-1}$ is [5]:

$$[T]^{-1} = \begin{bmatrix} \cos^2\theta & \sin^2\theta & -2\sin\theta\cos\theta \\ \sin^2\theta & \cos^2\theta & 2\sin\theta\cos\theta \\ \sin\theta\cos\theta & -\sin\theta\cos\theta & \cos^2\theta - \sin^2\theta \end{bmatrix} \quad (10)$$

Using the coordinate transformations, the relationship between stress and strain, in any arbitrary direction, can be found. This relationship is:

$$\{\sigma\}_{xyz} = [T]^{-1} \{\sigma\}_{123} = [\bar{Q}] \{\epsilon\}_{xyz} \quad (11)$$

where

$$[\bar{Q}] = [T]^{-1} [Q] [T]^{-T} \quad (12)$$

The stress-strain relationships for transverse isotropy in xyz coordinates are then represented in

matrix form as:

$$\begin{Bmatrix} \sigma_x \\ \sigma_y \\ \tau_{xy} \end{Bmatrix} = [\bar{Q}] \begin{Bmatrix} \epsilon_x \\ \epsilon_y \\ \gamma_{xy} \end{Bmatrix} = \begin{bmatrix} \bar{Q}_{11} & \bar{Q}_{12} & \bar{Q}_{16} \\ \bar{Q}_{12} & \bar{Q}_{22} & \bar{Q}_{26} \\ \bar{Q}_{16} & \bar{Q}_{26} & \bar{Q}_{66} \end{bmatrix} \begin{Bmatrix} \epsilon_x \\ \epsilon_y \\ \gamma_{xy} \end{Bmatrix} \quad (13)$$

in which:

$$\bar{Q}_{11} = C_{11} \cos^4 \theta + 2(C_{12} + 2C_{66}) \sin^2 \theta \cos^2 \theta + C_{22} \sin^4 \theta \quad (14)$$

$$\bar{Q}_{12} = (C_{11} + C_{22} - 4C_{66}) \sin^2 \theta \cos^2 \theta + C_{12} (\sin^4 \theta + \cos^4 \theta) \quad (15)$$

$$\bar{Q}_{16} = (C_{11} - C_{12} - 2C_{66}) \sin \theta \cos^3 \theta + (C_{12} - C_{22} + 2C_{66}) \sin^3 \theta \cos \theta \quad (16)$$

$$\bar{Q}_{22} = C_{11} \sin^4 \theta + 2(C_{12} + 2C_{66}) \sin^2 \theta \cos^2 \theta + C_{22} \cos^4 \theta \quad (17)$$

$$\bar{Q}_{26} = (C_{11} - C_{12} - 2C_{66}) \sin^3 \theta \cos \theta + (C_{12} - C_{22} + 2C_{66}) \sin \theta \cos^3 \theta \quad (18)$$

$$\bar{Q}_{66} = (C_{11} + C_{22} - 2C_{12} - 2C_{66}) \sin^2 \theta \cos^2 \theta + C_{66} (\sin^4 \theta + \cos^4 \theta) \quad (19)$$

Now that the stress-strain relationships for any arbitrary ply angle are developed, the equations relating strain to displacement for an anisotropic plate need to be derived. These equations will be derived in chapter III using the strain relationships derived in a rectangular cartesian coordinate system. A linear elastic theory will be used to describe this relationship. The coordinate system used in this development is shown in figure 7. The x and y axis are located at the mid-plane of the laminate. The displacements U_0 , V_0 , and W_0 are the laminate mid-surface displacements in the x, y, and z directions respectively.

Composite Tailoring

Composite tailoring has been used in aircraft and helicopter applications in the recent past. The tailoring of the composite material properties such as the strength, stiffness,

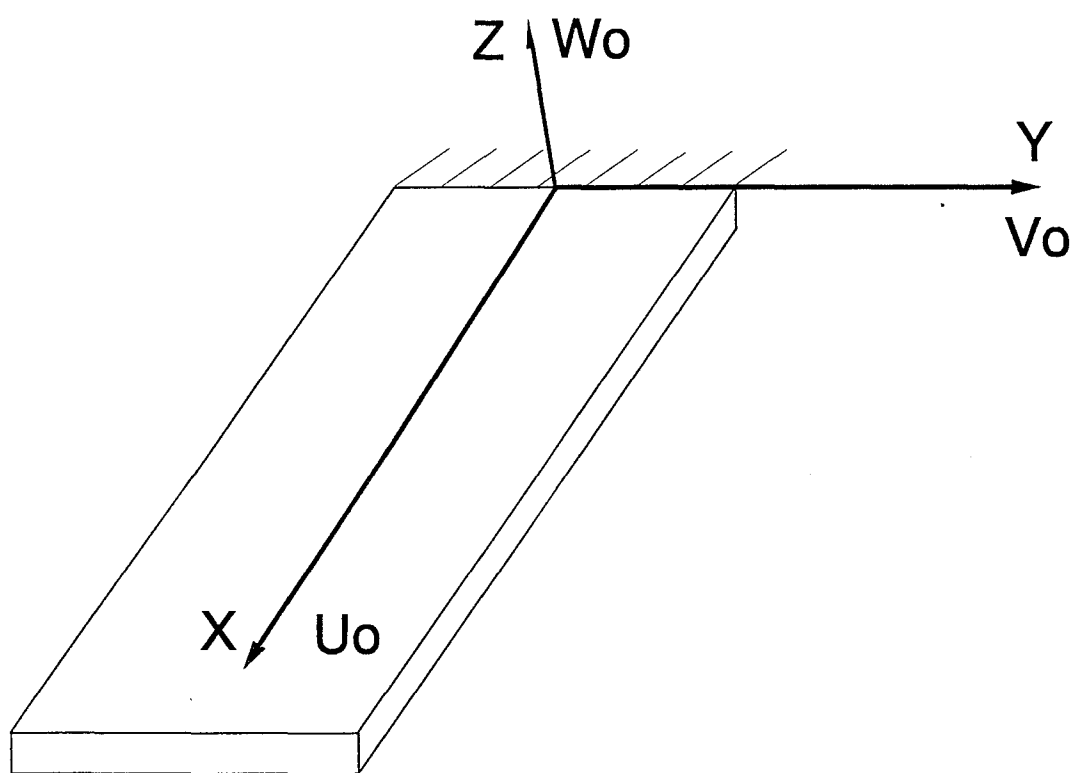


Figure 7 Coordinate System

thermal coefficients, and coupling terms to meet an objective is what makes them very attractive to use in all applications. This is especially true in the area of aeroelastic tailoring which is "the incorporation of directional stiffness into an aircraft structural design to control aeroelastic deformation, static or dynamic, in such a fashion as to affect the aerodynamic and structural performance of that aircraft in a beneficial way." (See [6],[7],[8],[9].) Aeroelasticity predominately deals with aircraft, but the same principles can also be applied to parts of the spacecraft such as the solar arrays. The solar arrays sometimes act as large wings on a spacecraft when in the presence of the low Earth orbit environment. Through the use of aeroelasticity, better control can be accomplished of the solar array structures. In recent years, most of the effort in aeroelastic tailoring has been conducted in identifying the effects of an anisotropic design on the deformation coupling of fixed and swept wing aircraft. (See [6] [7] [10] [11] [12] [14].) More recently, the shift in aeroelastic tailoring has turned to the effects on rotorcraft and rotorsystems. (See [2] [13] [15].) Composite tailoring through anisotropic design is ideal for this application since helicopter blades operate in an environment consisting of inertial, aerodynamic and elastic loadings. The benefits of aeroelastic tailoring for helicopter blades with an off-axis layup are that a twist will be induced in the blade when a non-torsion force is exerted which will improve the performance of the lifting surface.

In this research, the idea of composite tailoring will be extended to the area of controlling large space structures and modified slightly. The layup will remain symmetrical to prevent warping, but it will be unbalanced which will cause the required coupling in motion. The plates in a large space structure, with an anisotropic composite layup, will be optimized with respect to their directional stiffness and coupling terms to enhance the effect of the control system on the structure. The orientation of the composite fibers, which decide these

coupling and stiffness terms, will be optimized with respect to the active damping. The axial-bending and torsion-bending coupling due to an anisotropic, unbalanced ply-layup will be analyzed to provide the maximum energy to those vibratory modes that the control system can damp. Very few active damping systems work well in damping axial and torsion motion. If the energy from the axial and torsion modes can be transferred into a bending mode through ply coupling, then the disturbance can be damped out by the active control system.

The idea of composite tailoring for structural elements in a spacecraft has been presented only recently in the literature by Hwang and Gibson [16], Barrett [17] [18], Belknap and Kosmatka [19], Bronowicki and Diaz [20], Olcott [21] [22] [23], Hwang, Hwang, and Chul [24] [25] [26], and others [27] [28] [29] [31] [30]. Hwang and Gibson [16] presented the influence of the vibration coupling effects, such as bending-twist and bending-extension, on the damping of laminated composites. The only damping was the inherent material damping of the composite, modelled by the strain energy damping. They concluded that the coupling effects of the composite are dependent upon the fiber orientation and laminate geometry. The coupling effects were found maximized at fiber orientations of 30 degrees. Also, the coupling effects tended to increase the vibrational damping in the first two flexible modes.

Barrett [17] [18] discussed the improvement of damping properties of axially loaded structural members made up of anisotropic composite laminated and damping material. He formulated a structural theory that characterizes the behavior of an axially loaded composite cylinder and applied it to a three layered structure. This structure consisted of concentric layers of both stiffness and damping materials. In his theory, the stiffened cylinders were treated with thin wall theory that implies that the non-membrane stresses were negligible.

Different fiber orientation and layups were studied for controlling the resonant response of the structures. These design study comparisons were not made on an equal mass basis which accounts for some decrease in resonant frequency when the damping material is added to the structures. The design studies proved the effectiveness of the coupling in suppressing and controlling resonant vibration. Barrett discussed some difficulties associated with the addition of anisotropic effects. Anisotropy will result in shear stresses and circumferential displacements in the axial composite cylinder construction. These shear stresses may result in new modes of failure such as delaminations in the cylindrical structure. The circumferential displacements at the ends of the members will cause difficulties because they are usually constrained in most boundary conditions. Barrett discusses, but does not analyze, some possible solutions to these difficulties. One solution is to allow the stiffness to vary along the length of the structure. This can be accomplished by allowing the thickness to vary or the ply angle to change along the length. Barrett concludes that the anisotropic composite construction is resistant to all modes of vibration. The axially, torsional, and flexural modes of vibration are resisted by the coupling introduced by an anisotropic composite layup.

Belknap [19] discussed the design and fabrication of a thin walled composite structure with an inner and outer layer of graphite epoxy shells and a center layer of viscoelastic damping material. The graphite layers were fabricated so that when they are subjected to either a bending or axial load, they counter-rotate to produce a large shear area at the viscoelastic layer. Belknap used the stiffness characteristics of a laminated tube to choose ply orientations that maximize damping and structural stiffness. In his theoretical development he assumed a two-dimensional strain state when determining the displacement functions. A separation of variables technique combined with the Ritz method was used to solve for the

local cross-section warping functions. The extensional-bending-twisting coupling can be represented by applying solely an axial force. By varying the ply angle, Belknap demonstrated that the coupling is maximized when the angle is around 30 degrees. He also presented a very detailed fabrication plan and problems associated with incorporating the viscoelastic material into the tube. The main problem that he encountered was in testing the tube in the axial mode. He said that special end fittings need to be fabricated to couple the stiffness of the two composite shells with the viscoelastic core while allowing for the counter rotation of the two shells at the tube's end. However, by conducting a simple impact-hammer modal test with the tube in a near free-free suspension, the damping in the first mode was increased over seven times by optimizing the ply layers and incorporating the damping layer.

Bronowicki and Diaz [20] present a semi-analytical finite element approach using a pair of concentric cylindrical shells surrounding a viscoelastic medium. They present this theory in an attempt to damp extensional motions in a truss member commonly found in a space structure. The constitutive equations for the cylindrical shells are derived based upon a plane stress, linear strain-displacement relationship for an orthotropic material. The viscoelastic material is, as stated in this report, "assumed to be at a single operating frequency, which allows the elastic and shear modulus, E_v and G_v , to be defined as complex numbers representing magnitude and phase of stiffness." The analysis that is performed is for that single frequency and can be performed for different operating frequencies and temperatures. The stress-strain relationship is derived using Hooke's Law. The displacements of the viscoelastic material are assumed to vary linearly throughout the thickness between the inner and outer shell. The outer and inner orthotropic shells are coupled to the viscoelastic layer through surface tractions. From these combined equations, only allowing radial forces, a finite

element is defined for the composite structure. These finite elements are combined to form a coarse grid along the length of the tube. They say that due to the Bernoulli-Euler hypothesis, the axial results can be applied to bending.

In his dissertation and other papers, Olcot [21] [22] [23] discusses a new damping concept which uses the stress coupling effects inherent in composite materials to induce large shear strains in co-cured damping layers. The ply angle is varied along the length (as shown in figure 8) of the component to create multiple regions of high shear and to induce high damping loss factors within the component. This concept was analyzed by a computer program which was used to conduct parametric studies on the analytical models of flat membranes and cylindrical damped components. Finally, several damped cylinders and I-beams were built to test the validity of the theory and computer program. The model developed by the theory predicted the natural vibration frequency and damping loss factors of the cylinders to within 5%. The cylinders built and tested with this new concept have tested loss factors of up to 8.5%.

The work presented in the papers by Hwang, Hwang, and Chul [25] [26] is very similar to the work presented in this dissertation. Their theoretical model and approach are presented next. However, the conclusions of their paper will not be discussed in this chapter. A comparison of their theoretical and experimental work to the current approach is presented in chapter VI. The conclusions of the paper by Hwang, Hwang, and Chul will be used as an independent confirmation of this dissertation and compared with the results. Their basic premise is to use an intelligent system concept design for vibration control of a laminated composite plate with piezoelectric sensors and actuators attached. An intelligent system concept design is another name for smart structures which is the addition of sensors, actuators,

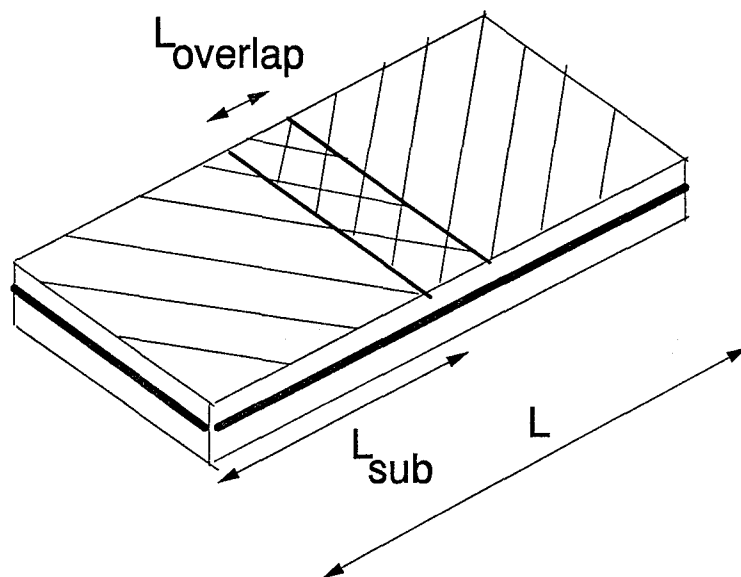


Figure 8 Ply Angle Varied Along X-Axis

and control electronics to a structure to control the vibrations. Also included is an analysis of altering the vibration modes of the composite structure by tailoring the stiffness and taking into account the bending-torsional coupling. They determine the optimal size and location of the sensor and actuator and the optimal ply layer angles which maximize the work done by the controller. If the work done by the controller is maximized by optimizing the structural and control parameters, then the control energy utilized is reduced. One of the major differences between the referenced paper and this dissertation is how the equations of motion are determined. Hwang et. al. derive the equations of motion by using Hamilton's Principle and then discretize them by using the finite element method. The kinematics are derived by expressing the displacement and curvature in terms of nodal displacements using the shape functions of a 4 node, 12 degree of freedom quadrilateral plate bending element. In this dissertation the equations of motion are formulated similarly using Hamilton's Principle. However, the discrete equations of motion are found by using the Rayleigh-Ritz or Assumed Modes method. Since finite element theory is a derivative of this energy methods, the theoretical results should compare very well.

Also in the paper by Hwang et.al., from finite element theory, the mass matrix M and stiffness matrix K are generated and used to solve the free vibration analysis for the natural frequencies and mode shape vector. The equations of motion are transformed into state space form through the use of modal state variables. The control equations are adjoined to the state space equation of motion by using negative velocity feedback. The combined control equations are written in terms of both the structural and control variables. An objective function is formed based upon these variables whose solution will maximize the work done by the feedback control forces, for a fixed energy input, by calculating the optimal solution. The

optimal solution is dependent upon the design variables which are the ply layer angles and number, size, location, and gains of each sensor and actuator pair. When the work done by the feedback control forces is maximized, the control system is more effective. In this paper [25], the numerical optimization is performed using the method of feasible directions.

Numerical calculations are performed on an eight ply laminated composite plate with two of the plies variable. The stacking sequence is defined as $[\theta_1/\theta_2/0^\circ/90^\circ]_s$, where θ_1 and θ_2 are the ply angle design variables. The optimization is first conducted for an orthotropic plate to determine the optimal size and location of the piezoelectric sensors and actuators. Initially, the size of the sensors and actuators are unconstrained while the locations are not allowed to vary. In the second case the sizes are constrained while the optimal locations are obtained. The optimization is next conducted to determine the optimal ply angles of the laminated plate which will maximize the control performance. The optimization is conducted with and without the dynamic stability constraints. The optimizations are not performed simultaneously or integrated as they are done in this dissertation. Instead they are performed sequentially which may or may not produce the optimal result. Sequential optimization may be the easier method because it reduces the number of parameters which are being searched for during the optimization, but may not produce the best result as shown by Dracopoulos and Oz [32]. They show that using simultaneous or integrated optimization produced a solution which lowered the control cost by 294.4% over a nonintegrated design procedure. The final result of the papers by Hwang [25], [26] and in this dissertation, is that the control system performance increases, as measured by the increased damping factors, as the bending-torsion coupling increases. This research described in the referenced paper presents only a theoretical analysis, but in this dissertation an experiment will be conducted to prove the feasibility of this

proposed theory. However, the results of Hwang et.al. are very close to the results found in this research even though the methodology is completely different: finite element method versus Rayleigh-Ritz approximation and sequential versus simultaneous optimization.

III. Theory

Introduction

This chapter is separated into five main sections: derivation of the equations of motion for the composite plate, active control derivation, derivation of the complete equations of motion, control theory and structural/control optimization formulation and solutions by an optimization subroutine. In each section, the necessary equations are derived and main assumptions are stated for each particular subject. How these particular sections fit together is shown in figure 9 which is a flow chart outlining the theory. First the governing composite equations are formulated for a particular strain field. These equations are converted from partial differential equations to ordinary differential equations by incorporating assumed solutions to the equations of motion. Next, the active control system is augmented to the differential equations through the use of state space modelling. The equations are first order differential equations. The optimization performance index and constraint equations are determined next. These equations are coded into a FORTRAN program and an optimum solution is found using an optimization solver. Numerous cases are run and the lowest local optimum solution is determined. Based upon the results of the optimization, an experimental plate is fabricated and tested. Finally the results are documented comparing the theoretical predictions with the experimental results.

Composite Plate Theory

This plate is (see figure 10 for dimensions) modeled by classical laminated plate theory using a linear elastic strain-displacement theory when subjected to combined loading. The thickness is approximately 100 times less than the next smallest dimension, the width.

OUTLINE OF RESEARCH

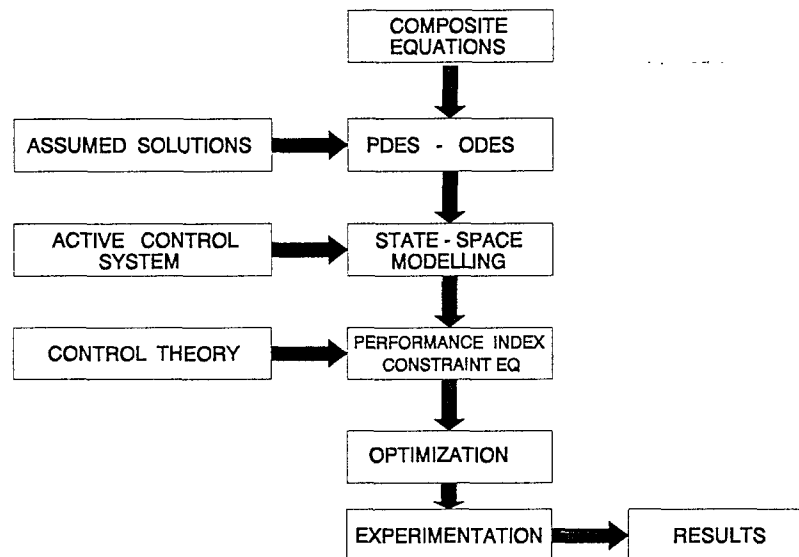


Figure 9 Outline of Research

DIMENSIONS OF THE PLATE

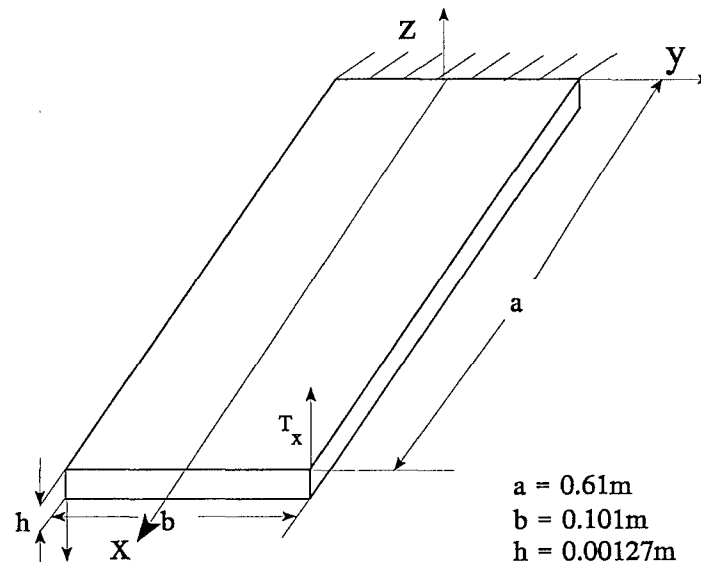


Figure 10 Dimensions of Composite Plate

The deflections of the plate are assumed to be small. Also the plate is assumed loaded only in torsion about the x-axis. The z-displacement, w_0 , is a function of both x and y. The force-displacement equations and equations of motion will now be stated for the plate.

Moment Displacement Equations. The generalized displacement field (see [3], [33]) is:

$$u(x,y,z,t) = -z \frac{\partial w_0}{\partial x} \quad (20)$$

$$v(x,y,z,t) = -z \frac{\partial w_0}{\partial y} \quad (21)$$

$$w(x,y,z,t) = w_0 \quad (22)$$

The strains considered in this analysis are derived from linear elastic theory. The linearized strain-displacement relationships are:

$$\epsilon_x = \frac{\partial u}{\partial x} \quad (23)$$

$$\epsilon_y = \frac{\partial v}{\partial y} \quad (24)$$

$$\gamma_{xy} = \frac{\partial v}{\partial x} + \frac{\partial u}{\partial y} \quad (25)$$

Substituting the above displacement relationships into the strain equations, the strain-displacement equations become:

$$\epsilon_x = -zw_{0,xx} \quad (26)$$

$$\epsilon_y = -zw_{0,yy} \quad (27)$$

$$\gamma_{xy} = -2zw_{0,xy} \quad (28)$$

Using classical laminated plate theory [3], the moment-strain relationship is presented using the above strain-displacement equations which will be used to assist with the derivation of the equations of motion is:

$$\begin{Bmatrix} M_x \\ M_y \\ M_{xy} \end{Bmatrix} = \begin{bmatrix} D_{11} & D_{12} & D_{16} \\ D_{12} & D_{22} & D_{26} \\ D_{16} & D_{26} & D_{66} \end{bmatrix} \begin{Bmatrix} \kappa_x \\ \kappa_y \\ \kappa_{xy} \end{Bmatrix} \quad (29)$$

where:

$$D_{ij} = \frac{1}{3} \sum_{k=1}^N (\bar{Q}_{ij})_k (z_k^3 - z_{k-1}^3) \quad (30)$$

where \bar{Q}_{ij} are given by eqs (14-19).

The above relationships are only valid if the ply layup is assumed to be symmetric.

Equations of Motion. The strain/displacement relationship developed previously will now be used to derive the equations of motion and boundary conditions for the composite plate. The equations of motion are derived using Hamilton's Principle [35] - [37] which is:

$$\int_{t_1}^{t_2} \delta(T - U - V) dt = 0 \quad (31)$$

where T is the kinetic energy, U is the potential or strain energy, and V symbolizes the work done by conservative or nonconservative external forces. The symbol δ represents the first variation with respect to the dependent variables.

The kinetic energy is defined as:

$$T = \int_{-b/2}^{b/2} \int_0^a \int_{-\frac{h}{2}}^{\frac{h}{2}} \frac{1}{2} \rho [(\dot{u}^2) + (\dot{v}^2) + (\dot{w}^2)] dz dx dy \quad (32)$$

where ρ is the mass density per unit volume for the composite plate and the displacement derivatives are with respect to time. The density is held constant throughout the laminate.

The displacement derivatives can now be calculated as:

$$(\dot{u}^2) = z^2 \dot{w}_{0,x}^2 \quad (33)$$

$$(\dot{v}^2) = z^2 \dot{w}_{0,y}^2 \quad (34)$$

$$(\dot{w}^2) = \dot{w}_0^2 \quad (35)$$

Before deriving the equation for the kinetic energy, the following simplifications are introduced:

$$I_1 = \int_{-\frac{h}{2}}^{\frac{h}{2}} \rho dz \quad (36)$$

$$I_3 = \int_{-\frac{h}{2}}^{\frac{h}{2}} \rho z^2 dz \quad (37)$$

The expression for the kinetic energy is:

$$T = \frac{1}{2} \int_{-b/2}^{b/2} \int_0^a [I_3 \dot{w}_{0,x}^2 + I_3 \dot{w}_{0,y}^2 + I_1 \dot{w}_0^2] dx dy \quad (38)$$

The first variation of the kinetic energy can now be found by taking the partial derivatives of

T with respect to the dependent variables which are w_0 , $w_{0,x}$, $w_{0,y}$. The first variation is now derived as:

$$\delta T = \int_{-b/2}^{b/2} \int_0^a [I_3 \dot{w}_{0,x} \delta \dot{w}_{0,x} + I_3 \dot{w}_{0,y} \delta \dot{w}_{0,y} + I_1 \dot{w}_0 \delta \dot{w}_0] dx dy \quad (39)$$

The variation of the kinetic energy is then integrated by parts (see appendix A) with respect to time to remove the partial derivatives from the variations. For simplification, this expression is broken out into four parts: contribution to the equation of motion, contribution to the initial conditions, contribution to the x-axis boundary conditions, and contribution to the y-axis boundary conditions. These expressions are represented as:

$$\int_{t_1}^{t_2} \delta T dt = T_1 + T_2 + T_3 + T_4 \quad (40)$$

Contribution to the Temporal Boundary Conditions can be stated as:

$$\begin{aligned} T_1 = & \int_{-b/2}^{b/2} I_3 \dot{w}_{0,x} \delta w_0 \Big|_{t_1}^{t_2} dy + \int_0^a I_3 \dot{w}_{0,y} \delta w_0 \Big|_{t_1}^{t_2} dx \\ & + \int_{-b/2}^{b/2} \int_0^a [(I_1 \dot{w}_0 - I_3 \dot{w}_{0,xx} - I_3 \dot{w}_{0,yy}) \delta w_0] \Big|_{t_1}^{t_2} dx dy \end{aligned} \quad (41)$$

Contribution to the Equation of Motion can be stated as:

$$T_2 = \int_{t_1}^{t_2} \int_{-b/2}^{b/2} \int_0^a [(I_3 \ddot{w}_{0,xx} + I_3 \ddot{w}_{0,yy} - I_1 \ddot{w}_0) \delta w_0] dx dy dt \quad (42)$$

Contribution to the X-Axis Boundary Condition can be stated as:

$$T_3 = - \int_{t_1 - b/2}^{t_2 b/2} I_3 \ddot{w}_{0,x} \delta w_0 \Big|_0^a dy dt \quad (43)$$

Contribution to the Y-Axis Boundary Condition can be stated as:

$$T_4 = - \int_{t_1 0}^{t_2 a} I_3 \ddot{w}_{0,y} \delta w_0 \Big|_{-b/2}^{b/2} dx dt \quad (44)$$

The strain energy is defined as:

$$U = \int_{-b/2 0}^{b/2 a} \int_{-\frac{h}{2}}^{\frac{h}{2}} (\sigma_x \epsilon_x + \sigma_y \epsilon_y + \tau_{xy} \gamma_{xy}) dz dx dy \quad (45)$$

or after taking the first variation, it can be written as:

$$\delta U = \int_{-b/2 0}^{b/2 a} \int_{-\frac{h}{2}}^{\frac{h}{2}} (\sigma_x \delta \epsilon_x + \sigma_y \delta \epsilon_y + \tau_{xy} \delta \gamma_{xy}) dz dx dy \quad (46)$$

This expression can be rewritten after substituting the terms for the displacements and integrating the z dependence out of the expressions. This equation for the potential energy is:

$$\delta U = \int_{-b/2 0}^{b/2 a} [M_x \delta w_{0,xx} + M_y \delta w_{0,yy} + 2M_{xy} \delta w_{0,xy}] dx dy \quad (47)$$

The variation of the potential energy is then integrated by parts twice with respect to x and y to remove the partial derivatives on the variations. Again for simplification, this expression is

broken out into four parts: contribution to the equation of motion, contribution to the boundary condition along the x - axis, contribution to the boundary condition along the y-axis, and contribution to the corner boundary condition. These expressions are represented as:

$$\int_{t_1}^{t_2} \delta U dt = U_1 + U_2 + U_3 + U_4 \quad (48)$$

Contribution to the Equation of Motion can be stated as:

$$U_1 = \int_{t_1}^{t_2} \int_{-b/2}^{b/2} \int_0^a [M_{xx} \delta w_0 + M_{yy} \delta w_0 + 2M_{xy} \delta w_0] dx dy dt \quad (49)$$

Contribution to the Boundary Condition Along the X - Axis can be stated as:

$$U_2 = \int_{t_1}^{t_2} \int_{-b/2}^{b/2} [M_x \delta w_{0,x} - M_{xx} \delta w_0 - 2M_{xy} \delta w_0] \Big|_0^a dy dt \quad (50)$$

Contribution to the Boundary Condition Along the Y - Axis can be stated as:

$$U_3 = \int_{t_1}^{t_2} \int_0^a [M_y \delta w_{0,y} - M_{yy} \delta w_0 - 2M_{xy} \delta w_0] \Big|_{-b/2}^{b/2} dx dt \quad (51)$$

Contribution to the Boundary Condition At the Corner of the Plate can be stated as:

$$U_4 = \int_{t_1}^{t_2} 2M_{xy} \delta w_0 \Big|_0^{a/b/2} dt \quad (52)$$

For this analysis, the structural eigenvalue problem associated with harmonic solutions

for the undamped free vibration case are formulated. Once that solution is found, the damped disturbed vibration case will be formulated based upon the solution to the above problem. The work done by external disturbances can be defined in terms of conservative torques and will show up in the boundary conditions for the damped disturbance vibration case. After the equations of motion are solved in the undamped free vibration case for their spatial relationships, the external disturbances and the control force are adjoined to them by LaGrange's Principle. Then the solutions for the damped disturbed vibration case are found.

The equations of motion, initial conditions, and boundary conditions can now be derived by substituting the appropriate equations from the variation of the kinetic and potential energies into Hamilton's Principle. The equations are:

Temporal Boundary Conditions are:

$$\begin{aligned} & \int_{-b/2}^{b/2} I_3 \dot{w}_{0,x} \delta w_0 \Big|_{t_1}^{t_2} dy + \int_0^a I_3 \dot{w}_{0,y} \delta w_0 \Big|_{t_1-b/2}^{t_2-b/2} dx \\ & + \int_{-b/2}^{b/2} \int_0^a [(I_1 \dot{w}_0 - I_3 \dot{w}_{0,xx} - I_3 \dot{w}_{0,yy}) \delta w_0] \Big|_{t_1}^{t_2} dx dy = 0 \end{aligned} \quad (53)$$

The Equations of Motion are:

$$\begin{aligned} & \int_{t_1-b/2}^{t_2-b/2} \int_0^a \int_{-b/2}^{b/2} (-M_{x^2xx} - M_{y^2yy} - 2M_{xy^2xy} \\ & + I_3 \ddot{w}_{0,xx} + I_3 \ddot{w}_{0,yy} - I_1 \ddot{w}_0) \delta w_0 dx dy dt = 0 \end{aligned} \quad (54)$$

The X-Axis Boundary Conditions are:

$$\int_{t_1-b/2}^{t_2-b/2} \int_{-b/2}^{b/2} [-M_x \delta w_{0,x} + (M_{x^2x} + 2M_{xy^2y} - I_3 \ddot{w}_{0,x}) \delta w_0] \Big|_0^a dy dt = 0 \quad (55)$$

The Y-Axis Boundary Conditions are:

$$+ \int_{t_1}^{t_2} \int_0^a [-M_y \delta w_{0,y} + (M_{y,y} + 2M_{xy,x} - I_3 \ddot{w}_{0,y}) \delta w_0] \Big|_{-b/2}^{b/2} dx dt = 0 \quad (56)$$

The Corner Boundary Conditions are:

$$- \int_{t_1}^{t_2} 2M_{xy} \delta w_0 \Big|_0^{a/2} \Big|_{-b/2}^{b/2} dt = 0 \quad (57)$$

If the initial and final conditions of the problem are completely specified, then the variations of the degrees of freedom over the interval t_1 to t_2 can be set to zero. The variations of the degree of freedom, δw_0 , is completely arbitrary and is not necessarily equal to zero. Therefore the quantities multiplied by this variation must be set equal to zero in order to satisfy Hamilton's Principle. The partial differential equation is defined as:

$$M_{x,xx} + M_{y,yy} + 2M_{xy,xy} - I_3 \ddot{w}_{0,xx} - I_3 \ddot{w}_{0,yy} + I_1 \ddot{w}_0 = 0 \quad (58)$$

No assumptions will be made about the material properties until the equations for the piezoceramic material are incorporated. Therefore, the natural and geometric boundary conditions which are derived from Hamilton's Principle are along the X - Axis:

$$M_x \delta w_{0,x} \Big|_0^a = 0 \quad (59)$$

$$(M_{x,x} + 2M_{xy,y} - I_3 \ddot{w}_{0,x}) \delta w_0 \Big|_0^a = 0, \quad (60)$$

along the Y - Axis:

$$(M_y) \delta w_{0,y} \Big|_{-b/2}^{b/2} = 0 \quad (61)$$

$$(M_{y,y} + 2M_{xy,x} - I_3 \ddot{w}_{0,y}) \delta w_0 \Big|_{-b/2}^{b/2} = 0 , \quad (62)$$

and at the corners:

$$2M_{xy} \delta w_0 \Big|_{0-b/2}^{a \ b/2} = 0 \quad (63)$$

In order to complete the development, the strain-displacement expressions and the moment resultants need to be substituted into the above equations. Also, the material constant I_3 is much smaller than the other constants in the equations of motion and boundary conditions by at least four orders of magnitude. Therefore, this constant can be neglected in the above equations. Finally, in order to simulate a solar array structure attached to a satellite, the boundary condition which approximates the physical conditions is a fixed-free condition in the x-axis and free-free condition in the y-axis. This is a satisfactory boundary condition in order to control the relative motion of the solar array with respect to the satellite bus. Both the displacement w_0 and the slope of the displacement $w_{0,x}$ are specified at the fixed end at ($x=0$), and the variation of these variables are also set equal to zero. For the free ends in the x-axis and y-axis, the displacement and slope cannot be specified so they are not necessarily zero. The shear and moments are zero. These equations can now be rewritten into their final form in terms of the unknown variables, material constants and proper boundary conditions. The partial differential equation is defined as:

$$\begin{aligned}
& D_{11}w_{0'xxx} + 2(D_{12} + 2D_{66})w_{0'xyy} + 4D_{16}w_{0'xxy} \\
& + D_{22}w_{0'yyy} + 4D_{26}w_{0'xyy} + I_1\ddot{w}_0 = 0
\end{aligned} \tag{64}$$

The natural and geometric boundary conditions become along the X - Axis,

at $X = 0$:

$$\delta w_{0'x}(0) = 0 \Rightarrow w_{0'x}(0) = 0 \tag{65}$$

$$\delta w_0(0) = 0 \Rightarrow w_0(0) = 0 \tag{66}$$

at $X = a$:

$$D_{11}w_{0'xx}(a) + D_{12}w_{0'yy}(a) + 2D_{16}w_{0'xy}(a) = 0 \tag{67}$$

$$\begin{aligned}
& D_{11}w_{0'xxx}(a) + (D_{12} + 4D_{66})w_{0'xyy}(a) \\
& + 4D_{16}w_{0'xxy}(a) + 2D_{26}w_{0'yyy}(a) = 0
\end{aligned} \tag{68}$$

and along the Y - Axis,

at $Y = -b/2$:

$$D_{12}w_{0'xx}(-b/2) + D_{22}w_{0'yy}(-b/2) + 2D_{26}w_{0'xy}(-b/2) = 0 \tag{69}$$

$$\begin{aligned}
& (D_{12} + 4D_{26})w_{0'xy}(-b/2) + D_{22}w_{0'yyy}(-b/2) \\
& + 2D_{16}w_{0'xxx}(-b/2) + 4D_{66}w_{0'xyy}(-b/2) = 0
\end{aligned} \tag{70}$$

at $Y = b/2$:

$$D_{12}w_{0,xx}(b/2) + D_{22}w_{0,yy}(b/2) + 2D_{26}w_{0,xy}(b/2) = 0 \quad (71)$$

$$\begin{aligned} (D_{12} + 4D_{26})w_{0,xy}(b/2) + D_{22}w_{0,yy}(b/2) \\ + 2D_{16}w_{0,xx}(b/2) + 4D_{66}w_{0,xy}(b/2) = 0 \end{aligned} \quad (72)$$

and at the Corners for $X = 0$ and $Y = -b/2$:

$$\delta w_0(0, -b/2) = 0 \Rightarrow w_0(0, -b/2) = 0 \quad (73)$$

for $X = 0$ and $Y = b/2$:

$$\delta w_0(0, b/2) = 0 \Rightarrow w_0(0, b/2) = 0 \quad (74)$$

for $X = a$ and $Y = -b/2$:

$$\begin{aligned} D_{16}w_{0,xx}(a, -b/2) + D_{26}w_{0,yy}(a, -b/2) \\ + 2D_{66}w_{0,xy}(a, -b/2) = 0 \end{aligned} \quad (75)$$

for $X = a$ and $Y = b/2$:

$$\begin{aligned} D_{16}w_{0,xx}(a, b/2) + D_{26}w_{0,yy}(a, b/2) \\ + 2D_{66}w_{0,xy}(a, b/2) = 0 \end{aligned} \quad (76)$$

Active Control Derivation

The equations of motion for the composite plate and the equations governing the active control elements will now be combined to form the complete set of equations that describe the structure. Figure 11 outlines how the active control elements are incorporated into the structural equations of motion. The structural equations of motion are combined with

the active control system by adjoining the equations of motions with the sensor and actuator dynamic model equations. The performance index and the constraint equations are formulated when the closed loop control equations are formulated from the combined state space model.

The active control elements, piezoceramic actuators and sensors, will be placed opposite one another through the thickness of the plate and will be wired such that for a given voltage, the actuator will either expand or contract producing a bending moment at the actuator location. They will primarily be used to control the bending and coupled torsion - bending modes of vibration. The equations for the bending force produced from the piezoceramic are now stated. (See [8], [39] - [45].) These equations were originally derived for a beam. They are applicable in this case due to the dimensions and directions of the capacitance of the actuators and sensors. When an electrical charge is applied through the piezoceramics, they will either expand or contract. The piezoelectric coefficient is significantly greater along the length of the actuators and sensors than the width. Therefore, they will produce predominately a pure bending moment along the length of the actuator. These equations will be derived for the actuators attached on the top and sensors attached to the bottom of a structure. (See figure 12.) Some assumptions made in deriving these expressions are:

1. A perfect bond between the actuator and sensor and the structure.
2. The actuator's and sensor's mass do not contribute to the structure.
3. The capacitances of the sensor's leads are negligible.

Considering a structure with no external moments and actuators mounted either on the top or

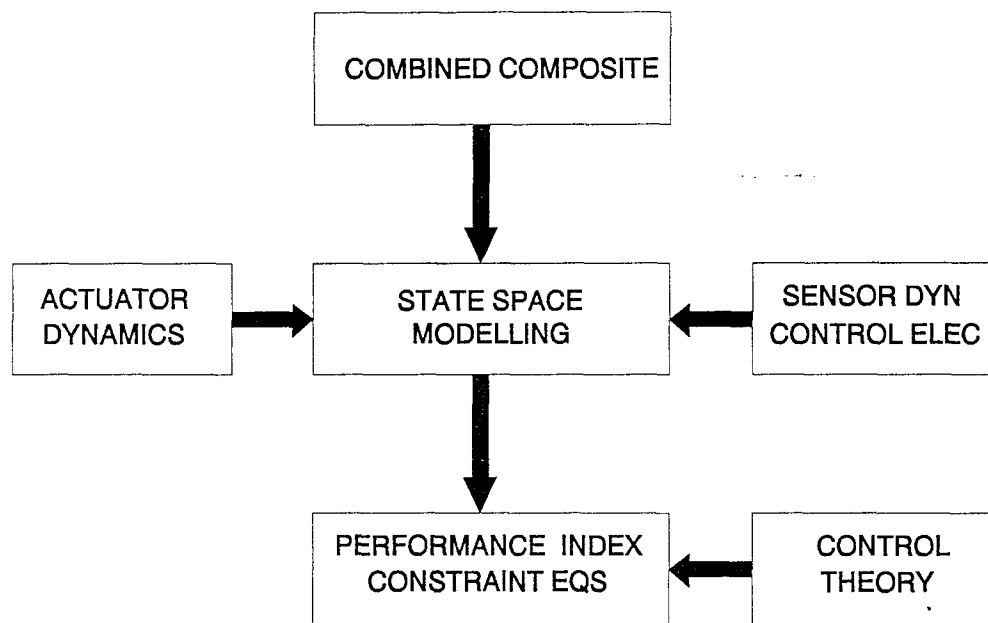


Figure 11 Combining Equations Of Motion with Control Theory

ATTACHMENT OF SENSOR AND ACTUATOR TO COMPOSITE

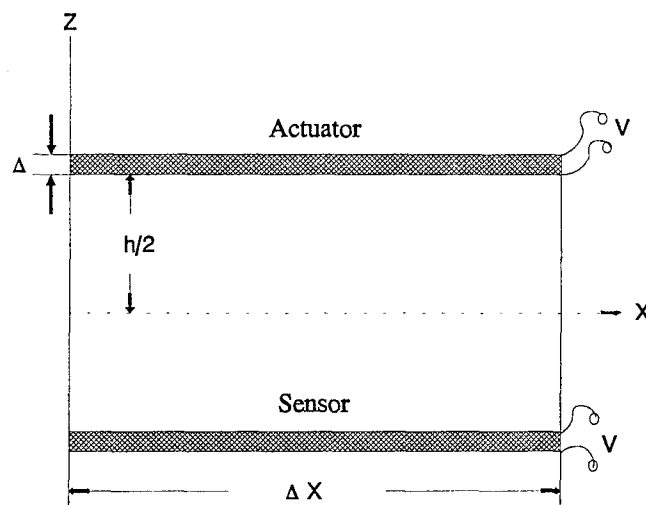


Figure 12 Actuator and Sensor Attached to Structure

bottom, the expression for the displacement caused by these actuators can be expressed as (see [39] - [45]):

$$w = \frac{K_D V_D x^2}{EI} \quad (77)$$

where K_D is the piezoceramic actuator coefficient and V_D is an applied DC voltage. This is similar to the expression when the structure has no actuators present and is acted upon by a point moment, M_0 :

$$w = \frac{M_0 x^2}{2EI} \quad (78)$$

Therefore, the piezoelectric actuators produce an equivalent point or concentrated moment proportional to the applied voltage. As stated previously, the above derivation was conducted for beams. Since the actuators and sensors only cover a small portion of the length and width of the plate, the moment produced and the strain sensed will be at the attachment point. This attachment point is assumed to be located at the center of both the piezoelectric actuator and sensor.

A similar expression is stated for the piezoelectric sensors which work opposite to that of the actuators. Instead of producing a strain from an applied voltage, the sensors produce a current from an applied strain rate. The results of these sensor equations found in references [39] - [45] are:

$$V_{0_k}(t) = K_s \int_{x_{k-1}}^{x_k} z \frac{\partial^2 \dot{w}}{\partial x^2}(x,t) dx, \quad k = 1, 2, \dots, N \quad (79)$$

After integrating, this equation becomes:

$$V_{0,k}(t) = K_s z \frac{\partial w}{\partial x}(x,t) \Big|_{x_{k-1}}^{x_k}, \quad k = 1, 2, \dots, N \quad (80)$$

where:

$$K_s = w_d \frac{h}{2} d_{31} c_{11}^E R_F \quad (81)$$

and

$V_{0,k}$	=	Measured voltage from the kth sensor
w_d	=	sensor width
$h/2$	=	one half plate thickness
N	=	number of sensor and actuator pairs
d_{31}	=	piezoelectric constant
c_{11}^E	=	elastic modulus of the sensor material
x_{k-1}	=	beginning point of kth sensor
x_k	=	endpoint of the kth sensor
R_F	=	resistor associated with an ideal operational amplifier used to acquire the signal

In this research, $N=2$, two actuator and sensor pairs will be used and their locations and control gains will be optimization parameters.

Discretization of the Equations of Motion

The equations of motion for the entire plate including the active control system will

now be reduced to ordinary differential equations with respect to time to formulate the closed loop state space equations based upon the control theory used. From these closed loop state space equations, the performance index and constraint equations are developed. This can be done by determining the approximate solution to the spatial dependence and integrating this solution over the volume of the plate leaving only an ordinary differential equation with respect to time. An assumption concerning the above equations must be made to simplify the expressions. This assumption is that the spatial dependence can be separated in the x and y directions and from the time dependence terms in the equations of motion. This assumption is hard to prove since it assumes that synchronous motion occurs from which orthogonality is shown. Taking into account these assumptions, the x and y spatial coordinates and the time dependence are separated and an approximate method such as the assumed-modes, Rayleigh-Ritz method (see [33], [35], [36], [46] - [49]) or Galerkin (see [33], [35], [36], [46], [47], [49]) is used to solve the equations of motion. A typical Rayleigh-Ritz approximate solution for this application is:

$$w_0(x,y,t) = \sum_{i=1}^N \sum_{j=1}^M A_{ij} \psi(t) X(x)_i Y(y)_j \quad (82)$$

Notice the spatial and temporal dependencies are separated. This approximate spatial relationship or admissible function is assumed to satisfy only the geometric boundary conditions. For this research with the above boundary conditions (eqs 65-76), fixed-free along the X-axis and free-free along the Y-axis, geometric boundary conditions are present only where the plate is fixed in the X-axis direction. The spatial properties or geometric boundary conditions for the X-axis are satisfied by the admissible function [33], [49], [50]:

$$X_m(x) = 1 - \cos\left[\frac{m\pi x}{2a}\right] \quad m = 1,2,3,4,\dots \quad (83)$$

For the Y-axis, the function used is a comparison function for the flexible motion of a beam made out of an isotropic material with free-free boundary conditions [33], [50]. This can be derived from assuming motion is the sum of four trigonometric functions: cos, sin, cosh, and sinh.

$$Y = c_1 \sin \frac{\lambda y}{b} + c_2 \cos \frac{\lambda y}{b} + c_3 \sinh \frac{\lambda y}{b} + c_4 \cosh \frac{\lambda y}{b} \quad (84)$$

where

c_1, c_2, c_3, c_4

constants derived from the boundary conditions

λ

solution to the characteristic equation

Substituting the above expression into the boundary conditions for free-free which are:

$$\begin{aligned} \frac{\partial^2 Y}{\partial y^2}(0) &= \frac{\partial^3 Y}{\partial y^3}(0) = 0 \\ \frac{\partial^2 Y}{\partial y^2}(b) &= \frac{\partial^3 Y}{\partial y^3}(b) = 0 \end{aligned} \quad (85)$$

yields the following four expressions:

$$\frac{\lambda^2}{b^2}(-c_2 + c_4) = 0 \Rightarrow c_2 = c_4 \quad (86)$$

$$\frac{\lambda^3}{b^3}(-c_1 + c_3) = 0 \Rightarrow c_1 = c_3 \quad (87)$$

$$\frac{\lambda^2}{b^2}(-c_1 \sin \lambda - c_2 \cos \lambda + c_1 \sinh \lambda + c_2 \cosh \lambda) = 0 \quad (88)$$

$$\frac{\lambda^3}{b^3}(-c_1 \cos \lambda + c_2 \sin \lambda + c_1 \cosh \lambda + c_2 \sinh \lambda) = 0 \quad (89)$$

Solving equations (88, 89), assuming λ doesn't equal 0 which would be the trivial solution, one obtains:

$$\cos \lambda \cosh \lambda = 1 \quad \lambda = 4.73, 7.8532, 10.996, 14.137, \dots \quad (90)$$

and

$$c_1 = -\frac{[\cosh \lambda - \cos \lambda]}{[\sinh \lambda - \sin \lambda]} c_2 \quad (91)$$

Using the above equations, the expression for the flexible motion of a beam made out of an isotropic material with free-free boundary conditions is:

$$Y = \cosh\left[\frac{\lambda y}{b}\right] + \cos\left[\frac{\lambda y}{b}\right] - \frac{(\cosh[\lambda] - \cos[\lambda])}{(\sinh[\lambda] - \sin[\lambda])} \left(\sinh\left[\frac{\lambda y}{b}\right] + \sin\left[\frac{\lambda y}{b}\right]\right) \quad (92)$$

However, additional terms are needed since the assumed comparison function modeled only the flexible motion of the beam and the rigid body motion of the beam in the Y-axis also needs to be taken into account. These additional terms capture the rigid body motion of the plate in the Y-axis while the plate in the X-axis is undergoing flexible body motion. Also in

order to simplify the equations, the coordinate system for the Y-axis was shifted from the center of the plate to one end. This shift occurred over a distance of $b/2$ or half the width of the plate. (See figure 13 for the new coordinate system.)

$$\begin{aligned}
 Y_1 &= 1 \\
 Y_2 &= 1 - \frac{2y}{b} \\
 Y_n(y) &= \cosh\left[\frac{\lambda_{(n-2)}y}{b}\right] + \cos\left[-\frac{\lambda_{(n-2)}y}{b}\right] \\
 &- \frac{(\cosh[\lambda_{(n-2)}] - \cos[\lambda_{(n-2)}])}{(\sinh[\lambda_{(n-2)}] - \sin[\lambda_{(n-2)}])} \left(\sinh\left[\frac{\lambda_{(n-2)}y}{b}\right] + \sin\left[\frac{\lambda_{(n-2)}y}{b}\right]\right) \quad n = 3, 4, \dots
 \end{aligned} \tag{93}$$

where λ_n is a solution to the characteristic equation given in equation (90). The approximate periodic solution is a combination of both solutions and $\psi(t) = \sin[pt]$:

$$w_0(x, y, t) = \sum_{i=1}^m \sum_{j=1}^n A_{ij} X_i Y_j \sin[pt] \tag{94}$$

using a finite number of terms for X and Y (in this case 2 terms each):

$$\begin{aligned}
 w_0(x, y, t) &= [A_{11}(1 - \cos\frac{\pi x}{2a}) + A_{12}(1 - \cos\frac{\pi x}{2a})(1 - \frac{2y}{b}) \\
 &+ A_{21}(1 - \cos\frac{\pi x}{a}) + A_{22}(1 - \cos\frac{\pi x}{a})(1 - \frac{2y}{b})] \sin pt
 \end{aligned} \tag{95}$$

and:

$$p = \text{Modal frequency}$$

Following the Rayleigh-Ritz approach, this approximation is then substituted into the following expression for kinetic and potential energy from which the equations of motion for the undamped, unforced plate were derived to determine the frequencies and mode shapes of the plate:

PLATE LOCAL COORDINATE SYSTEM

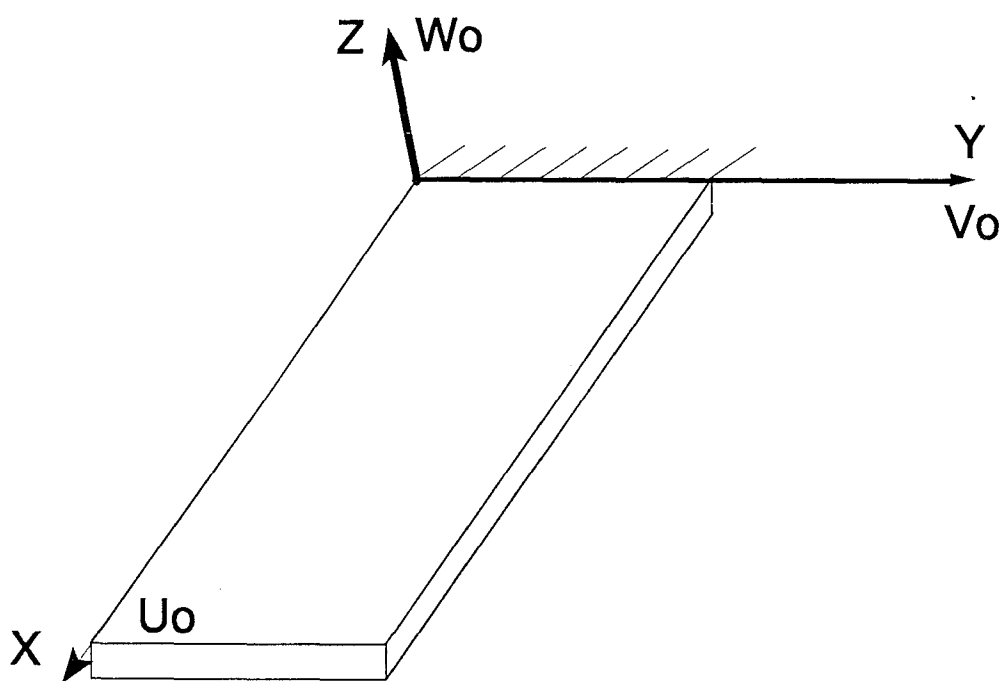


Figure 13 New Plate Coordinate System

$$V_{\max} - T_{\max} = 0 \quad (96)$$

where:

$$T_{\max} = \max_t \left(\frac{1}{2} \int_0^b \int_0^a [I_3 \dot{w}_{0,x}^2 + I_3 \dot{w}_{0,y}^2 + I_1 \dot{w}_0^2] dx dy \right) \quad (97)$$

$$V_{\max} = \max_t \int_0^b \int_0^a \int_{-\frac{h}{2}}^{\frac{h}{2}} (\sigma_x \epsilon_x + \sigma_y \epsilon_y + \tau_{xy} \gamma_{xy}) dz dx dy \quad (98)$$

$$= \max_t \int_0^b \int_0^a \frac{1}{2} [M_x w_{0,xx} + M_y w_{0,yy} + 2M_{xy} w_{0,xy}] dx dy$$

These are used to solve for the constants, A_{ij} , and the frequencies of the approximate solution.

After the integrations with respect to x , y , and z are completed and the numerical values are substituted in for the constants found in figure 10, the expressions for the potential and kinetic energies become:

$$T_{\max} = p^2 \rho [.54A_{11}^2 + .18A_{12}^2 + 2.8A_{11}A_{21} + 3.6A_{21}^2 + 1.2A_{22}^2] \quad (99)$$

$$\begin{aligned} V_{\max} = & .00044A_{11}^2 D_{11} + .00015A_{12}^2 D_{11} + .0015A_{11}A_{21}D_{11} \\ & + .0071A_{21}^2 D_{11} + .0005A_{12}A_{22}D_{11} + .0023A_{22}^2 D_{11} \\ & - .0086A_{11}A_{12}D_{16} + .023A_{12}A_{21}D_{16} - .023A_{11}A_{22}D_{16} \\ & + .10A_{12}^2 D_{66} + .35A_{12}A_{22}D_{66} + .41A_{22}^2 D_{66} \end{aligned} \quad (100)$$

The derivative of the above equation is taken with respect to the constants A_{ij} and each is set

equal to zero. This is used [36] to calculate the constants A_{ij} from which the eigenvector can be determined. This forms four separate equations in terms of the unknown A_{ij} and frequencies. These four equations are combined into a matrix/vector equation in order to solve for the constants and frequencies. The constants and frequencies are then found by solving the equations simultaneously.

The method that is used in this research is evaluated by differentiating each term separately and formulating the following equation:

$$\begin{Bmatrix} \frac{\partial V_{\max}}{\partial A_{11}} \\ \frac{\partial V_{\max}}{\partial A_{12}} \\ \frac{\partial V_{\max}}{\partial A_{21}} \\ \frac{\partial V_{\max}}{\partial A_{22}} \end{Bmatrix} - \begin{Bmatrix} \frac{\partial T_{\max}}{\partial A_{11}} \\ \frac{\partial T_{\max}}{\partial A_{12}} \\ \frac{\partial T_{\max}}{\partial A_{21}} \\ \frac{\partial T_{\max}}{\partial A_{22}} \end{Bmatrix} = 0 \quad (101)$$

Each term can be represented as a matrix multiplication using the symbols K and M for the stiffness and mass matrices respectively.

$$\begin{Bmatrix} \frac{\partial V_{\max}}{\partial A_{11}} \\ \frac{\partial V_{\max}}{\partial A_{12}} \\ \frac{\partial V_{\max}}{\partial A_{21}} \\ \frac{\partial V_{\max}}{\partial A_{22}} \end{Bmatrix} = [K] \begin{Bmatrix} A_{11} \\ A_{12} \\ A_{21} \\ A_{22} \end{Bmatrix} \quad (102)$$

$$\begin{Bmatrix} \frac{\partial T_{\max}}{\partial A_{11}} \\ \frac{\partial T_{\max}}{\partial A_{12}} \\ \frac{\partial T_{\max}}{\partial A_{21}} \\ \frac{\partial T_{\max}}{\partial A_{22}} \end{Bmatrix} = p^2 [M] \begin{Bmatrix} A_{11} \\ A_{12} \\ A_{21} \\ A_{22} \end{Bmatrix} \quad (103)$$

where

$$[K] = \begin{bmatrix} .00088D_{11} & -.0086D_{16} & .0015D_{11} & -.023D_{16} \\ -.0086D_{16} & .00029D_{11}+.21D_{66} & .023D_{16} & .0005D_{11}+.35DD_{66} \\ .0015D_{11} & .023D_{16} & .014D_{11} & 0 \\ -.023D_{16} & .0005D_{11}+.35D_{66} & 0 & .0047D_{11}+.82D_{66} \end{bmatrix} \quad (104)$$

and

$$[M] = \rho \begin{bmatrix} 1.1 & 0 & 2.76 & 0 \\ 0 & .36 & 0 & .92 \\ 2.76 & 0 & 7.2 & 0 \\ 0 & .92 & 0 & 2.4 \end{bmatrix} \quad (105)$$

Substituting these expressions into the above equation, one obtains the following equation:

$$[K] \begin{Bmatrix} A_{11} \\ A_{12} \\ A_{21} \\ A_{22} \end{Bmatrix} = p^2 [M] \begin{Bmatrix} A_{11} \\ A_{12} \\ A_{21} \\ A_{22} \end{Bmatrix} \quad (106)$$

The frequencies and constants A_{ij} are found by solving the generalized eigenvalue problem for the above equation. The frequencies squared are the eigenvalues and the constants A_{ij} are the

eigenvectors.

As a check to see if the selected approximate solution models the plate sufficiently, the numerical frequencies and mode shapes were found by using typical realistic material constants and various ply layups. For this check, typical composite parameters were substituted for the composite properties. (See Table 1.)

TABLE 1 TYPICAL COMPOSITE PROPERTIES

Composite Parameter	Value
E_1	137.25 GPa
E_2	11.42 GPa
G_{12}	6.39 GPa
ν_{12}	0.3
ν_{21}	0.025
ρ	.043

These results for the four-mode approximation (2 "x" terms and 2 "y" terms) also compare, at least in first bending, to the one-mode approximation. The frequencies for the one-mode approximation are now calculated for the following four test case ply layups: 1. $[0/90/\pm 45/0]_s$, 2. $[0/\pm 45_2]_s$, 3. $[\pm 45_5]_s$, 4. $[+30_5]_s$ and shown in table 2. They differ by between 1-3% for all four cases. Since the Rayleigh-Ritz solution is an upper bound, the frequencies should decrease for the more accurate four-mode approximation.

TABLE 2 FREQUENCIES FOR THE TEST CASES FOR THE ONE MODE
APPROXIMATION

Case #	Frequency (Hz)
1	1.3857
2	1.03544
3	1.46278
4	1.0116

These are the frequencies for the first bending mode of the structure. The frequencies and associated mode shapes are now calculated for the four-mode approximate solution for the above test cases and shown in table 3.

TABLE 3 FREQUENCIES AND MODE SHAPES FOR THE TEST CASES FOR THE
FOUR MODE APPROXIMATION

Case #	Frequency (Hz)	Mode Shape
1	1.3416	1st bending
	11.207	1st torsion
	12.45	2nd bending
	49.11	2nd torsion
2	1.00831	1st bending
	9.2879	1st torsion
	18.745	2nd bending
	81.138	2nd torsion
3	1.41583	1st bending
	12.9074	1st torsion

	14.7732	2nd bending
	63.697	2nd torsion
4	1.00395	1st bending
	7.535	1st torsion
	17.67	2nd bending
	73.43	2nd torsion

The mode shapes are what one would have expected for a plate geometry. However, it is difficult to prove this, because there is no known solution for this problem and no one has modelled this particular plate before. Other people have modelled plates with fixed-free end conditions before, but one was not found for these particular ply layups and plate dimensions [9], [33], [50], [51]. For a plate structure which is very long in one direction and very thin, one would expect the low frequency mode shapes to be in the dominant direction. Also with the purposeful ply angle selection to enhance the bending/torsion coupling, one would also expect the combined bending/torsional mode shape to appear in the first few modes of vibration. Furthermore, the frequency changes among the different test cases (ply angles) make sense. The more rigid the plate is in torsion, the more the frequency for that particular mode will increase. Also if there are 0 degree plies in the layup, the frequencies for the bending modes will increase due to the increased longitudinal stiffness of the plate. Based upon the calculated frequencies and mode shapes, it is assumed that the approximate solution models the plate sufficiently for this research. As a final check, the frequencies of a nine-mode approximation (3 "x" terms and 3 "y" terms) are solved numerically for case number 1. These results are compared with the one and four mode approximations for case 1. The frequencies for all modes are presented in table 4.

TABLE 4 TEST CASE 1 FREQUENCIES FOR THE NINE MODE APPROXIMATION

Mode Number	Frequency (Hz)
1	1.31765
2	8.736
3	10.812
4	34.25
5	49.838
6	102.59
7	320.36
8	327.5
9	365.94

Table 5 shows the comparison of the first four modal frequencies for the one, four, and nine mode approximations.

TABLE 5 TEST CASE 1 FREQUENCIES FOR THE ONE, FOUR, AND NINE MODE
APPROXIMATION

Mode Shape	One Mode	Four Mode	Nine Mode	Percent Difference 4 vs 9 Mode
1st Bending	1.3857	1.3416	1.31765	1.8%
2nd Bending	X	11.207	8.736	22%
1st Torsion	X	12.45	10.812	13.2%
2nd Torsion	X	49.11	34.25	30%

As one can see, the frequencies for the nine mode approximation are lower than both the one and four mode approximation. The frequencies for the four mode approximation vary from the nine mode approximation by 2-30%. Clearly, the nine mode approximation would be a better solution to use, but a symbolic solution was never calculated due to the limitation of the computer workstations. It is assumed that the four mode approximation is sufficient for this research. Also in Chapter VI, this approximation will be compared to experimental results and the referenced paper by Hwang [25] which used a finite element method. These comparisons will show that this approximate solution models the plate sufficiently.

The Rayleigh-Ritz solution using generalized time functions, versus periodic expressions for time, for the modal amplitudes can now be formulated using the approximate solution. The dimensions of the plate are substituted into the appropriate equations prior to the formulation. This solution is:

$$w_0(x,y,t) = w(x,y)_1\psi_1(t) + w(x,y)_2\psi_2(t) + w(x,y)_3\psi_3(t) + w(x,y)_4\psi_4(t) \quad (107)$$

where:

$$w(x,y)_i = A_{11i}X_1Y_1 + A_{12i}X_1Y_2 + A_{21i}X_2Y_1 + A_{22i}X_2Y_2 \quad (108)$$

and:

$$X_m = (1 - \cos \frac{m\pi x}{48}) \quad m = 1, 2 \quad (109)$$

$$Y_1 = 1 \quad (110)$$

$$Y_2 = (1 - \frac{y}{2}) \quad (111)$$

In the above equations, the numerical plate dimensions were used versus the symbols, a and b. The constants A_{ij} vary for each spatial solution, $w(x,y)_i$. These assumed modes, $w_0(x,y,t)$, can not be substituted directly back into the equations of motion because not all of the boundary conditions are satisfied. Only the geometric boundary conditions are satisfied. (Note that an admissible function versus a comparison function was used in the Rayleigh-Ritz approximation so only the geometric boundary conditions should be satisfied.) If we use only the equations of motion, then we completely ignore the natural boundary conditions. The assumed modes are then substituted into the expressions for potential and kinetic energies and the spatial dependence is integrated out. To generate the new equations of motion we can use either Hamilton's Principle with the $\psi_i(t)$'s as independent variables or the Lagrange equation, since we are dealing with conservative forces and motions in nature. For ease of use to generate the new equations of motion and the ability to incorporate external forces, the Lagrange equation is chosen. The Lagrange equation will generate four equations of motion for each of the

independent variables.

$$\frac{d}{dt} \left(\frac{\partial T}{\partial \dot{\Psi}_i(t)} \right) - \frac{\partial T}{\partial \Psi_i(t)} + \frac{\partial V}{\partial \Psi_i(t)} = Q_i \quad i = 1,2,3,4 \quad (112)$$

The complete equation of motion for the plate is formed by combining the four equations of motion into a matrix equation:

$$[M]\ddot{\Psi}(t) + [K]\Psi(t) = Q \quad (113)$$

where M and K are given in equation (102) and (103)

$$\Psi(t) = \{\psi(t)_i\} \quad (114)$$

and $\psi(t)$ represents the time dependent modal amplitudes of the approximated solution. The next step is transforming this set of ordinary differential equations into a state space representation. This is done in the next section in conjunction with adjoining the control system dynamics to the flexible body equations of motion.

Control Theory and Optimization

In this section the equations of motion from the previous section are transformed from a second-order ordinary differential equation into a state space format that is a first order ordinary differential equation and then incorporated into a control theory for the active control system. A performance index and constraint equations which formulate the optimization problem are then determined by using the state space equations.

Control Theory. The control theory used in this research is output feedback from collocated sensors and actuators. Collocated is defined as occupying the same location on the

plate along the X-axis and Y-axis. The sensors and actuators can be located on opposite sides of the plate and still be collocated. Output feedback is defined as taking the signal obtained by a sensor, multiplying the signal by a gain and transmitting it to a control actuator to produce a force which could be a moment. This sensor senses the strain rate of the plate. An active control electronic filter is sometimes needed to process the output signal that comes from the sensors and is converted into a high voltage control signal that is provided to the actuators. This filter is used only to eliminate any high frequency noise which is also detected by the sensor. A standard active control feedback filter used with piezoceramic sensors and actuators consists of a preamplifier, a bandpass filter, a phase shifting circuit, and a high voltage output amplifier. A filter was needed and the center frequency was set to the torsional frequency of the plate. From the definition of direct output feedback, one sensor controls only one actuator.

The actuator moments and disturbance torques are added to the equations of motion now by equating the individual equations of motion resulting from LaGrange's equation to a work term.

$$\frac{d}{dt} \left(\frac{\partial T}{\partial \dot{\Psi}_i(t)} \right) - \frac{\partial T}{\partial \Psi_i(t)} + \frac{\partial V}{\partial \Psi_i(t)} = Q_i \quad i = 1,2,3,4 \quad (115)$$

where:

$$Q_i = \sum_{k=1}^N \vec{F}_k \cdot \frac{\partial \vec{r}_k}{\partial \Psi_i(t)} \Big|_{act} + \vec{F}_j \cdot \frac{\partial \vec{r}_j}{\partial \Psi_i(t)} \Big|_{disturbance} \quad (116)$$

The force, \vec{F}_k , in the above equation is the point actuator moment applied anywhere on the structure where the actuator sensor pair is located. The force, \vec{F}_j , in the above equation is the

disturbance torque applied to the structure. Since the force is treated as a moment, the vector \vec{r}_j is the vector whose magnitude is the angle over which the moment acts. For the actuators, the vector \vec{r}_k is the vector whose magnitude is the angle or X-axis rotation of the plate where the actuator is located at $x = x_{A,k}$ and $y = y_{A,k}$. This is modelled as:

$$\vec{F}_k \cdot \frac{\partial \vec{r}_k}{\partial \psi_i} \Big|_{act} = M_{A_k} \frac{\partial \left(\frac{\partial w}{\partial x} \right)}{\partial \psi_i} \Big|_{x = x_{A_k}, y = y_{A_k}} \quad (117)$$

$$M_{A_k} = K_{D_k} V_{D_k} \quad (118)$$

The disturbance torque is applied to the free end of the plate producing a twisting of the plate. Again, since the force, \vec{F}_j , is a torque, the vector \vec{r}_j is the vector whose magnitude is the angle over which the moment acts. This is modelled as:

$$\vec{F}_j \cdot \frac{\partial \vec{r}_j}{\partial \psi_i} \Big|_{disturbance} = d \frac{\partial \left(\frac{\partial w}{\partial y} \right)}{\partial \psi_i} \Big|_{x = x_D, y = y_D} \quad (119)$$

where d is the disturbance torque amplitude and $x_D = a$ and $y_D = b/2$. The vector \vec{r}_j , in this case, is the vector whose magnitude is the angle or Y-axis rotation of the plate.

Before reducing the ordinary differential equations to state space equations the above actuator and disturbance models are incorporated into the model.

$$[M]\ddot{\Psi} + [K]\Psi = \left[\sum_{k=1}^N K_{D_k} V_{D_k} \frac{\partial \left(\frac{\partial w}{\partial x} \right)}{\partial \psi} \Big|_{x = x_{A_k}, y = y_{A_k}} + d \frac{\partial \left(\frac{\partial w}{\partial y} \right)}{\partial \psi} \Big|_{x = x_D, y = y_D} \right] \quad (120)$$

The sensor equation makes up the last part of the state space transformation. This equation is:

$$V_{s_k}(t) = K_{s_k} z \frac{\partial \dot{w}}{\partial x}(x, t) \Big|_{x_{k-1}}^{x_k} = \left[K_{s_k} z \frac{\partial \left(\frac{\partial w}{\partial x} \right)}{\partial \dot{\psi}_i} \Big|_{x_{k-1}}^{x_k} \right] \{\dot{\psi}\} \quad (121)$$

where x_k is the end point and x_{k-1} is the beginning point of the sensor corresponding to the actuator location. The second order equation of motion is rewritten as:

$$\ddot{\psi} = -[M]^{-1}[K]\psi + [M]^{-1}[b] [V_{D_k}] + [M]^{-1} \left[\frac{\partial \left(\frac{\partial w}{\partial y} \right)}{\partial \psi} \Big|_{x=x_D, y=y_D} \right] d \quad (122)$$

where

$$[V_{D_k}] = \begin{Bmatrix} V_{D_1} \\ V_{D_2} \end{Bmatrix} \quad (123)$$

is a vector of the control voltages and the ik_{th} element of $[b]$ is:

$$b_{ik} = K_{D_k} \frac{\partial \left(\frac{\partial w}{\partial x} \right)}{\partial \dot{\psi}_i} \Big|_{x=x_{A_k}, y=y_{A_k}} \quad (124)$$

The state variable q is related to the physical variables with:

$$q = \begin{Bmatrix} \psi \\ \dot{\psi} \end{Bmatrix} \quad (125)$$

$$\dot{q} = \begin{Bmatrix} \dot{\psi} \\ \ddot{\psi} \end{Bmatrix} \quad (126)$$

The second order differential equation can now be rewritten in first order state space notation in which the vector q represents the assumed modal displacements and first derivatives. The first order state space notation is given by:

$$\dot{q} = [A]q + [B]u + [H]d \quad (127)$$

$$y = [C]q \quad (128)$$

where:

$$A = \begin{bmatrix} 0 & I \\ -[M]^{-1}[K] & 0 \end{bmatrix} \quad (129)$$

$$B = \begin{bmatrix} 0 \\ [M]^{-1}[b] \end{bmatrix} \quad (130)$$

$$H = \begin{bmatrix} 0 \\ [M]^{-1} \left[\frac{\partial \left(\frac{\partial w}{\partial y} \right)}{\partial \psi} \right]_{x=x_D, y=y_D} \end{bmatrix} \quad (131)$$

$$C = [0 \quad [c]] \quad (132)$$

where the k_i th element of $[c]$ is:

$$c_{ki} = K_{s_k} z_{s_k} \frac{\partial \left(\frac{\partial w}{\partial x} \right)_{x_k}}{\partial \psi_i} \bigg|_{x_{k-1}} \quad (133)$$

and:

- [A] = Plant matrix determined from the stiffness matrix and the inverse of the mass matrix
- [B] = Control matrix determined from the actuator coupling coefficients, location matrix and the inverse of the mass matrix
- u = $[V_{d,k}]$, Control input vector which is the actuator voltages at specific locations
- y = Sensor voltage signal (strain rate of the plate) collocated at actuator position
- [C] = Sensor matrix determined from the sensor and dynamic coupling coefficients
- [H] = Disturbance matrix determined from the disturbance location matrix and the inverse of the mass matrix
- d = Torsional disturbance amplitude at free end of plate

In output feedback, the control vector u (voltages sent to the actuator) is proportional to the output sensor vector y (strain rate of the plate) by a gain multiplier.

$$u = -[G]y \quad (134)$$

where:

$$[G] = \text{constant control gains}$$

Substituting equation (128) into the expression for y , one obtains:

$$u = -[G][C]q \quad (135)$$

Substituting the above equation into the state-space relationship, the closed loop state-space equation can now be derived.

$$\dot{q} = [A]q - [B][G][C]q + [H]d \quad (136)$$

$$\dot{q} = [A_{cl}]q + [H]d \quad (137)$$

where:

$$[A_{cl}] = [A] - [B][G][C] \quad (138)$$

Performance Index and Sensitivity Equations. The performance index or objective function is a scalar measure that is to be minimized during the structural/control optimization. The primary objective of the active damping system is to minimize the bending and torsional motion of the plate while staying within the actuator voltage constraints. Previous papers that use output feedback as their control system tend to minimize the norm of the output feedback gain matrix [54] which was a function of the structural and control parameters or the expectation of the standard Linear Quadratic Gaussian plus the penalized gain matrix [39]. This research will be similar to the work accomplished by Slater [56] in which he states "the structure-control design is to find the structural parameters and the control law to minimize a performance index while satisfying control energy and displacement constraints." The structural equations of motion are assumed disturbed by a torsional zero mean white Gaussian

noise disturbance with an intensity of D . A white Gaussian noise was chosen as the disturbance to optimize the performance of the plate to a wide range of frequencies versus one set of frequencies as in harmonic motion.

The performance index or objective function J used in this research will be based upon the mean square motion of the free end of the plate $w_{tip}(p_i)$, where the p_i are the structural and control parameters to be optimized, e.g., the ply angle, location of the actuators, and magnitude of the actuator gains. The stiffness of the plate, which reacts against the disturbance force, is determined from the lamina stiffness which depends on the ply angle. Also the coupling parameter is determined directly from the ply angle. Just increasing the ply angle does not cause the coupling parameter to increase as shown by the equations for the lamina stiffness. The coupling parameter will reach a relative maximum for some optimum ply angle.

The determination of this optimum angle is shown next. This will show that there is only one ply angle which maximizes the torsional/bending coupling coefficient, D_{16} . Because the Y-axis approximation used in this research is linear, the D_{26} coefficient is not taken into account when calculating the equations of motion. The D_{26} coefficient is multiplied by the second derivative of the displacement function, $w_0(x,y,t)$, with respect to y when forming the potential energy equation. This expression is zero due to the linear Y-axis displacement function. (See equations 110,111.) The equation for the D_{16} coefficient can be expressed as:

$$D_{16} = \sum_{k=1}^N [\bar{Q}_{16}]_k^* \int_{z_{k-1}}^{z_k} z^2 dz \quad (139)$$

where:

$$\bar{Q}_{16}^* = \bar{Q}_{16} - \frac{\bar{Q}_{12}\bar{Q}_{26}}{\bar{Q}_{22}} \quad (140)$$

and $[\bar{Q}_{ij}]$ given by eqs (14-19). For this problem, the experimentally determined values, with the exception of ν_{21} which is calculated, used for the material properties are:

$$E_1 = 156.45 \text{ GPa}$$

$$E_2 = 9.95 \text{ GPa}$$

$$G_{12} = 5.99 \text{ GPa}$$

$$\nu_{12} = .3056$$

$$\nu_{21} = .01925$$

The angle which optimizes the D_{16} coefficient can be determined by plotting this expression for magnitude D_{16} versus θ or by taking the first derivative of the expression for D_{16} and setting it equal to zero and determining θ . (See Figure 14.) The angle (expressed in radians) which maximizes the D_{16} coefficient is:

$$\theta_{\text{opt}} = .312$$

or expressed in degrees:

$$\theta_{\text{opt}} = 18.0^\circ$$

The objective of the optimization problem in this research was to find the feedback law or gain G , actuator locations and ply angles which minimize J subject to certain constraints which are related to the mean square control energy. The mean square control energy constraint provides an upper limit on the amount of control energy expended since the piezoceramic actuators do have an upper limit. This optimization problem can be stated as:

Minimize:

$$J = \zeta E(w_r w_r^T) + (1 - \zeta) E(w_b w_b^T) \quad (141)$$

MAXIMUM D16 COEFFICIENT

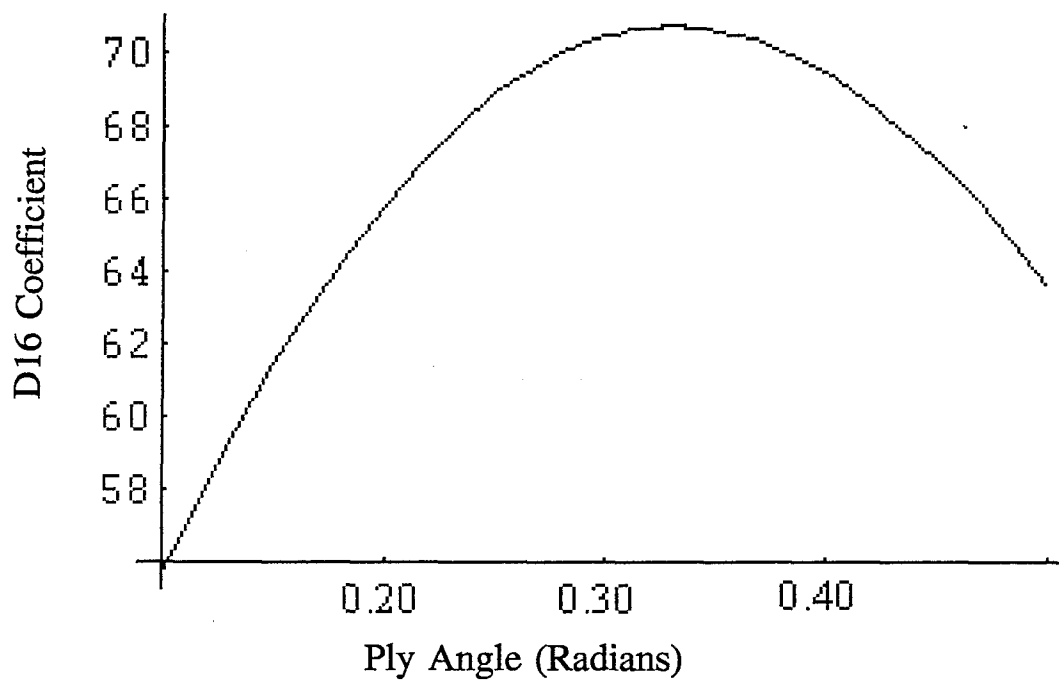


Figure 14 D_{16} Coefficient versus Ply Angle

subject to:

$$E(uu^T) \leq [\Xi] \quad (142)$$

where:

- ζ = Parameter to vary the weight on a torsional versus bending motion
- w_r = Difference of the corner displacement vector and the center displacement vector of the plate tip
- w_b = Center displacement vector of the plate tip
- Ξ = Fixed mean square control energy
- $E(\)$ = Expectation operator
- u = Control vector {actuator voltages}

The performance index and inequality constraints can be converted from statistical notation in terms of the expectation operator to matrix notation using the Lyapunov equation solution of the covariance matrix. The motion of the tip w_r and w_b are determined from multiplying the location matrix by the state response:

$$\begin{aligned} w_r &= [C_r]q \\ w_b &= [C_b]q \end{aligned} \quad (143)$$

For large time behavior the motion can be represented by the steady state covariance of the states:

$$E(qq^T) = Q \quad (144)$$

The steady state covariances can be calculated by solving a Lyapunov equation [56]. Both the performance index and the constraint equations can be rewritten in terms of matrix equations due to the relationship between the mean square response of the states and the covariance matrix Q . The mean square responses of the states will be the diagonals of the covariance matrix Q . Before the Lyapunov equation is solved, the closed loop plant matrix is calculated. The closed loop plant is solved by substituting the output and control expression into the equation of motion. This is represented as:

$$[A_{cl}] = [A] - [B][G][C] \quad (145)$$

The Lyapunov equation [56]:

$$[A_{cl}][Q] + [Q][A_{cl}]^T + [H][D][H]^T = 0 \quad (146)$$

is solved for the covariance matrix Q , where D is the intensity of the white Gaussian noise. For steady state optimization, the performance index and actuator energy constraints can be replaced by their respective covariance relationships. The performance index is rewritten in matrix form by substituting the covariance matrix in for the expected value of the state:

$$\begin{aligned} E(w_r w_r^T) &= E(C_r q q^T C_r^T) \\ &= C_r E(q q^T) C_r^T \\ &= C_r Q C_r^T \end{aligned} \quad (147)$$

$$\begin{aligned} E(w_b w_b^T) &= E(C_b q q^T C_b^T) \\ &= C_b E(q q^T) C_b^T \\ &= C_b Q C_b^T \end{aligned} \quad (148)$$

The constraint equations are rewritten in matrix form by substituting the covariance matrix in for the expected value of the state:

$$\begin{aligned}
 E(u u^T) &= E(GCqq^TC^TG^T) \\
 &= GCE(qq^T)C^TG^T \\
 &= GCQC^TG^T
 \end{aligned} \tag{149}$$

The constraint equations form a two-by-two diagonal matrix whose elements are required to be less than or equal to the total control energy the actuators can produce.

$$GCQC^TG^T = \begin{bmatrix} c_1 & 0 \\ 0 & c_2 \end{bmatrix} \tag{150}$$

The total control energy, Ξ , is also a two-by-two diagonal matrix whose elements are equal and equate to the allowable control energy each actuator can produce.

$$\Xi = \begin{bmatrix} \xi_1 & 0 \\ 0 & \xi_2 \end{bmatrix} \tag{151}$$

The performance index and constraint equation can be finally rewritten as:

minimize

$$J = \zeta[C_r]Q[C_r]^T + (1 - \zeta)[C_b]Q[C_b]^T \tag{152}$$

subject to

$$\begin{aligned}
 c_1 &\leq \xi_1 \\
 c_2 &\leq \xi_2
 \end{aligned} \tag{153}$$

where:

ζ	=	Parameter to vary the weight on a torsional versus bending motion
C_r	=	Location matrix for the difference between the left corner and the center of the plate tip
C_b	=	Location matrix for center of the plate tip
Q	=	Covariance matrix from Lyapunov equation (152)
Ξ	=	Fixed voltage control energy
ξ_1	=	Fixed mean square control energy for actuator one
ξ_2	=	Fixed mean square control energy for actuator two
C	=	Location matrix for sensor output
G	=	Actuator gain matrix

The optimality conditions or sensitivity equations which arise from the optimization are calculated by taking the partial derivative of the performance index and the constraint equations with respect to the parameters to be optimized. These parameters for this performance index are the structural and control parameters p_i which include the actuator locations, and the control gains G . These gradients are calculated numerically by the finite difference method by an optimization program called DOT [55]. The search gradients determine which direction the optimization program proceeds. This will be discussed in the next chapter on optimization.

IV. Optimization Results

A FORTRAN computer optimization program called DOT [55] was used to solve the optimization problem in this research using numerical optimization. Numerical optimization determines the "best" solution using a logical, systematic decision-making procedure. DOT is a computer program created by VMA Engineering for optimization. DOT uses numerical optimization to change the selected parameters based upon the search gradients to either maximize or minimize an objective function nonlinear in the design variables. The main optimization program DOT is coupled with an application program, which determines both the constraints and the objective function, by writing a small interface FORTRAN program which controls both programs [57]. An outline of the optimization process is shown in figure 15. Prior to running the optimization, realistic material data on the piezoceramics and composite need to be determined. The data on the piezoceramic is provided by the literature from the various vendors [43]. The sensor and actuator width, w_d , is 0.01905 m and the length of the actuator is 0.0635 m and sensor 0.01905 m. The resistor associated with an ideal operational amplifier used to acquire the sensor signal, R_F , is $1E10^6$ ohms. The elastic modulus of both the sensor and actuator material, c_{11}^E , is 5.847 MPa. The actuator location in the thickness or z-direction is set equal to 0.000635 m. Finally, the piezoelectric constant, d_{31} , is $1.498E10^{-4}$ m/V. The rest of the constants used in the optimization are combinations of the piezoelectric material constants. However, the composite data cannot be taken directly from the user material data sheet because the material ages and the properties are distinct for each fabrication. These material properties must be determined experimentally. Tensile testing on

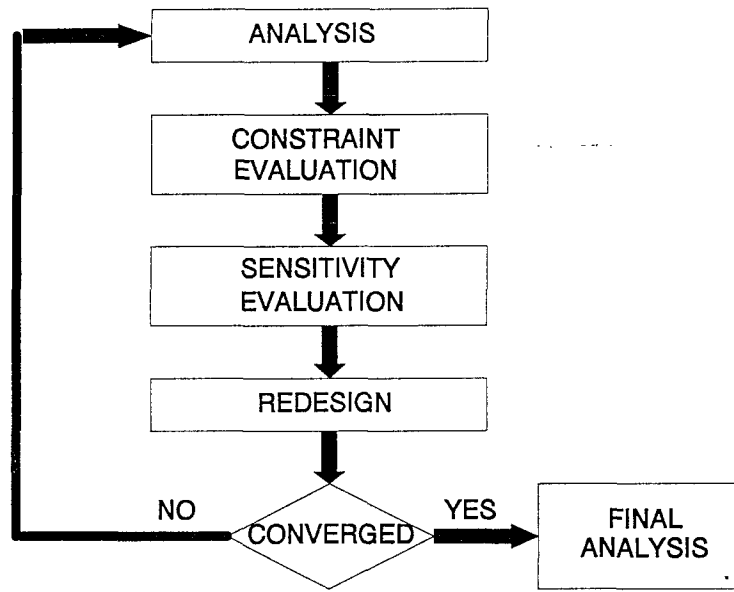


Figure 15 Outline of Optimization

TEST FOR CONVEXITY

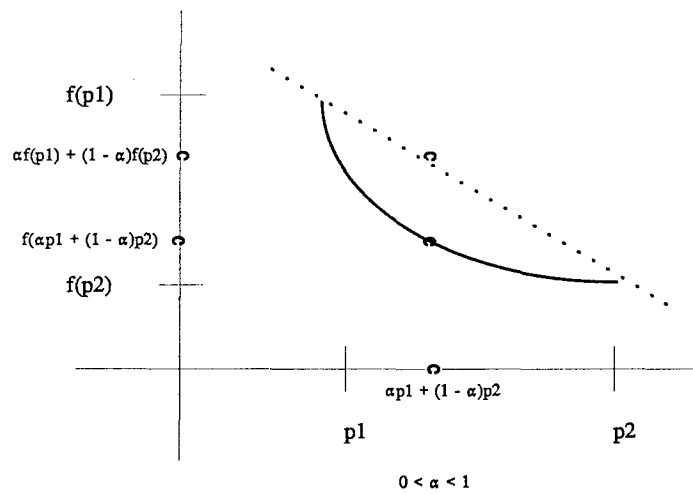


Figure 16 Test for Convexity

three sets of specimens with different ply angles was completed to determine the various composite properties required for this research.

The procedure, testing method, and results of determining the composite properties are given in the next section when the experimental apparatus is discussed. Only the results of the testing are presented in table 6.

TABLE 6 EXPERIMENTALLY DETERMINED COMPOSITE PROPERTIES

Composite	E_1	G_{12}	ν_{21}	E_2	ν_{12}	ρ
Value	156.45 GPa	5.91 GPA	.0107	9.95 GPa	.306	1455 kg/m ³

Prior to running the optimization computer program, the objective function was tested for convexity. The objective function and the constraint equations defined as the functions $f(p)$, $f1(p)$, and $f2(p)$ respectively.

$$f(p) = \zeta [C_r] Q [C_r]^T + (1 - \zeta) [C_b] Q [C_b]^T \quad (154)$$

$$f1(p) = c_1 \quad (155)$$

$$f2(p) = c_2 \quad (156)$$

In this research, the functions $f1$ and $f2$ pertain to each actuator and sensor pair. Convexity was tested for each of the functions. (See figure 16.) The symbol p represents a complete set of optimization parameters such as the ply angle, control gains, and actuator locations. The symbol α is an arbitrary multiplier which satisfies $0 \leq \alpha \leq 1$. Some randomly generated optimization parameters within the appropriate ranges were examined. The following test case

variables are calculated from the above functions:

$$\text{TEST} = \alpha f(p1) + (1 - \alpha)f(p2) - f(\alpha p1 + (1 - \alpha)p2)$$

$$\text{TEST1} = \alpha f1(p1) + (1 - \alpha)f1(p2) - f1(\alpha p1 + (1 - \alpha)p2)$$

$$\text{TEST2} = \alpha f2(p1) + (1 - \alpha)f2(p2) - f2(\alpha p1 + (1 - \alpha)p2)$$

With this setup, convexity was tested for. If any of the TEST, TEST1, or TEST2 variables were negative then the objective function or the constraint equations are not convex. After thousands of runs, the objective function was determined to be not convex, because there were cases in which the TEST function was negative. This means that a local minimum may not be the global minimum for the function. However, there could be some local minima which can be located using the optimization computer program. The constraint equations are considered to be convex, because in every case both the TEST1 and TEST2 function were positive. This is not a conclusive test for convexity, but it leads one to believe that they are perhaps convex. The optimization is performed in order to determine the local minima and try to find the smallest one by varying the optimization parameters.

In order to use DOT, a host program is required to control the optimization by defining the optimization method used, number of design variables and constraints, and by calling the main optimization program as a subroutine. This shell program is also used to define the programming constants, upper and lower bounds, and initial designs. The shell program also calls a subroutine which evaluates the objective function and the constraints for the optimization. (See equations 152-153.) This subroutine takes the experimentally determined composite constants, see table 1, and the sensor and actuator constants given by equations (80) and (77) and formulates the mass and stiffness matrices defined by equations

(104-105). From these matrices, the eigenvalues and eigenvectors are determined for the free motion system. Both the eigenvalues and eigenvectors are determined by using subroutines from the IMSL math libraries. Using the closed loop matrices, the Lyapunov equation (146) is solved and used to calculate the performance index, equation (152). Finally, the constraint inequality, equation (153), is calculated. All of these programs can be found in Appendix B of this dissertation.

In this research the optimization method used by DOT is Modified Method of Feasible Directions. This method is reliable and uses low amounts of computer memory. The expressions for the gradients from the previous theoretical section are calculated numerically by the finite difference method. The gradients determine which search direction along which the optimization program is to proceed. In this type of optimization, the process moves down to the minimum in the direction of the gradient as far as possible until a constraint is reached. Once a constraint is reached, a new search direction is looked for. The number of design variables used in the optimization is 14: 10 angles from each of the plies in the composite layup, 2 from the control gain of each of the actuators, and 2 from the x-location of each of the actuators. Actually, there are only 5 design variables for the ply angles due to the forced symmetry. For each of the ply angles, the upper bound is +90 degrees and the lower bound is -90 degrees. Anything beyond this range, the material properties are just repeating themselves. The upper bound on the actuator control gains is 40000 and the lower bound is 0. This upper bound is well beyond anything we could produce in the laboratory, since this is a gain multiplier which amplifies the voltage signal from the sensor. The upper and lower bounds on the actuator x axis locations are 0.5696m and 0.0127m which correspond to the beginning and end dimensions of the plate. The complete actuator has to fit on the plate which is why 0 and

0.6096 were not used. Finally, ζ was set equal to .5 which corresponds with minimizing the combined bending and torsion motion of the plate. The parameters that were held fixed during the optimization runs were the piezoelectric actuator and sensor material properties, composite material properties, dimensions of the plate, location of the sensors and actuators along the width of the plate, and the constant ζ . The constant ζ was used to weigh equally the bending tip motion with the torsional tip motion of the plate. The main objective of this research is to stop the complete motion, both bending and torsion, of the plate which is best accomplished by setting ζ to 0.5. (See Table 7) Later, ζ was allowed to vary from 0 to 1 by increments of .1 for one of the test cases to show the affect this parameter has on the optimization.

TABLE 7 DEFINITION OF OPTIMIZATION PARAMETERS

Optimization Parameter	Held Constant	# of Variables Optimized
Ply Angle, θ		5
Sensor/Actuator X-Location		2
Control Gains, G		2
Actuator/Sensor Properties	X	
Composite Properties	X	
Plate Dimensions, a,b,t	X	
Weighting Parameter ζ	X	
Sensor/Actuator Y-Location	X	

In order to determine if the minimum objective reached during the optimization routine is the lowest local minimum or possibly the global minimum, the optimization routine was started at numerous locations for the design variables. The starting ply was varied from 5 to

90 degrees by a 5 degree differential while the starting gain multiplier is varied from 10 to .00001. Both starting actuators locations were varied from 0.0254 to 0.55 meters along the length of the plate. The results of the optimization parameter study can be found in Appendix C of this dissertation. Hundreds of computer runs were made to determine if a possible global minimum solution could be found. From the computer runs, the value of the objective function reached a maximum of 26875 which occurred with a starting ply angle of 90 degrees, actuator location of 0.2032 and 0.4064 and gain multipliers of 10. The final results of this optimization run were ply angles of 80.2 degrees, actuator location of 0.188 and 0.577, and actuator gain multipliers of 8.86 and 0.12. This particular result from the optimization program must be near one of the local minima since the optimized parameters are located near the starting parameters. The minimum objective function of approximately 60-70 was reached consistently by about 50% of the optimization runs. The final optimized results of these optimization runs were all 10 ply angles with angles of about 20 degrees, actuator locations of 0.184 and 0.577 and actuator gains of 8.23 and 0.142. (See Table 8 for optimization details)

TABLE 8 SUMMARY OF "GLOBAL MINIMUM" SOLUTIONS FROM STARTING POSITIONS

Parameters to be Optimized	Starting Value	Optimized Value
Ply Angle 1	5° - 75°	20°
Ply Angle 2	5° - 75°	20°
Ply Angle 3	5° - 75°	20°
Ply Angle 4	5° - 75°	20°
Ply Angle 5	5° - 75°	20°
Ply Angle 6	5° - 75°	20°
Ply Angle 7	5° - 75°	20°

Ply Angle 8	5° - 75°	20°
Ply Angle 9	5° - 75°	20°
Ply Angle 10	5° - 75°	20°
Actuator 1 Location	.2032 - .4064 meters	0.184 meters from base
Actuator 2 Location	.2032 - .4064 meters	0.577 meters from base
Control Gain 1	.01 - 10.0	8.23
Control Gain 2	.01 - 10.0	0.142
Objective Function		60 - 70

Based upon the number of times this result was reached no matter where the optimization was started, it was surmised that this was the "global optimal" solution for this problem.

There is a physical significance for the optimization program to choose those particular parameters as the global solution. Both the coupled motion, bending, and torsional stiffness of the plate are being used to stop the motion. For maximum bending stiffness, the optimum angle is 0 degrees. For maximum torsional stiffness, the optimum angle is 45 degrees. Finally, the angle which maximizes the bending/torsional coefficient, D_{16} , is 18 degrees. It is reasonable to conclude that the optimum angle would occur near the angle which maximizes this coefficient. It turns out to be slightly larger due to the fact that the disturbance is a torsional force which excites predominately only the torsion and bending/torsional modes.

In order to verify the conclusions concerning the optimized ply layup, the optimization program is rerun with different performance indices as ζ varies. The constant, ζ , is varied from 0 to 1 by increments of 0.1. The results are presented in table 9.

TABLE 9 EFFECTS OF ζ ON THE PLY ANGLE, ACTUATOR LOCATION AND
OBJECTIVE FUNCTION

ζ	PLY ANGLE (degrees)	ACTUATOR LOCATIONS (meters)	OBJECTIVE FUNCTION
0	$[-45/45_2/34/28]_s$.156/.577 from base	2.81
0.1	$[26_2/9.8/21/16]_s$.186/.577 from base	21.3
0.2	$[22/17/21/18/15]_s$.185/.577 from base	32.2
0.3	$[20_3/19/16]_s$.185/.577 from base	42.2
0.4	$[20_4/17]_s$.183/.577 from base	52.3
0.5	$[20_5]_s$.184/.577 from base	61.7
0.6	$[20_4/19]_s$.183/.577 from base	71.3
0.7	$[19/20_3/18]_s$.180/.577 from base	81.4
0.8	$[20_4/17]_s$.169/.577 from base	92.2
0.9	$[20_2/17]_s$.161/.577 from base	101.3
1.0	$[20_2/19/16]_s$.149/.577 from base	109.5

From table 9, one notices that the objective function increases linearly as ζ changes from 0 to 1. This general increase in the objective function, with increasing ζ , makes physical sense due to the torsional disturbance input. The disturbance excites primarily the torsional modes of vibration with bending coming from the coupling. One would expect that the torsional motion of the plate would be larger than the bending motion so the objective function would increase as the dependence upon the torsional motion is increased. One should note that for the $\zeta = 0$ case which is controlling pure bending, the objective function should approach 0 by choosing a balanced layup which prevents any bending/torsional coupling. The optimization run for this case is tending towards a balanced layup but hits a local minimum or simply terminates

prematurely. This run was performed for only one starting ply and actuator location. Also, notice that in all three cases the actuator location does not vary greatly.

Finally, it is important to determine how sensitive the optimized objective function is to small changes in the optimized parameters. If the ply angle changes a few degrees, or if the location of the actuators are not exactly .184 and .577 meters, what affect does this have on the objective function? Using slightly different parameters, the computer program which calculates the objective function when supplied the optimized parameters was run again. From these results, it seems clear that the objective function is not sensitive to either minor deviations in the ply angle or even several different ply angles as part of the 10. In fact, in certain cases some of the ply angles ended up at 40 degrees and the objective function only changed by less than 0.1%. Also, the objective is not sensitive to very small changes in the actuator locations, but anything larger such as a couple of centimeters from the optimal locations changes the objective function greatly. If the actuator location varies by more than 0.0762 to 0.1016 meters, then the objective function will change by over 20%. Also, changing the disturbance force does not change some of the optimization parameters such as the actuator and sensor locations and ply layup. However, the change in the disturbance force greatly effects the actuator control gains. This effect is almost a one-to-one change. If the disturbance force is doubled, then the actuator control gains are reduced by one half. Also if the disturbance force is halved, then the actuator control gains are doubled. This relationship between the disturbance force and the actuator control gains occurs because of the constraints placed upon the total amount of energy supplied to the actuators. Because of physical limitations of the actuator, such as shorting out and depoling, the total voltage supplied to them is limited. This voltage is dependent upon both the strain signal of the sensor and the

actuator control gains. In fact it is the product of the two. Therefore if the sensor strain signal increases, then the actuator control gains must decrease in order for the total voltage to remain constant. When the disturbance force is increased, the strain on the plate is also increased which causes the sensor strain signal to increase. This is why the actuator control gains decrease proportionally. The same is true if the disturbance force is decreased.

The next chapter contains information regarding the experimental portion of this research. A plate was fabricated and tested with a ply angle of 21 degrees. The results of this testing were then compared with a plate fabricated with a quasi-isotropic layup.

V. *Experimental Apparatus and Procedure*

The information presented in this chapter covers the experimental apparatus and procedure for the fabrication, the testing methodology, the material characterization results of the composite test specimens and the testing methodology and characterization of the vibration testing. The procedures used to characterize the material follow the guidelines provided by ASTM. The standards followed for determining the tensile and shear properties are ASTM D3039-76 and ASTM D3518-76. The size of the specimen and the testing procedure are taken from the reference, Experimental Characterization of Advanced Composite Materials by Carlsson and Pipes [58]. The specimens were fabricated and prepared for testing at the Composites Structures Laboratory of the Applied Composite Branch, Phillips Laboratory Edwards AFB, CA. The material used was Fiberite Graphite/Epoxy tape or specifically, IM-7 fiber and 977-2 thermoset epoxy resin on 12" wide preimpregnated tape. IM-7 fiber is a high strength, medium modulus graphite fiber that has been used extensively for space applications. The resin, 977-2, is a dicyanate ester resin which is space qualified and provides very little microcracking and outgassing. This material definitely needed to be characterized because it had surpassed its shelf life by about 2 years. The material had aged significantly. In order to completely characterize the composite material, 3 sets of samples were fabricated with different lay-ups to determine all of the material properties. The samples were fabricated with the following ply angles: $[0]_8$ to determine E_1 and ν_{12} , $[90]_{16}$ to determine E_2 and ν_{21} , and $[\pm 45]_{28}$ to determine G_{12} . Also, the density of the composite material was determined by measuring the volume and the weight of some of the test specimens.

The fabrication method used to make the specimens was hand layup. This is the simplest method for making flat panels from which the test specimens were machined. First,

the composite material was taken out of a freezer and allowed to thaw while the mold surface was being prepared. This preparation involves cleaning the mold with acetone to remove any contaminants, spraying it with a release agent such as McLube or Freecote, and then attaching a release cloth to the surface using teflon tape to prevent the composite from adhering to the mold. The composite material used was .304 meters wide graphite/epoxy unidirectional tape which means the reinforcing fibers all run in only one direction. The composite tape was then cut into square and rectangular strips depending upon which layup was being fabricated. These strips were then laid on top of one another in the proper fiber orientation on the mold to form the specimens. A combination of release and bleeder cloth is then attached to the top of the mold to capture the excess resin which flows from the prepreg material out of the specimen panel. The release cloth is used to prevent the excess resin from sticking to the formed part. A vacuum bag is then formed around the part by taping, with double-sided tape, a thick plastic sheet to the mold. (See figure 17.) Using a vacuum pump, the air is removed from the bag in order to apply uniform pressure on the composite part during the curing cycle. The part is now ready for the cure cycle which completes the fabrication of the composite material. (See figure 18) The cure cycle used ramps the temperature up to 180 degrees F. At this temperature the resin becomes less viscous and starts to flow. Once this temperature is reached 80 psig of pressure is applied. This temperature is maintained for 30 minutes to allow the resin to heat up and begin to flow creating a uniform cross-sectional area of matrix material. After 30 minutes the temperature ramps up to 350 degrees F and is held for 4 hours. The resin or matrix material has then reached its T_g , or gel temperature, and begins to set. The pressure is held constant during this time. After four hours both the temperature and pressure are lowered gradually to minimize any residual thermostresses which could be

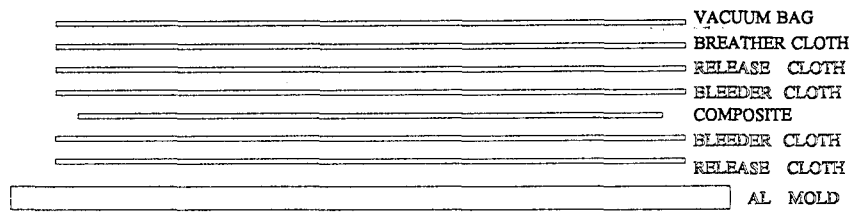


Figure 17 Bagging the Composite Layup

STANDARD CURE CYCLE

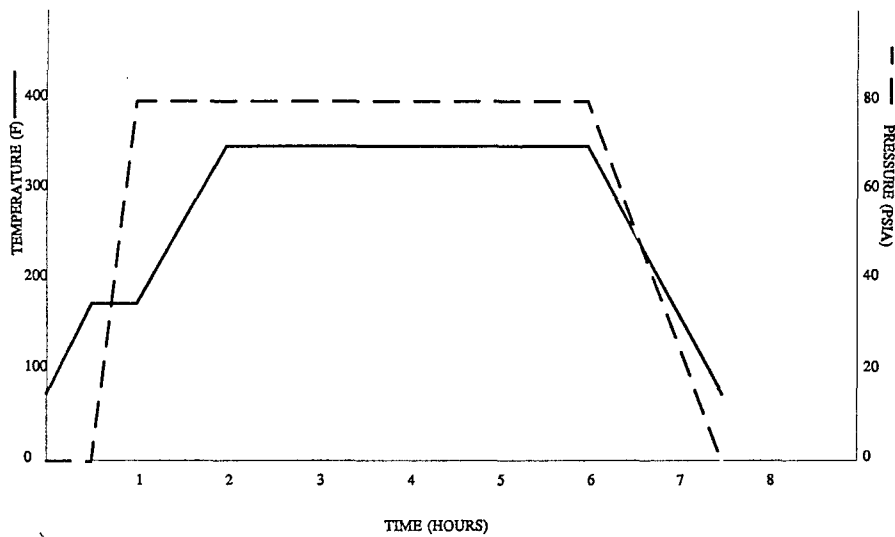


Figure 18 Standard Cure Cycle of Graphic Epoxy Materials

induced into the composite material. The specimen panels are now complete and ready to be machined to test specimens.

Loading tabs are attached to the specimen panels in order for the material testing machine to grip the individual test specimens. These loading tabs are made out of glass epoxy and are attached to the specimen using a Hysol 9394 epoxy resin. The resin has a 3-5 day cure time at ambient temperature of 77 degrees F or an accelerated cure time of 1 hour at 150 degrees F. The loading tabs are cut into strips 0.0381 meter length and glued to the specimen panels prior to machining. The reason the loading tabs are attached prior to machining is to insure that the specimen and tabs are aligned with one another. This prevents any unwanted bending force from entering into the tensile test. After the resin has cured, the specimen panels are cut into their proper dimensions depending upon the ply angle orientation of the fiber and what type of test is going to be performed. The test specimen panels were cut according to the specifications stated in the relevant standards for shear and tension testing, ASTM D3039-76 and D3518-76. Prior to testing, electric resistance foil strain gages are attached both in the longitudinal and transverse directions to measure the strains in those directions. These gages were purchased from Measurements Group, Inc. and are from the CEA - Series. They are self compensating strain gages with a fully encapsulated copper grid and exposed copper-coated integral solder tabs. From each test, different material constants are derived. The specimens were loaded into a MTS material testing machine, making sure they are aligned properly to prevent bending from occurring. The specimens are loaded at a constant rate with data taken continuously until failure. Since the composite material properties are directly related to minute changes in the environment during the fabrication and curing cycle, numerous tests must be performed and then averaged to obtain the material

constants. Nine specimens of each ply layup were tested to determine a statistical average of the material properties. The results of the tests for 0 degrees are shown in table 10.

TABLE 10 RESULTS FOR THE 0 DEGREE COMPOSITE MATERIAL TESTS

Test Number	E_1	ν_{12}
1	166.93 GPa	Bad Data
2	173.75 GPa	Bad Data
3	163.54 GPa	.360564
4	174.71 GPa	.38231
5	152.21 GPa	.285173
6	159.14 GPa	.307589
7	147.76 GPa	.296064
8	127.49 GPa	.263132
9	142.52 GPa	.244482
Average	156.45 GPa	.305616286

The results of the tests for 45 degrees are shown in table 11.

TABLE 11 RESULTS FOR THE 45 DEGREE COMPOSITE MATERIAL TESTS

Test Number	G_{12}
1	5.4 GPa
2	5.65 GPa
3	6.05 GPa
4	5.5 GPa
5	6.099 GPa
6	6.22 GPa
7	6.14 GPa
8	6.041 GPa
Average	5.91 GPa

The results of the tests for 90 degrees are shown in table 12.

TABLE 12 RESULTS FOR THE 90 DEGREE COMPOSITE MATERIAL TESTS

Test Number	E_2	ν_{21}
1	10.54 GPa	.012422949
2	9.52 GPa	.016004

3	Bad Data	.018734
4	8.83 GPa	.007410486
5	10 GPa	Bad Data
6	9.38 GPa	0.004059426
7	10.61 GPa	.008723356
8	10.2 GPa	.009075485
9	9.72 GPa	.0098146
Average	9.95 GPa	.010780538

The density was determined by cutting off a square piece of composite to exact dimension using a computer controlled milling machine. The dimensions are checked with a calibrated measuring device. Once the exact volume is known, the specimen is weighed on a precision scale. The density is then calculated from these experimental measurements. The results of these characterization tests are shown in table 6. However, as one can see there is a lot of variance between the measured values of v_{21} . It is extremely difficult to experimentally measure v_{21} , because the strain gage slips and eventually falls off prior to completing the testing. Prior to using these measured numbers, a simple check was made using the equation:

$$\frac{E_1}{E_2} = \frac{v_{12}}{v_{21}} \quad (157)$$

It was determined that the measured value for v_{21} , 0.010718, was inaccurate and the number used in the optimization subroutine was calculated to be 0.01925. A similar fabrication

procedure described above to make the test specimens was used to fabricate the optimized plate for the experiment.

The results from the optimization program from the previous chapter, include the optimal ply orientation and locations of the actuators, are used in the fabrication of the composite plate. This structure was fabricated at the Composite Structures Laboratory, Applied Composite Branch, Phillips Laboratory at Edwards AFB, CA. The plate was hand layed up on an aluminum mandrel, vacuum bagged, and cured. The material used was Fiberite Graphite/Epoxy tape or specifically, IM-7 fiber and 977-2 Thermoset Epoxy Resin on 0.304 meter wide preimpregnated tape. Plates having a quasi-isotropic and 21 degree layup were fabricated. Quasi-isotropic means that the properties are the same in both the length and width direction. This is accomplished by creating a layup that provides both the stiffness of the fibers and the elasticity of the matrix in all directions. Plates that are quasi-isotropic usually have a layup with a combination of 0, ± 45 , and 90° plies. Fabricating these plates with various ply orientations is extremely difficult. The composite material is similar to a fabric with sticky glue on it prior to its being cured. Trying to cut this fabric to the exact geometry such as 21 or 45 degrees is nearly impossible. Since the optimized plies varied between 20 and 22.05 degrees, all of the plies of the optimized plate were attempted to be cut at 21 degrees. The difficulty involved in cutting causes at least a ± 3 degree error in the ply angle. Another factor which influences the ply angles is how the cut composite sheets are laid on top of one another. When the plies are compacted to provide adequate bonding, the stretch in the matrix directions causes the ply angle to change somewhat. These errors should not affect the overall results of this research since it was shown in the last chapter that the optimized objective function is not extremely sensitive to changes in the ply orientation. The plates were

cured using a standard cure cycle at 176.67 degrees C at 551.6 kPa of pressure, the same as the test coupons. After the plates were fabricated, the piezoceramic actuators and sensors were attached to the plate at the optimized locations as determined by the optimization computer program. The sensors and actuators were attached using room temperature cure epoxy resin. The sensors are attached on one side of plate and the actuators are attached in the exact location on the opposite side of the plate. (See figure 19.) Once finished, this completed plate is then attached to the control electronics.

The structural assembly described above is attached to the control electronics described in the theoretical section which contains among other things, a strain rate feedback circuit. This circuit is shown in figure 20. For the testing, two circuits were built out of breadboard electronics. The responses of both circuits targeted the torsional mode of the plate. This means that the circuits provided the most damping at the torsional theoretical resonance frequency of the plate. This response is shown in figures 21, 22. The output of the piezoceramic sensors is conditioned by the feedback electronics which then supply a high voltage control signal to an actuator. One sensor will control only one actuator in this research. The feedback electronics consist of a preamplifier which converts the sensor signal to a voltage, a bandpass filter with an adjustable center frequency and bandwidth which changes the signals phase, and a high power output amplifier which amplifies the voltage signal to power the actuators. The center frequency of the electronic circuit is centered around the torsional and bending/torsional modes of the plates. The torsional vibration is provided by using a piezoceramic sensor and actuator pair mounted halfway along the length of the plate at a 45 degree to the longitudinal axis. A pseudo-random signal of 500 mVrms is sent to the actuators as the disturbance source.

Location of Actuator and Sensor on Plate

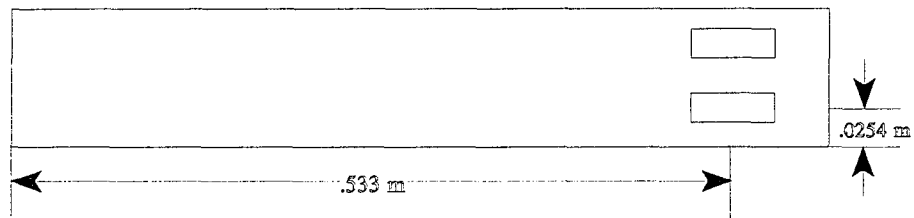


Figure 19 Location of Sensor and Actuator on Plate

Strain Rate Feedback Circuit

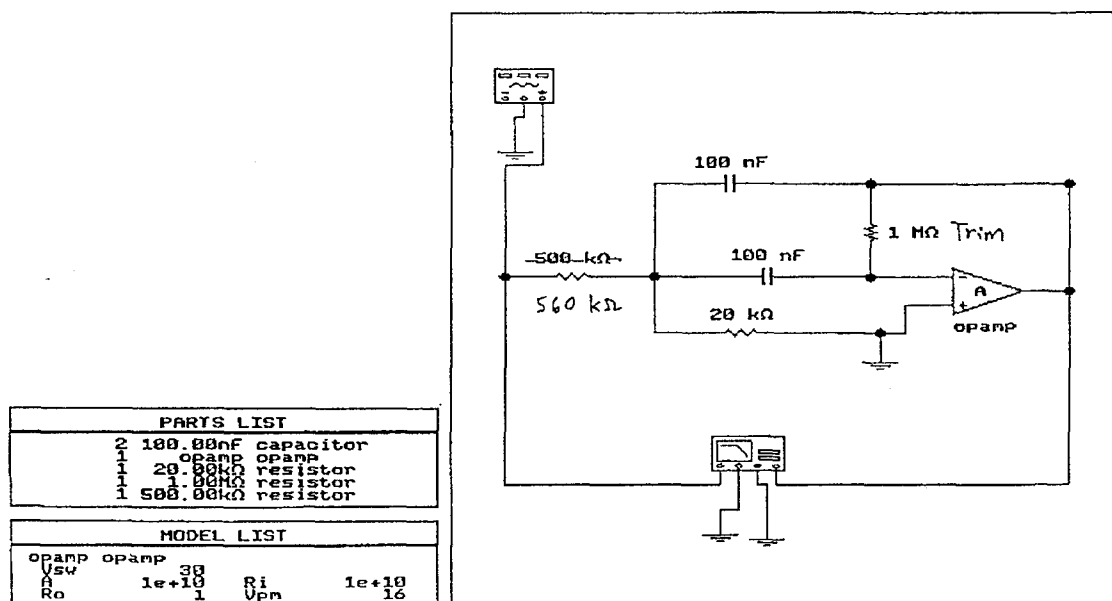


Figure 20 Strain Rate Feedback Circuit

RESPONSE - STRAIN RATE FEEDBACK CIRCUIT 1

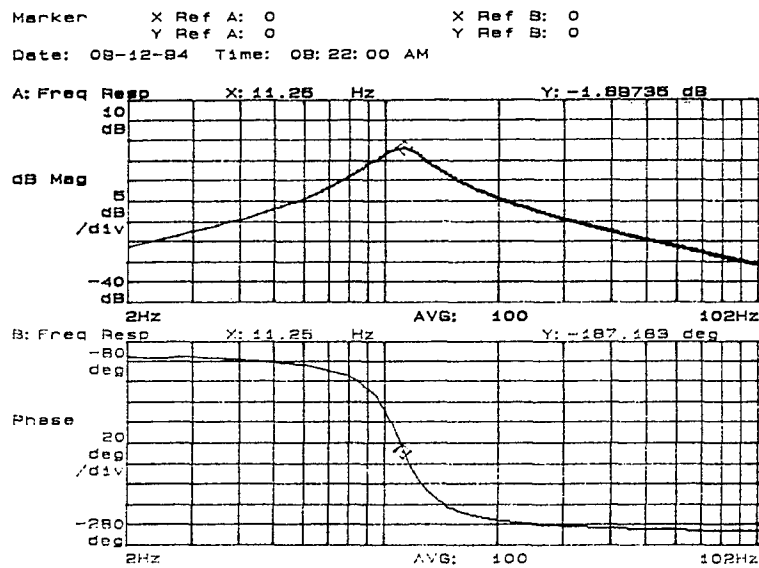


Figure 21 Response - Strain Rate Feedback Circuit 1

RESPONSE - STRAIN RATE FEEDBACK CIRCUIT 2

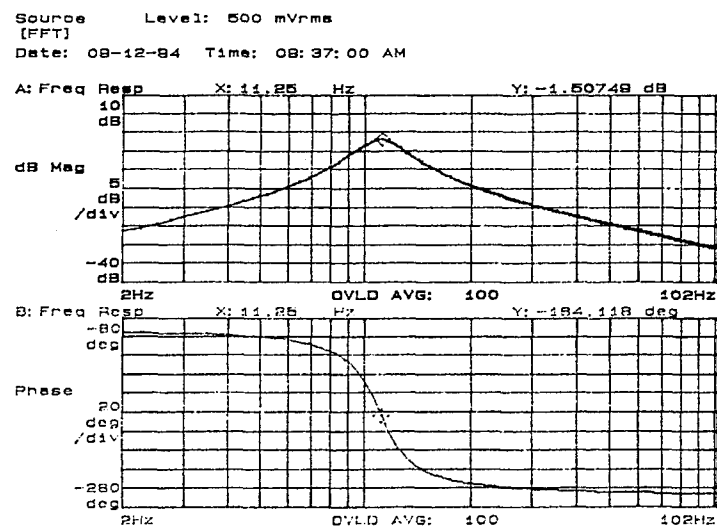


Figure 22 Response - Strain Rate Feedback Circuit 2

A schematic of the control electronics is shown in figure 23.

The main objective of the experimental portion is to characterize the damping of the plate and its performance when subjected to random noise disturbances. The structural response can be measured by exciting the structure with a piezoceramic actuator and measuring the response with a piezoceramic sensor. The complex modal parameters and mode shapes of the structure will be calculated using transfer function analysis techniques as determined by the frequency response functions (FRF). Initially, the plates are characterized with the control system turned off. The random noise signal is sent to the disturbance piezoceramic actuator and the structural response is detected by the collocated sensor. The response is the real time average of 100 signals. Once the plates are characterized, then the above procedure is repeated with the control system turned on. The closed loop response of the 21 degree plate is measured. The magnitude of the natural frequencies are compared with the theoretical predictions. A HP 35665A Hewlett Packard Dynamic Signal Analyzer is used to create the random noise signal and to calculate the (FRF)'s of the plates. The signal analyzer is also used to characterize the response of each of the electronic circuits used to control the plate.

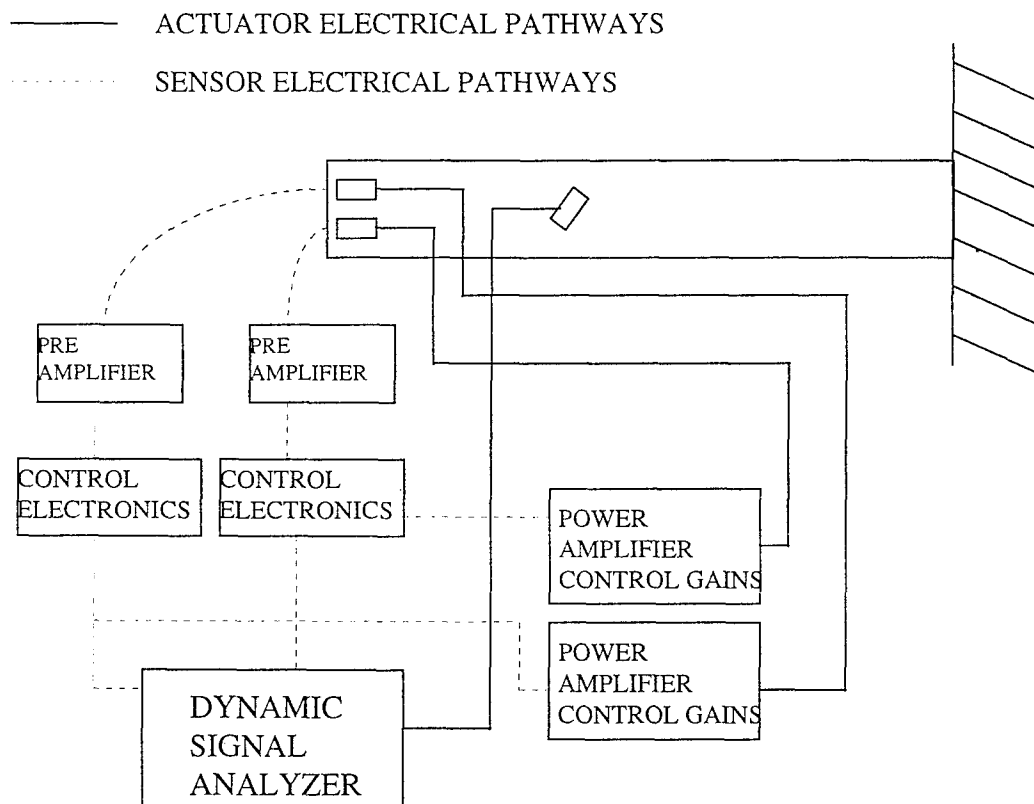


Figure 23 Schematic of Control Electronics

VI. Comparisons Between Baseline, Modified Plate and Theory

In this chapter, the 21 degree optimized plate is compared to a quasi-isotropic baseline plate as well as the theoretical calculations in terms of performance. When comparing the optimized plate to the theoretical calculations, one should note that the actuator locations for the experimental plate are not at the optimized locations. They were placed at their current location of 0.531m based upon theoretical calculations that were in error. That error has been corrected producing the new actuator locations, however a new experimental plate was not fabricated. One should also note that the optimal ply angles did not change due to the error in the theory. The theoretical calculations and experiments are also compared with the work done by Hwang, Hwang, and Chul [25] [26]. Their work is very similar to the work accomplished here with the exception of their modelling method. As stated previously, the results found in Hwang, Hwang, and Chul's report are very close to the results found in this dissertation even though the modelling methodology is completely different: finite element method versus classical Rayleigh-Ritz modelling and sequential versus simultaneous optimization. First, the work accomplished in the above paper is compared to theoretical calculations in this dissertation.

In the papers by Hwang, Hwang, and Chul [25] [26], numerical calculations are performed on an eight-ply laminated composite plate with two of the plies variable. The stacking sequence is $[\theta_1/\theta_2/0^\circ/90^\circ]_s$, where θ_1 and θ_2 are the ply angle design variables. The optimization is first conducted for an orthotropic plate with the design angles set equal to 0 degrees to determine the optimal size and location of the piezoelectric sensors and actuators. Initially, the size of the sensors and actuators are unconstrained while the locations are not allowed to vary. In the second case the actuator sizes are constrained while the optimal

locations are obtained. The optimization conducted next is to determine the optimal ply layer angles of the laminated plate which will maximize the control performance. The optimization is conducted with and without dynamic stability constraints. The optimization is performed for only a limited number of cases. The results of the optimized actuator locations are shown in figure 24. As the reader can see they compare favorably with what this dissertation predicts. The theory in this dissertation places the actuators at the optimum location of 0.184 and 0.577 meters from the base out of a plate length of 0.6096 meters or 30% and 95% down the length of the plate. In Hwang's paper, the optimum location of the actuators are .41m from the base out of a plate length of .5m or 82% down the length of the plate. Thus there is only a 13% difference between one actuator location in these two theories which were developed differently and independently. The results of the optimized ply angles also compare very favorably to the theoretical predictions in this dissertation. These results are shown in table 13. The results from this dissertation predicts the ply angles to be 20-21 degrees while the results from HHC's paper vary from 24.98 - 29.04 degrees. These ply angles differ from this dissertation by 20 - 31% depending upon which ply angle you choose. This may seem high, but remember that only two of the ply angles are allowed to vary in Hwang's paper and the others are fixed. Since the fixed ply angles offer very little torsional stiffness, the optimized ply angles are expected to be higher or closer to the 45 degree maximum torsional stiffness. Table 14 shows the final optimized results of the two theories.

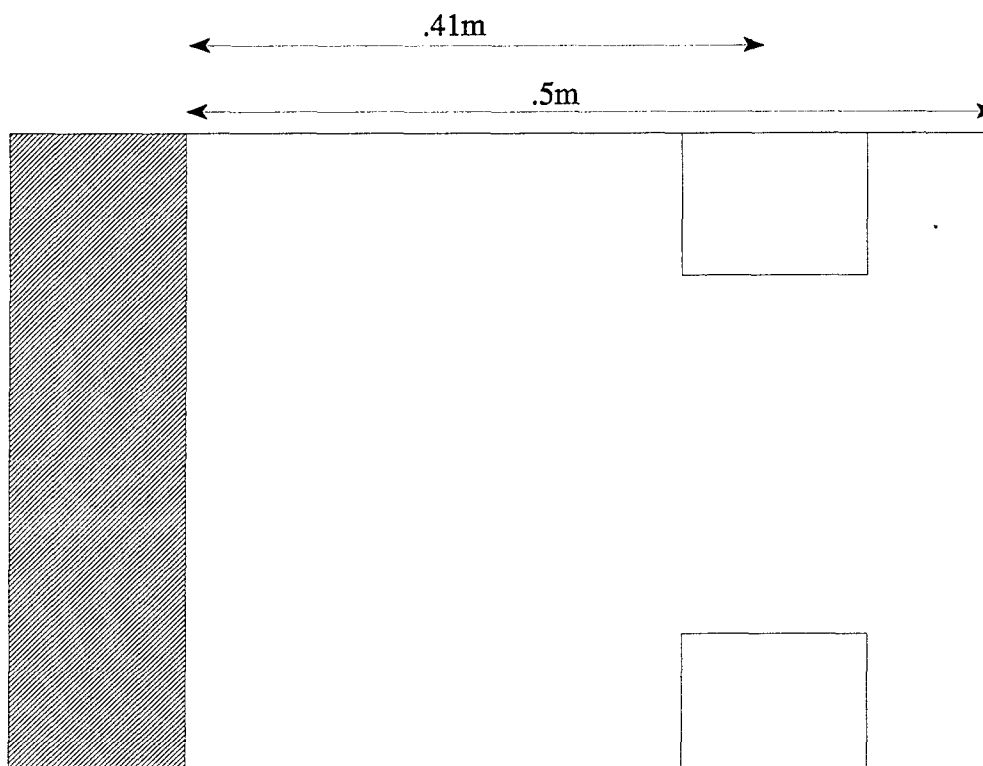


Figure 24 Optimal Location of Actuators from [24] [25] [26]

TABLE 13 OPTIMAL PLY ANGLE FROM [24] [25] [26]

Objective Function	Case No.	Design Variable θ_1	Design Variable θ_2
C3 for 1B	1	30.00/26.19	30.00/28.75
C3 for 1B	2	30.00/25.10	-30.00/26.10
C3 for 1T	1	30.00/26.12	30.00/29.04
C3 for 1T	2	30.00/25.94	-30.00/24.98

TABLE 14 COMPARISON BETWEEN REFERENCED PAPER AND DISSERTATION
PARAMETERS

Optimized Parameter	Referenced Paper Theory	Dissertation Theory
Actuator Location #1	.41m/.5m 82%	0.184m/0.6096m 30%
Actuator Location #2	.41m/.5m 82%	0.577m/0.6096m 94%
Ply Angle #1	24.98 - 29.04 degrees	20-21 degrees
Ply Angle #2	24.98 - 29.04 degrees	20-21 degrees

The results of the experiment will now be presented and compared with the theoretical calculations. The theoretical modes of vibration are shown in figures 25 - 28. Each figure displays a different mode of vibration: figure 25 - 1st bending, figure 26 - 2nd bending, figure 27 - 1st torsion, figure 28 - 2nd torsion. The frequencies for the theoretical, both 4 and 9

mode models, and experimental calculations of the 21 degree plate are shown in table 15.

TABLE 15 FREQUENCY COMPARISON OF THEORETICAL CALCULATIONS AND
EXPERIMENTAL MEASUREMENTS OF THE 21 DEGREE PLATE

Frequency	4 Mode	9 Mode	Exp	4 Mode vs Exp	9 Mode vs Exp
1st Bending	1.224	1.15	1	22%	15%
2nd Bending	8.62	7.00	6	44%	17%
1st Torsion	16.35	14.66	18	-9.2%	-19%
2nd Torsion	64.54	53.10	54	20%	-1.7%

The percent difference in the frequencies between both the theoretical calculations and the experimental measurements are not that significant when modelling composite structures especially with the nine mode theoretical model. As one can see, in all but one case the Rayleigh-Ritz approximate solution provides an upper bound to the experimental frequencies. One reason that theoretically determined and experimentally measured frequencies varied is the added weight and stiffness associated with the piezoceramics were not accounted for in the analysis. The plate itself weighed only 149.9 g, each of the three actuator elements weighed 4.8 g, and each of the three sensor elements weighed 2.4 g bring the total weight of the structure to 171.5 g. This is an increase in weight of 14.4%. The actuators and sensors also provide extra stiffness in certain modes of the structure such as the torsional mode.

As far as how the optimized plate performed experimentally, both the open and closed loop response to the 21 degree optimized plate showed a significant improvement in stopping the tip motion over the open loop baseline isotropic plate. The performance of the open loop

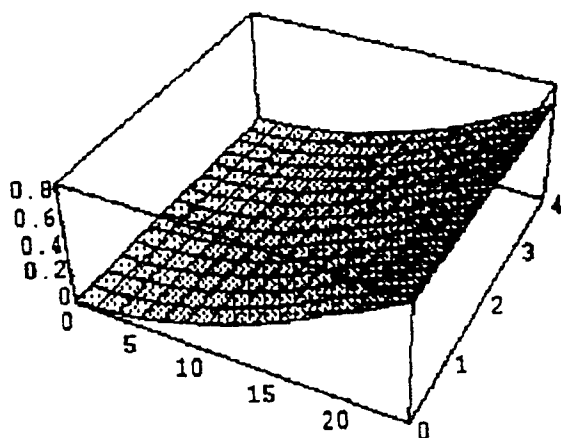


Figure 25 1st Bending Mode of the Plate

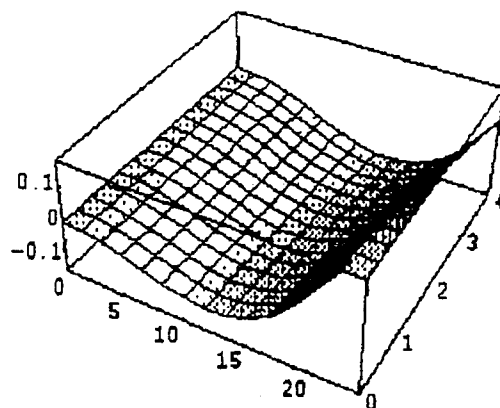


Figure 26 2nd Bending Mode of the Plate

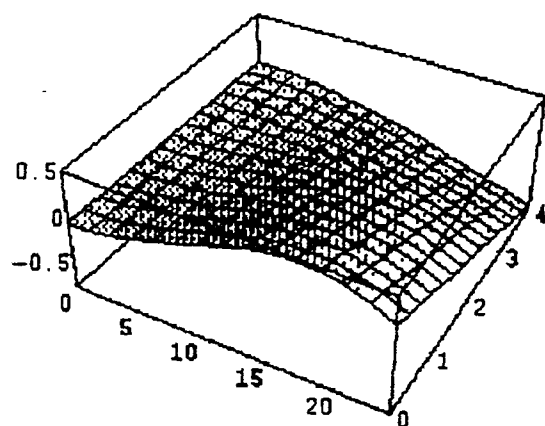


Figure 27 1st Torsional Mode of the Plate

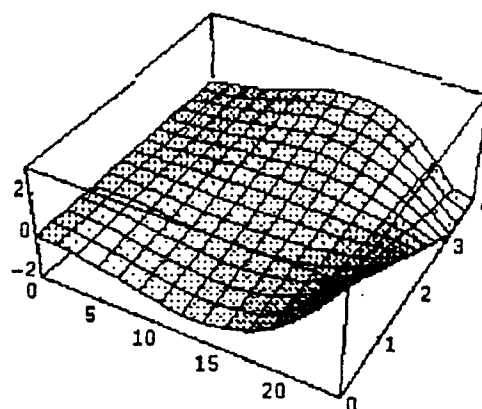


Figure 28 2nd Torsional Mode of the Plate

response of the isotropic plate is shown in figure 29. The performance comparison between the open and closed loop response of the optimized plates are shown in figure 30. Figures 29 and 30 show that both the open and closed loop response of the optimized plate perform significantly better than the open loop response of the isotropic plate. The open loop response of the optimized plate was 16.6% lower than the open loop response of the isotropic plate. The closed loop response performed even better. The closed loop response of the optimized plate was 29.8% lower than the open loop response of the isotropic plate.

In the case of the optimized plate, the performance improved with the addition of the control system. The magnitude of the harmonic peak for the 1st torsional mode decreased by 11.3% and for the 2nd torsional mode by 6.7%. Both the isotropic and the optimized plate tests were repeated 10 times with excellent repeatable results. One comparison that was unable to be made due to the limitations with the equipment that was used, was comparing the damping factors of the theoretical predictions with the experimental measurements. The damping factors are measurements of the inherent structural damping or added damping due to the active control system. Next, the changes in the damping factors for the different ply are presented. Note, the actuator gains and locations are the same for both plates in this comparison. These are shown in table 16. These were determined from the theoretical analysis from the closed loop plant matrix.

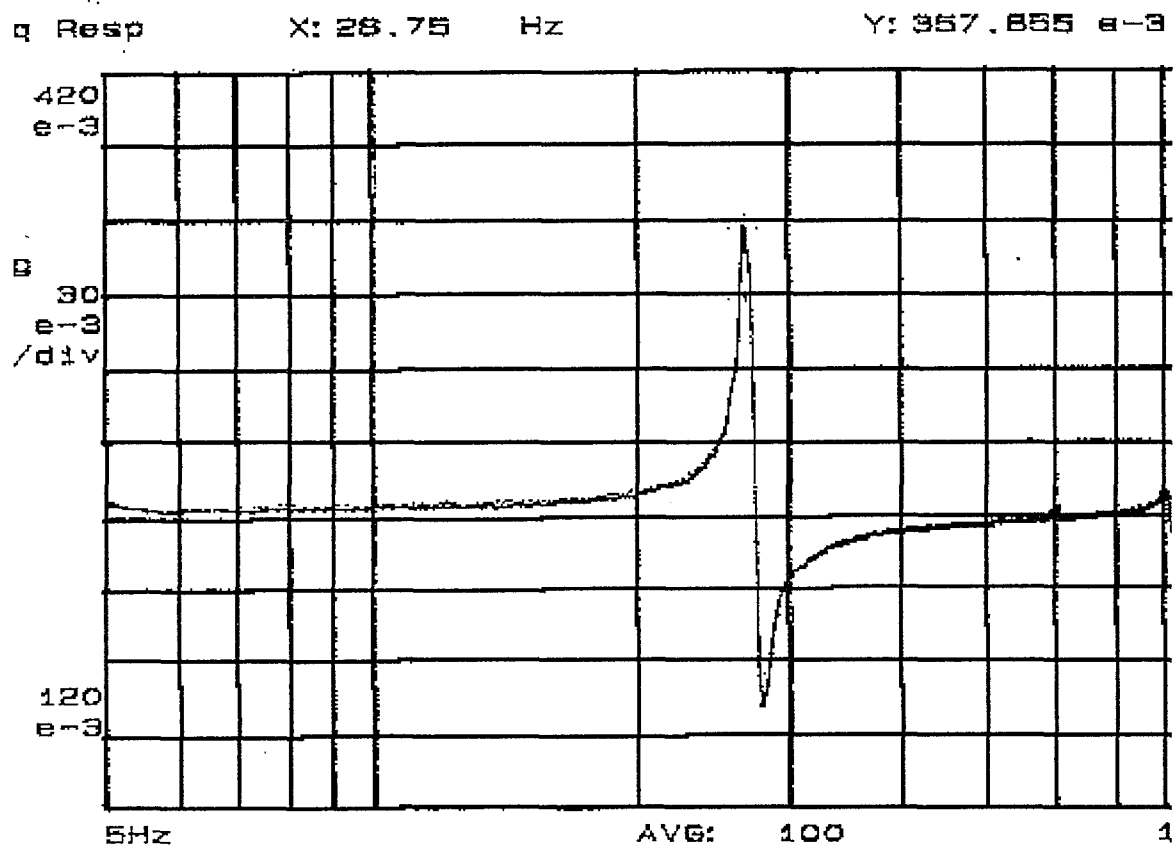


Figure 29 Open Loop Frequency Response of Isotropic Plate

Marker X Ref A: 0 X Ref B: 0
Y Ref A: 0 Y Ref B: 0

Date: 08-13-84 Time: 11:42:00 AM

A: Freq Resp X: 17.75 Hz Y: 275.801 e-3
B: D1 Freq Resp X: 18 Hz Y: 308.083 e-3

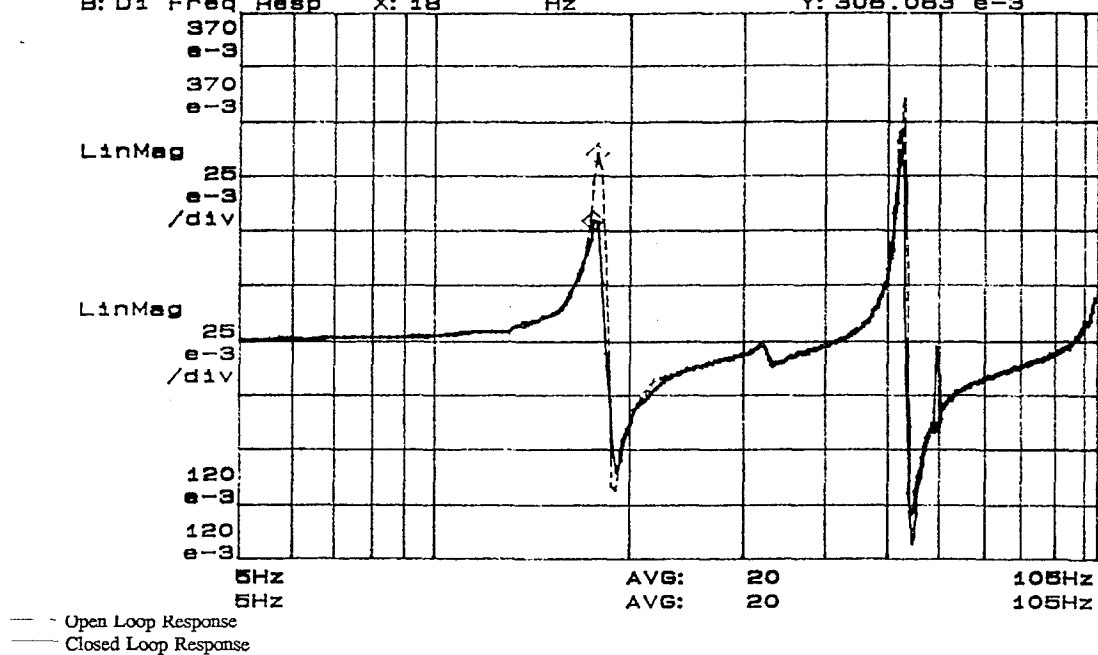


Figure 30 Open and Closed Loop Response of Optimized Plate

TABLE 16 THEORETICAL DAMPING FACTORS FOR ISOTROPIC AND 21 DEGREE
PLATE

Mode of Vibration	Isotropic Plate	21 degree Optimized Plate
1st Bending	.00039	.000248
2nd Bending	.0945	.025
1st Torsion	.0129	.0685
2nd Torsion	.0000009781	.000084936

The damping factor is greater in the isotropic plate than in the optimized plate for the bending modes of vibration. However, as one would expect, the damping factors are greater in the torsion and combined bending/torsion modes of vibration. In fact, for the first torsional mode the difference is a factor of 5 and for the second torsional mode the difference is two orders of magnitude. This implies that the isotropic plate damps out the bending modes of vibration better than the optimized plate. However, the optimized plate damps out both the 1st torsional and 2nd torsional modes of vibration better than the isotropic plate. Since the optimized plate was designed specifically to stop the motion of the plate when subjected to a torsional disturbance, these results are expected.

VII. Summary

The results from this research are a design methodology and a plate which is optimized with respect to both structural and control parameters. The design methodology demonstrates how to achieve simultaneous structural and control optimization using the basic elastic and dynamic equations. The ply layup and location of the piezoelectric actuators that provide bending torque only are determined from the optimization routine. The ply orientation of the plate is optimized to enhance the active control elements. The active control system is optimized with respect to actuator and sensor location and the amount of voltage being applied to each of the actuators. Finally, the optimized ply orientation produces coupling between the bending and torsion modes of vibration. With this "tailored" coupling not only will the piezoelectric actuators damp bending, but they will also damp the rotation motion.

The theoretical calculations provided the natural frequencies, mode shapes and damping factors for the plates which corresponded very well with the measured experimental values. The percent difference of the natural frequencies varied by only 9% to 44% which is well within experimental error when modelling composite structures. The theory also predicted that the optimized plate would achieve higher damping in the torsional mode than the quasi-isotropic plate. The factor of 5 increase in torsional damping is a significant increase in damping considering the fact that the method used secondary effects. The torsion modes are not being damped directly as in the 1st or 2nd bending modes. Recall that the piezoceramic actuators only produce a bending moment which easily reacts against the bending motion of the plate. This direct stopping motion produces large damping in the 1st or 2nd bending modes of the plate. Only the bending/torsional coupling motion of the plate caused by the optimized ply layup and actuator location produces any increase in damping for a torsional disturbance force. This is verified by the figures in chapter VI, which show both the open and closed loop response for the baseline plate and the optimized plate.

The present theoretical calculations compare favorably with independent papers written by Hwang, Hwang, and Chul [25] [26]. The concept of their papers and referenced PhD dissertation by W. S. Hwang in 1993, is almost identical to what is proposed in this dissertation. However, it was shown that in both chapters II and VI, their theory and approach are different. Their theory is based upon finite element modelling and their optimization subroutine is performed sequentially whereas this dissertation models the plate by using energy method models and simultaneous optimization. An even greater difference between the two theories is in the geometry of the plate and materials used. Also, experiments were conducted in this dissertation to back up the theory, while the referenced papers discuss only theoretical work. Even though the differences in the theory are significant, what is even more outstanding is the fact that the results compare so well. One of the optimized actuator locations differ by only 13% and the optimized ply angles differ by 20% to 31%. Based upon the results of this dissertation and the other referenced work, the concept of damping out torsional vibrations using bending actuators enhanced by the coupled bending torsional motion of a plate is achievable and worthwhile.

Further refinement of this theory with the addition of a combined bending/torsional disturbance force and taking into account the viscoelastic damping effects of the matrix material would be a good topic for further research. Substituting a combined bending/torsional force as the disturbance instead of a torsional force would more than likely change the ply orientation and at least one of the actuator locations. These would change in order to provide directly damping to the induced bending modes of vibration of the plate. Also, taking into account the inherent damping effects of the composite material would show conclusively the effects of the active control system. One other minor modification which could be made to refine this theory would be to allow some of the fixed structural parameters to vary such as the y - direction location of the actuator/sensor pair. If this theory and design approach was used in an operational satellite system, the plate length and width could also be

allowed to vary to determine the complete optimized structure for a given disturbance profile.

As stated in the introduction, as satellites require more power, the size of the solar array increases tremendously which causes the solar arrays to be prone to vibrations due to their large size and light weight. A design methodology and structure fully optimized with respect to its size, shape, and structural makeup which can damp out both bending and torsional vibration would be greatly beneficial to the military and commercial space community. This research centered on developing and testing this design methodology by fabricating an optimized plate which provides positive proof of the theoretical calculations.

Bibliography

1. Agrawal, B. N., Design of Geosynchronous Spacecraft, Prentice-Hall, Inc., Englewood Cliffs, NJ, 1986.
2. Forrester, P. G., "Effects of Aeroelastic Tailoring on Anisotropic Composite Material Beam Models of Helicopter Blades," Master's of Science Thesis University of Virginia, Richmond, VA, May 1989.
3. Jones, R. M., Mechanics of Composite Materials, Hemisphere Publishing Corp., New York, 1975.
4. Murray, Y. D., "Fibrous Composite Laminates - An Introduction to the Theory and Verification of the DYNA3D Implementation," Technical Report #APTEK, Aug 1988.
5. Cook, R. D., Malkus, D. S., and M. E. Plesha, Concepts and Applications of Finite Element Analysis, Wiley Publishing, New York, 1989.
6. Weisshaar, T. A., "Aeroelastic Tailoring - Creative Uses of Unusual Materials," AIAA-87-0976 AIAA Paper, 1987.
7. Shirk, M. H., Hertz, T. A., and T. A. Weisshaar, "Aeroelastic Tailoring - Theory, Practice, Promise," Journal of Aircraft, Vol 23, No. 1, pp. 6-18, Jan 1986.
8. Crawley, E. F., and K. B. Lazarus, "Induced Strain Actuation of Isotropic and Anisotropic Plates," AIAA Journal, Vol. 29, No. 6., pp. 944-951, June 1991.
9. Fukunaga, H. and H. Sekine, "A Laminate Design for Elastic Properties of Symmetric Laminates with Extension-Shear or Bending-Twisting Coupling," Journal of Composite Material, Vol. 28, No. 8, pp.708-731, 1994.
10. Collar, A. R., "The First Fifty Years of Aeroelasticity," Aerospace, Vol 5, No. 2, pp. 111-125, May 1978.
11. Ashley, H., "The Constructive Uses of Aeroelasticity," AIAA-80-0877 AIAA Paper, 1982.
12. Garfinkle, M., "Twisting Smartly in the Wind," Aerospace America, Vol. 32, No. 7, pp. 18-20, 1994.
13. Lake, R. C., and M. W. Nixon, "A Preliminary Investigation of Finite-Element Modeling for Composite Rotor Blades. Aerostructures Directorate," Proceeding of the 3rd Workshop on Dynamics of Aeroelastic Structures, NASA Langley Research Center, Virginia, Vol. 1, pp. 354-365, 1990.

14. Weisshaar, T. A. and S. M. Ehlers, "Adaptive Aeroelastic Composite Wings-Control and Optimization Issues," Journal of Composite Engineering, Vol. 2, No. 5-7, pp. 457-476, 1992.
15. Hodges, D. H., Atilgan, A. R., Fulton, M. V. and L. W. Rehfield, "Free-Vibration Analysis of Composite Beams," Proceedings of American Helicopter Society National Specialists Conference, Vol. 1, pp. 36-47, Arlington, TX, 1989.
16. Hwang, S. J., and R. F. Gibson, "The Influence of Vibration Coupling on Damping of Laminated Composites," AIAA Journal, Vol. 29, No. 10, pp. 1678-1685, Oct 1991.
17. Barrett, D. J., "A Design For Improving the Structural Damping Properties of Axial Members," Proceedings of Damping 1989, WRDC-TR-89-3116, Vol. III, pp. HCB-1-HCB-20, 8-10 February 1989.
18. Rotz, C. A. and D. J. Barrett, "Cocured Damping Layers in Composite Structures," Proceedings 23rd International SAMPE Technical Conference, Vol. 23, pp. 352-362, Anaheim, CA, Oct 1991.
19. Belknap, F. M. and J. B. Kosmatka, "Vibration Suppression of Thin-Walled Composite Tubes using Embedded Viscoelastic Layers," Proceedings - Damping 1991, pp. HAC-1 - HAC-16, San Diego, CA, Feb 1991.
20. Bronowicki, A. J. and H. P. Diaz, "Analysis, Optimization, Fabrication, and Test of Composite Shells with Embedded Viscoelastic Layers," Proceedings of Damping 1989, WRDC-TR-89-3116, Vol. III, pp. GCA-1-GCA-21, 8-10 February 1989.
21. Olcott, D. D., Improved Damping in Composite Structures Through Stress Coupling, Co-cured Damping Layers, and Segmented Stiffness Layers, Ph.D. Dissertation, Brigham Young University, Salt Lake City, UT, 1992.
22. Olcott, D. D., Rotz, C. A., and D. J. Barrett, "Improved Damping in Composite Tubes Through Stress Coupling and Co-cured Damping Layers," Proceedings 23rd International SAMPE Technical Conference, Vol. 23, pp. 373-387, Anaheim, CA, Oct 1991.
23. Olcott, D. D., Rotz, C. A., and P. F. Eastman, "Improved Vibration Damping in Composite Structures Using 'Zig-Zag' Fibers and Embedded Viscoelastic Damping Layers," Proceedings 38th International SAMPE Symposium, Vol. 1, pp. 1357-1370, Anaheim, CA, May 1993.
24. Hwang, W., Park, H. C., and W. Hwang, "Tailoring of a Laminated Composite Plate Under Structural Control," Proceedings of ICCM/9: Composite Modelling and Processing Science, Madrid, Spain, Vol. 3, pp. 592-598, 12-16 July 1993.
25. Hwang, W.; Park, H. C.; and W. Hwang, "Vibration Control of Laminated Plate with Piezoelectric Sensor/Actuator: Finite Element Formulation and Modal Analysis," Journal of

Intelligent Material Systems and Structures, Vol 4, pp. 317-329, July 1993.

26. Hwang, W.; Hwang, W., and H. C. Park, "Integration of Composite Structural Design with the Intelligent System Concept," Proceedings of the 34th AIAA/ASME/ASCE/AHS/ASC Structures, Structural Dynamics, and Materials Conference, part 6 pp. 3534-3539, 1993.
27. Shen, I. Y., "Bending and Torsional Vibration Control of Composite Beams Through Intelligent Constrained-Layer Damping Treatment," Proceedings of 1995 Smart Structures and Materials Conference, San Diego, CA, Vol. 2445, pp. 110-122, Mar 1-2 1995.
28. Napolitano, K. L. and J. B. Kosmatka, "Extension-Twist Coupled Damped Composite Strut: Analytical and Experimental Evaluation," Proceedings of 1995 Smart Structures and Materials Conference, San Diego, CA, Vol. 2445, pp. 362-373, Mar 1-2 1995.
29. Humphreys, E. A., and B. W. Rosen, "Passive Damping Characteristics of Satellite Structural Components", WRDC Technical Report, WRDC-TR-89-4048, July 1989.
30. Adali, S., and V. Verijenko, "Minimum Weight Design of Symmetrical Angle-Ply Laminates Under Multiple Uncertain Loads," Journal of Structural Optimization, Vol. 9, No. 2, pp. 89-95, Apr 1995.
31. Walker, M., Adali, S., and V. Verijenko, "Optimization of Symmetric Laminates for Maximum Buckling Load Including the Effects of Bending-Twisting Coupling," Journal of Computers and Structures, Vol. 58, No. 2, pp. 313-319, Jan 1996.
32. Dracopoulos, T. N., and H. Oz, "Integrated Aeroelastic Control Optimization of Laminated Composite Lifting Surfaces," Journal of Aircraft, Vol. 29, No. 2, pp. 280-288, March-April 1992.
33. Szilard, R., Theory and Analysis of Plates, Prentice-Hall, Inc., Englewood Cliffs, NJ, 1974.
34. Fung, Y. C., Foundations of Solid Mechanics, Prentice-Hall Inc., Englewood Cliffs, NJ, 1965.
35. Meirovitch, L., Analytical Methods in Vibration, Macmillan Publishing Co. Inc., New York, NY, 1967.
36. Clark, S. K., Dynamics of Continuous Elements, Prentice Hall Inc., Englewood Cliffs, NJ, 1972.
37. Meirovitch, L., Methods of Analytical Dynamics, McGraw-Hill Publishing Company, New York, NY, 1970.
38. Crawley, E. F. and E. H. Anderson, "Detailed Models of Piezoceramic Actuation of Beams," Journal of Intelligent Material Systems and Structures, Vol. 1, pp. 4-25, Jan 1990.

39. Obal, M. W., "Vibrations Control of Flexible Structures using Piezoelectric Devices as Sensors and Actuators," Doctorate of Philosophy Dissertation at Georgia Institute of Technology, Atlanta, GA, Sept 1986.
40. Hanagud, S., Obal, M. W., and M. Meyyappa, "Electronic damping techniques and active vibration control," AIAA Journal, Vol. 23, No. 5, pp. 443-453, May 1985.
41. Crawley, E. F., and J. de Luis, "Use of Piezoelectric Actuators as Elements of Intelligent Structures," AIAA Journal, Vol. 25, No. 10, pp. 1377-1385, October 1987.
42. Hagood, N., Crawley, E. F., Luis, Javier de, and Eric H. Anderson, "Development of Integrated Components for Control of Intelligent Structures," Proceedings of the 1988 American Control Conference, Vol. 3, p 1890-6, June 1988.
43. Wadin, J. R., Vernitron Corporation - A Guide to Modern Piezoelectric Ceramics, Sales Manual, Morgan Matroc-Vernitron Division, El Toro, CA, 1994.
44. Hanagud, S., Won, C. C., and M. W. Obal, "Optimal Placement of Piezoceramic Sensors and Actuators," American Control Conference 3, pp. 1884-1889, 1988.
45. Kulkarni, G. and S. V. Hanagud, "Modeling Issues in the Vibration Control with Piezoceramic Actuators," Journal of Smart Materials and Structures, Vol 24, pp. 7-17, 1991.
46. Shames, I. H. and C. L. Dym, Energy and Finite Element Methods in Structural Mechanics, Hemisphere Publishing Corporation, Washington, 1985.
47. Wang, C., Applied Elasticity, McGraw-Hill Book Company, Inc., NY, 1953.
48. Buhariwala, K. J., "Dynamics of Viscoelastic Structures," PhD Disseration University of Toronto - Institute For Aerospace Studies, Toronto, Canada, 1986.
49. Leissa, A. W., and T. H. Young, "Extensions of the Ritz-Galerkin Method for the Forced, Damped Vibrations of Structural Elements," Proceedings of the 1984 Vibration Damping Workshop, pp. EE-2 - EE-20, 1984.
50. Flugge, W. (ed.), Handbook of Engineering Mechanics, McGraw-Hill Book Company, New York, 1962.
51. Lang, D. and L. Reithler, "Active Control of a Composite Plate: From the Specific Problem to an Optimized Solution," Proceedings of 1995 Smart Structures and Materials Conference, San Diego, CA, Vol. 2443, pp. 597-608, Mar 1-2 1995.
52. Plass, H. J., Gaines, J. H., and C. D. Newson, "Application of Reissner's Variational Principle to Cantilever Plate Deflection and Vibration Problems," Journal of Applied Mechanics, Vol 29, #1, pp. 127-135, Mar 1962.

53. Wolfram, S., Mathematica - A System for Doing Mathematics by Computer, Addison-Wesley Publishing Co., Reading, MA, 1988.
54. Bodden, D. S., and J. L. Junkins, "Eigenvalue Optimization Algorithms for Structure/Control Design Iterations," AIAA Journal of Guidance, Control and Dynamics, Vol 8 No. 6 , pp 697-706, Nov - Dec 1985.
55. Vanderplaats, Miura & Associates, Inc., Dot Users Manual Version 4.00, VMA Engineering, 1993.
56. Slater, G. L., "A Disturbance Model for the Optimization of Control/Structure Interactions for Flexible Dynamic Systems," AIAA Guidance, Navigation and Control Conference, Minneapolis, NM, August 15 - 17, 1988, pp 57-63; AIAA Paper 88-4058-CP.
57. Valentino, J., Fortran for Technologists and Engineers, Holt, Rinehart, and Winston, Chicago, IL, 1985.
58. Carlsson, L. A. and R. B. Pipes, Experimental Characterization of Advanced Composite Materials, Prentice-Hall, Inc., Englewood Cliffs, NJ, 1987.

Appendix A

The information in this appendix will show the development of how the kinetic, strain, and work energy expressions are integrated by parts. In the energy expressions there are four different integrations to be performed for the dependent variables. The first involves only one derivative with respect to x on the variation:

$$\begin{aligned} \int_0^a A(x, t) \delta B(x, t) ,_x = A(x, t) \delta B(x, t) \Big|_0^a \\ - \int_0^a A(x, t) ,_x \delta B(x, t) dx \end{aligned} \quad (158)$$

This integral contributes to the x boundary condition and the equation of motion.

The second integral to be performed involves two derivatives with respect to x on the variation.

$$\begin{aligned} \int_0^a A(x, t) \delta B(x, t) ,_{xx} = A(x, t) \delta B(x, t) ,_x \Big|_0^a \\ - A(x, t) ,_x \delta B(x, t) \Big|_0^a + \int_0^a A(x, t) ,_{xx} \delta B(x, t) dx \end{aligned} \quad (159)$$

This integral contributes to the x boundary conditions and the equation of motion.

The third integral to be performed involves one derivative with respect to t on the variation.

$$\begin{aligned}
\int_{t_1}^{t_2} \int_0^a A(x, t) \delta \dot{B}(x, t) dx dt &= \int_0^a A(x, t) \delta B(x, t) \Big|_{t_1}^{t_2} dx \\
&- \int_{t_1}^{t_2} \int_0^a \dot{A}(x, t) \delta B(x, t) dx dt
\end{aligned}
\tag{160}$$

This integral contributes to both the initial conditions and the equation of motion.

The fourth integral to be performed involves one derivative with respect to t and one with respect to x on the variation.

$$\begin{aligned}
\int_{t_1}^{t_2} \int_0^a A(x, t) \delta \dot{B}(x, t) ,_x dx dt &= \int_0^a A(x, t) \delta B(x, t) ,_x \Big|_{t_1}^{t_2} dx \\
&- \int_{t_1}^{t_2} \dot{A}(x, t) \delta B(x, t) \Big|_0^a dt + \int_{t_1}^{t_2} \int_0^a \dot{A}(x, t) ,_x \delta B(x, t) dx dt
\end{aligned}
\tag{161}$$

This integral contributes to both the initial conditions and the equation of motion.

The optimization program is divided up into many different parts. There is an overall shell program which calls the various subroutines to perform the optimization. Figure 31 shows a flow chart diagramming this optimization program.

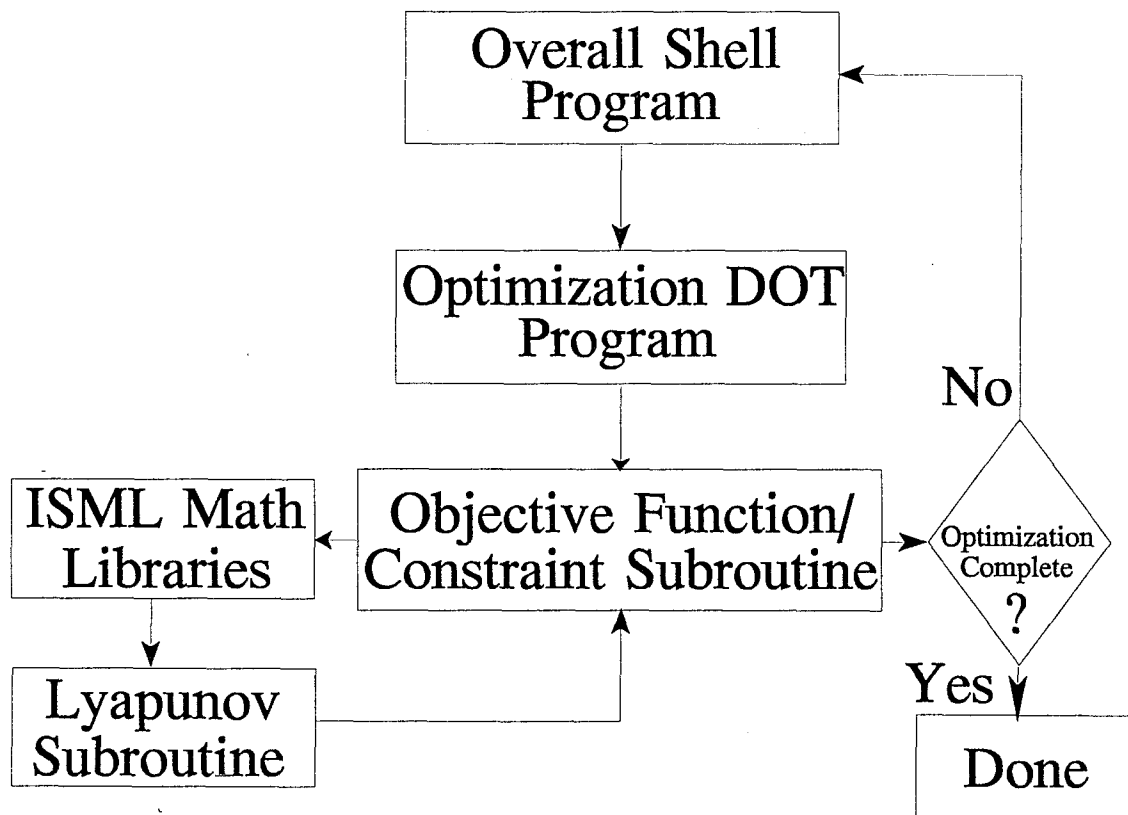


Figure 31 Optimization Program Flow Chart

This program is:

```
c  Optimization Program
c
c  Define Constants Make All Variables Double Precision
c
c  DOUBLE PRECISION X(14), OBJ, XL(14), XU(14), G(2),
c  * WK(2000), RPRM(200)
c
c  DIMENSION IWK(2000), IPRM(200)
c
c  Define NRWK, NRIWK
c
c  NRWK = 2000
c  NRIWK = 2000
c
c  Zero RPRM And IPRM
c
c  DO 10 I = 1,200
c      RPRM(I) = 0.0D0
10  IPRM(I) = 0
c
c  Define Method, NDV, NCON
c  Sequential Quadratic Programming Method
c
c  METHOD = 1
c
c  Design Variables
c
c  NDV = 14
c
c  2 Constraints
c
c  NCON = 2
c
c  Define Bounds and Initial Design For Theta's
c
c  DO 20 K = 1,10
c      X(K) = 1.570796327D0
c
c  Lower Bounds
c
c  XL(K) = -1.570796327D0
c
c
```

```

20    XU(K) = 1.570796327D0
c
c    Define Bounds and Initial Design For Other Variables
c
c
c    X(11) = 4 8.D0
c    X(12) = 16.D0
c    X(13) = .00001D0
c    X(14) = .00001D0
c
c    Lower Bounds
c
c    XL(11) = 1.25D0
c    XL(12) = 1.25D0
c    XL(13) = 0.0D0
c    XL(14) = 0.0D0
c
c    Upper Bounds
c
c    XU(11) = 22.75D0
c    XU(12) = 22.75D0
c    XU(13) = 400000.D0
c    XU(14) = 400000.D0
c
c    Define IPRINT, MINMAX, INFO
c
c    Print Control
c
c    IPRINT = 3
c
c    MINIMIZE
c
c    MINMAX = -1
c
c    Initialize INFO To Zero
c
c    INFO = 0
c
c    Optimize
c
100 CALL DOT (INFO, METHOD, IPRINT, NDV, NCON, X, XL, XU, OBJ,
* MINMAX, G, RPRM, IPRM, WK, NRWK, IWK, NRIWK)
c
c    Finished
c
c    IF(INFO.EQ.0) STOP

```



```

c
c Evaluate Objective and Constraint

c
c Call Subprog(OBJ, X, G)

c
c Go Continue with Optimization
c
c GO TO 100
c
c end

```

The first subroutine called is the optimization program DOT. This program is too long to list in this document. The second subroutine call evaluates the objective function and the constraints. This program is:

```

SUBROUTINE Subprog(OBJ, X, G)
c
c Subroutine to Calculate Objective Function
c
c Define Constants Make All Variables Double Precision
c
c INTEGER LDSF,LDMF,LDEVEC,N,K,NOUT,LDS,LDM,IROW(8),NA,NDIM
c
c PARAMETER (LDM=4, LDMINV=4, LDS=4, LDT=4, NCIM=4, NCS=4, NCT=4,
* NRIM=4, NRS=4, NRT=4, N=4, LDT1=4, NCT1=2, NRT1=4, LDT2=4,
* NCT2=2, NRT2=4, LDT3=4, NCT3=1, NRT3=4, LDT4=4, NCT4=1, NRT4=4,
* LDG=2, NCG=2, NRG=2, LDC=2, NCC=8, NRC=2, LDT5=2, NCT5=8,
* NRT5=2, LDB1=8, NCB1=2, NRB1=8, LDT6=8, NCT6=8, NRT6=8, LDSF=4,
* LDMF=4, LDEVEC=4, NCD=1, NRD=1, LDD=1, NCH=1, NRH=8, LDH=8,
* NCB=8, NRB=8, LDB=8, NCB=8, NRBD=8, LDBD=8, NCA=8, NRA=8,
* LDA=8, NRASYS=8, NCASYS=8, LDASYS=8, NCW1=8, NRW1=1, LDW1=1,
* NCW2=8, NRW2=1, LDW2=1, NCT8=8, NRT8=1, LDT8=1, NCT11=8,
* NRT11=1, LDT11=1, NCT9=1, NRT9=1, LDT9=1, NCXRMS=1, NRXRMS=8,
* LDXRMS=8, NRT10=1, NCT10=1, LDT10=1, NRT12=2, NCT12=8, LDT12=2,
* NRT13=2, NCT13=8, LDT13=2, NRT14=2, NCT14=2, LDT14=2, NRT15=2,
* NCT15=2, LDT15=2, NCW3=8, NRW3=1, LDW3=1)
c
c DOUBLE PRECISION E1, E2, nu12, nu21, g12, rho, e31, actloc,
* wd, C11e, Rf, A1(4), A2(4), A3(4), A4(4), d111, d112, d113, d11,
* d161, d162, d163, d164, d16, d661, d662, d663, d66,
* mfree(LDMF,N), sfree(LDSF,N), AMACH, BETA(N), mass(LDM,LDM),
* invmas(LDMINV,LDMINV), stiff(LDS,NCS), KD, KS, d31,
* GAIN(LDG,NCG), xd, Ls, Asys(LDASYS,NCASYS), B1(LDB1,NCB1),
* C(LDC,NCC), H(8,1), A(LDA,NCA), TEMP(LDT,NCT), TEMP1(LDT1,NCT1),
* TEMP2(LDT2,NCT2), TEMP3(LDT3,NCT3), TEMP4(LDT4,NCT4),

```

```

* TEMP5(LDT5, NCT5), TEMP6(LDT6,NCT6), X(14), G(2), OBJ,
* BETA1(N), B(LDB,NCB), BD(LDBD,NCBD), D(LDD, NCD),
* TEMP7(LDH, NCH), W1(LDW1,NCW1), W2(LDW2,NCW2), TEMP8(LDT8,NCT8),
* ZETA, TEMP9(LDT9,NCT9), TEMP10(LDT10, NCT10),
* TEMP11(LDT11, NCT11), TEMP12(LDT12,NCT12), TEMP13(LDT13, NCT13),
* thick,TEMP14(LDT14, NCT14), TEMP15(LDT15, NCT15), W3(LDW3,NCW3)
c
DOUBLE COMPLEX ALPHA(N), EVAL(N), EVEC(LDEVEC,N), ALPHA1(N),
* EVAL1(N), EVEC1(LDEVEC,N)
c
EXTERNAL DMRRRR, AMACH, GPIGR, DGVCRG, UMACH, DWRRRN
c
NA = 8
NDIM = 8
c
Define Composite Constants
c
E1 = 22691551.44D0
E2 = 1429537.875D0
g12 = 868816.825D0
nu12 = .305616286D0
nu21 = .019253424D0
rho = .052598707D0
c
Weighting Matrices for the Performance Index
c
ZETA = .5D0
c
Location of Disturbance Torque
c
xd = 24.D0
c
Strength of the Disturbance Torque
c
D(1,1) = 1.D0
c
Define PZT Actuator and Sensor Constants
c
wd = 1.5D0
Rf = 1.D+7
C11e = 8.844D+06
Ls = 2.5D0
actloc = .025D0
d31 = 6.7323D-9
e31 = C11e*d31

```

KS = -wd*actloc*d31*C11e*Rf
 KD = e31*wd*actloc

c

c Evaluate Composite Constants

c

d111 = 2.54167D-6*E1*Cos(X(1))**4.D0/(1.D0-nu12*nu21) +
 * 2.54167D-6*E1*Cos(X(10))**4.D0/(1.D0-nu12*nu21)+
 * 1.54167D-6*E1*Cos(X(2))**4.D0/(1.D0-nu12*nu21)+
 * 7.91667D-7*E1*Cos(X(3))**4.D0/(1.D0-nu12*nu21)+
 * 2.91667D-7*E1*Cos(X(4))**4.D0/(1.D0-nu12*nu21)+
 * 4.16667D-8*E1*Cos(X(5))**4.D0/(1.D0-nu12*nu21)+
 * 4.16667D-8*E1*Cos(X(6))**4.D0/(1.D0-nu12*nu21)+
 * 2.91667D-7*E1*Cos(X(7))**4.D0/(1.D0-nu12*nu21)+
 * 7.91667D-7*E1*Cos(X(8))**4.D0/(1.D0-nu12*nu21)+
 * 1.54167D-6*E1*Cos(X(9))**4.D0/(1.D0-nu12*nu21)+
 * 0.000010166666666666667D0*g12*Cos(X(1))**2*Sin(X(1))**2.D0+
 * 5.08333D-6*E2*nu12*Cos(X(1))**2.D0*Sin(X(1))**2.D0/(1.D0-nu12*
 * nu21)+2.54167D-6*E2*Sin(X(1))**4.D0/(1.D0-nu12*nu21)+
 * 0.000010166666666666667D0*g12*Cos(X(10))**2.D0*Sin(X(10))**2.D0+
 * 5.08333D-6*E2*nu12*Cos(X(10))**2.D0*
 * Sin(X(10))**2.D0/(1.D0-nu12*nu21)+
 * 2.54167D-6*E2*Sin(X(10))**4.D0/(1.D0- nu12*nu21)

c

d112 = 6.16667D-6*g12*Cos(X(2))**2.D0*Sin(X(2))**2.D0 +
 * 3.08333D-6*E2*nu12*Cos(X(2))**2.D0*Sin(X(2))**2.D0/(1.D0-nu12*
 * nu21)+1.54167D-6*E2*Sin(X(2))**4.D0/(1.D0- nu12*nu21) +
 * 3.16667D-6*g12*Cos(X(3))**2.D0*Sin(X(3))**2.D0 +
 * 1.58333D-6*E2*nu12*Cos(X(3))**2.D0*Sin(X(3))**2.D0/(1.D0-nu12*
 * nu21)+7.91667D-7*E2*Sin(X(3))**4.D0/(1.D0- nu12*nu21) +
 * 1.16667D-6*g12*Cos(X(4))**2.D0*Sin(X(4))**2.D0 +
 * 5.83333D-7*E2*nu12*Cos(X(4))**2.D0*Sin(X(4))**2.D0/(1.D0-nu12*
 * nu21)+2.91667D-7*E2*Sin(X(4))**4.D0/(1.D0- nu12*nu21) +
 * 1.66667D-7*g12*Cos(X(5))**2.D0*Sin(X(5))**2.D0 +
 * 8.33333D-8*E2*nu12*Cos(X(5))**2.D0*Sin(X(5))**2.D0/(1.D0-nu12*
 * nu21)+4.16667D-8*E2*Sin(X(5))**4.D0/(1.D0- nu12*nu21) +
 * 1.66667D-7*g12*Cos(X(6))**2.D0*Sin(X(6))**2.D0 +
 * 8.33333D-8*E2*nu12*Cos(X(6))**2.D0*Sin(X(6))**2.D0/(1.D0-nu12*
 * nu21)

c

d113 = 4.16667D-8*E2*Sin(X(6))**4.D0/(1.D0- nu12*nu21) +
 * 1.16667D-6*g12*Cos(X(7))**2.D0*Sin(X(7))**2.D0 +
 * 5.83333D-7*E2*nu12*Cos(X(7))**2.D0*Sin(X(7))**2.D0/(1.D0-nu12*
 * nu21)+2.91667D-7*E2*Sin(X(7))**4.D0/(1.D0- nu12*nu21) +
 * 3.16667D-6*g12*Cos(X(8))**2.D0*Sin(X(8))**2.D0 +
 * 1.58333D-6*E2*nu12*Cos(X(8))**2.D0*Sin(X(8))**2.D0/(1.D0-nu12*

* nu21)+7.91667D-7*E2*Sin(X(8))*3.D0/(1.D0- nu12*nu21) +
 * 6.16667D-6*g12*Cos(X(9))*2.D0*Sin(X(9))*2.D0 +
 * 3.08333D-6*E2*nu12*Cos(X(9))*2.D0*Sin(X(9))*2.D0/(1.D0-nu12*
 * nu21)+1.54167D-6*E2*Sin(X(9))*3.D0/(1.D0- nu12*nu21)

c

d11 = d111 + d112 + d113

c

d161 = -5.08333D-6*g12*Cos(X(1))*3.D0*Sin(X(1)) +
 * 2.54167D-6*E1*Cos(X(1))*3.D0*Sin(X(1))/(1.D0- nu12*nu21) -
 * 2.54167D-6*E2*nu12*Cos(X(1))*3.D0*Sin(X(1))/(1.D0-nu12*nu21)+
 * 5.08333D-6*g12*Cos(X(1))*Sin(X(1))*3.D0 -
 * 2.54167D-6*E2*Cos(X(1))*Sin(X(1))*3.D0/(1.D0-nu12*nu21) +
 * 2.54167D-6*E2*nu12*Cos(X(1))*Sin(X(1))*3.D0/(1.D0-nu12*nu21)-
 * 5.08333D-6*g12*Cos(X(10))*3.D0*Sin(X(10)) +
 * 2.54167D-6*E1*Cos(X(10))*3.D0*Sin(X(10))/(1.D0-nu12*nu21)-
 * 2.54167D-6*E2*nu12*Cos(X(10))*3.D0*Sin(X(10))/(1.D0-nu12*nu21)+
 * 5.08333D-6*g12*Cos(X(10))*Sin(X(10))*3.D0 -
 * 2.54167D-6*E2*Cos(X(10))*Sin(X(10))*3.D0/(1.D0-nu12*nu21) +
 * 2.54167D-6*E2*nu12*Cos(X(10))*Sin(X(10))*3.D0/(1.D0-nu12*nu21)-
 * 3.08333D-6*g12*Cos(X(2))*3.D0*Sin(X(2)) +
 * 1.54167D-6*E1*Cos(X(2))*3.D0*Sin(X(2))/(1.D0-nu12*nu21) -
 * 1.54167D-6*E2*nu12*Cos(X(2))*3.D0*Sin(X(2))/(1.D0-nu12*nu21)+
 * 3.08333D-6*g12*Cos(X(2))*Sin(X(2))*3.D0 -
 * 1.54167D-6*E2*Cos(X(2))*Sin(X(2))*3.D0/(1.D0-nu12*nu21)

c

d162 = 1.54167D-6*E2*nu12*Cos(X(2))*Sin(X(2))*3.D0/(1.D0-nu12*
 * nu21)-1.58333D-6*g12*Cos(X(3))*3.D0*Sin(X(3)) +
 * 7.91667D-7*E1*Cos(X(3))*3.D0*Sin(X(3))/(1.D0- nu12*nu21) -
 * 7.91667D-7*E2*nu12*Cos(X(3))*3.D0*Sin(X(3))/(1.D0-nu12*nu21)+
 * 1.58333D-6*g12*Cos(X(3))*Sin(X(3))*3.D0 -
 * 7.91667D-7*E2*Cos(X(3))*Sin(X(3))*3.D0/(1.D0- nu12*nu21) +
 * 7.91667D-7*E2*nu12*Cos(X(3))*Sin(X(3))*3.D0/(1.D0-nu12*nu21)-
 * 5.83333D-7*g12*Cos(X(4))*3.D0*Sin(X(4)) +
 * 2.91667D-7*E1*Cos(X(4))*3.D0*Sin(X(4))/(1.D0- nu12*nu21) -
 * 2.91667D-7*E2*nu12*Cos(X(4))*3.D0*Sin(X(4))/(1.D0-nu12*nu21)+
 * 5.83333D-7*g12*Cos(X(4))*Sin(X(4))*3.D0 -
 * 2.91667D-7*E2*Cos(X(4))*Sin(X(4))*3.D0/(1.D0- nu12*nu21) +
 * 2.91667D-7*E2*nu12*Cos(X(4))*Sin(X(4))*3.D0/(1.D0-nu12*nu21)-
 * 8.33333D-8*g12*Cos(X(5))*3.D0*Sin(X(5)) +
 * 4.16667D-8*E1*Cos(X(5))*3.D0*Sin(X(5))/(1.D0- nu12*nu21) -
 * 4.16667D-8*E2*nu12*Cos(X(5))*3.D0*Sin(X(5))/(1.D0-nu12*nu21)+
 * 8.33333D-8*g12*Cos(X(5))*Sin(X(5))*3.D0 -
 * 4.16667D-8*E2*Cos(X(5))*Sin(X(5))*3.D0/(1.D0- nu12*nu21) +
 * 4.16667D-8*E2*nu12*Cos(X(5))*Sin(X(5))*3.D0/(1.D0-nu12*nu21)

c

$$\begin{aligned}
d163 = & -8.33333D-8*g12*\cos(X(6))^3.D0*\sin(X(6)) + \\
& * 4.16667D-8*E1*\cos(X(6))^3.D0*\sin(X(6))/(1.D0-\nu12*\nu21) - \\
& * 4.16667D-8*E2*\nu12*\cos(X(6))^3.D0*\sin(X(6))/(1.D0-\nu12*\nu21)+ \\
& * 8.33333D-8*g12*\cos(X(6))*\sin(X(6))^3.D0 - \\
& * 4.16667D-8*E2*\cos(X(6))*\sin(X(6))^3.D0/(1.D0-\nu12*\nu21) + \\
& * 4.16667D-8*E2*\nu12*\cos(X(6))*\sin(X(6))^3.D0/(1.D0-\nu12*\nu21)- \\
& * 5.83333D-7*g12*\cos(X(7))^3.D0*\sin(X(7)) + \\
& * 2.91667D-7*E1*\cos(X(7))^3.D0*\sin(X(7))/(1.D0-\nu12*\nu21) - \\
& * 2.91667D-7*E2*\nu12*\cos(X(7))^3.D0*\sin(X(7))/(1.D0-\nu12*\nu21)+ \\
& * 5.83333D-7*g12*\cos(X(7))*\sin(X(7))^3.D0 - \\
& * 2.91667D-7*E2*\cos(X(7))*\sin(X(7))^3.D0/(1.D0-\nu12*\nu21) + \\
& * 2.91667D-7*E2*\nu12*\cos(X(7))*\sin(X(7))^3.D0/(1.D0-\nu12*\nu21)- \\
& * 1.58333D-6*g12*\cos(X(8))^3.D0*\sin(X(8)) + \\
& * 7.91667D-7*E1*\cos(X(8))^3.D0*\sin(X(8))/(1.D0-\nu12*\nu21) - \\
& * 7.91667D-7*E2*\nu12*\cos(X(8))^3.D0*\sin(X(8))/(1.D0-\nu12*\nu21)+ \\
& * 1.58333D-6*g12*\cos(X(8))*\sin(X(8))^3.D0 - \\
& * 7.91667D-7*E2*\cos(X(8))*\sin(X(8))^3.D0/(1.D0-\nu12*\nu21) + \\
& * 7.91667D-7*E2*\nu12*\cos(X(8))*\sin(X(8))^3.D0/(1.D0-\nu12*\nu21)
\end{aligned}$$

c

$$\begin{aligned}
d164 = & -3.08333D-6*g12*\cos(X(9))^3.D0*\sin(X(9)) + \\
& * 1.54167D-6*E1*\cos(X(9))^3.D0*\sin(X(9))/(1.D0-\nu12*\nu21) - \\
& * 1.54167D-6*E2*\nu12*\cos(X(9))^3.D0*\sin(X(9))/(1.D0-\nu12*\nu21)+ \\
& * 3.08333D-6*g12*\cos(X(9))*\sin(X(9))^3.D0 - \\
& * 1.54167D-6*E2*\cos(X(9))*\sin(X(9))^3.D0/(1.D0-\nu12*\nu21)+ \\
& * 1.54167D-6*E2*\nu12*\cos(X(9))*\sin(X(9))^3.D0/(1.D0-\nu12*\nu21)
\end{aligned}$$

c

$$d16 = d161 + d162 + d163 + d164$$

c

$$\begin{aligned}
d661 = & 2.54167D-6*g12*\cos(X(1))^4.D0 + \\
& * 2.54167D-6*g12*\cos(X(10))^4.D0 + \\
& * 1.54167D-6*g12*\cos(X(2))^4.D0+7.91667D-7*g12*\cos(X(3))^4.D0+ \\
& * 2.91667D-7*g12*\cos(X(4))^4.D0+4.16667D-8*g12*\cos(X(5))^4.D0+ \\
& * 4.16667D-8*g12*\cos(X(6))^4.D0+2.91667D-7*g12*\cos(X(7))^4.D0+ \\
& * 7.91667D-7*g12*\cos(X(8))^4.D0+1.54167D-6*g12*\cos(X(9))^4.D0- \\
& * 5.08333D-6*g12*\cos(X(1))^2.D0*\sin(X(1))^2.D0 + \\
& * 2.54167D-6*E1*\cos(X(1))^2.D0*\sin(X(1))^2.D0/(1.D0-\nu12*\nu21)+ \\
& * 2.54167D-6*E2*\cos(X(1))^2.D0*\sin(X(1))^2.D0/(1.D0-\nu12*\nu21)- \\
& * 5.08333D-6*E2*\nu12*\cos(X(1))^2.D0* \\
& * \sin(X(1))^2.D0/(1.D0-\nu12*\nu21)+2.54167D-6*g12*\sin(X(1))^4.D0- \\
& * 5.08333D-6*g12*\cos(X(10))^2.D0*\sin(X(10))^2.D0 + \\
& * 2.54167D-6*E1*\cos(X(10))^2.D0*\sin(X(10))^2.D0/(1.D0-\nu12*\nu21)+ \\
& * 2.54167D-6*E2*\cos(X(10))^2.D0*\sin(X(10))^2.D0/(1.D0-\nu12*\nu21)- \\
& * 5.08333D-6*E2*\nu12*\cos(X(10))^2.D0* \\
& * \sin(X(10))^2.D0/(1.D0-\nu12*\nu21)+2.54167D-6*g12* \\
& * \sin(X(10))^4.D0-3.08333D-6*g12*\cos(X(2))^2.D0*\sin(X(2))^2.D0+
\end{aligned}$$

$$* 1.54167D-6 * E1 * \cos(X(2))^{**2.D0} * \sin(X(2))^{**2.D0} / (1.D0 - \text{nu}12 * \text{nu}21)$$

c

$$\begin{aligned} d662 = & 1.54167D-6 * E2 * \cos(X(2))^{**2.D0} * \\ & * \sin(X(2))^{**2.D0} / (1.D0 - \text{nu}12 * \text{nu}21) - \\ & * 3.08333D-6 * E2 * \text{nu}12 * \cos(X(2))^{**2.D0} * \sin(X(2))^{**2.D0} / (1.D0 - \text{nu}12 * \\ & * \text{nu}21) + 1.54167D-6 * g12 * \sin(X(2))^{**4.D0} - \\ & * 1.58333D-6 * g12 * \cos(X(3))^{**2.D0} * \sin(X(3))^{**2.D0} + \\ & * 7.91667D-7 * E1 * \cos(X(3))^{**2.D0} * \sin(X(3))^{**2.D0} / (1.D0 - \text{nu}12 * \text{nu}21) + \\ & * 7.91667D-7 * E2 * \cos(X(3))^{**2.D0} * \sin(X(3))^{**2.D0} / (1.D0 - \text{nu}12 * \text{nu}21) - \\ & * 1.58333D-6 * E2 * \text{nu}12 * \cos(X(3))^{**2.D0} * \\ & * \sin(X(3))^{**2.D0} / (1.D0 - \text{nu}12 * \text{nu}21) + 7.91667D-7 * g12 * \sin(X(3))^{**4.D0} - \\ & * 5.83333D-7 * g12 * \cos(X(4))^{**2.D0} * \sin(X(4))^{**2.D0} + \\ & * 2.91667D-7 * E1 * \cos(X(4))^{**2.D0} * \sin(X(4))^{**2.D0} / (1.D0 - \text{nu}12 * \text{nu}21) + \\ & * 2.91667D-7 * E2 * \cos(X(4))^{**2.D0} * \sin(X(4))^{**2.D0} / (1.D0 - \text{nu}12 * \text{nu}21) - \\ & * 5.83333D-7 * E2 * \text{nu}12 * \cos(X(4))^{**2.D0} * \\ & * \sin(X(4))^{**2.D0} / (1.D0 - \text{nu}12 * \text{nu}21) + 2.91667D-7 * g12 * \sin(X(4))^{**4.D0} - \\ & * 8.33333D-8 * g12 * \cos(X(5))^{**2.D0} * \sin(X(5))^{**2.D0} + \\ & * 4.16667D-8 * E1 * \cos(X(5))^{**2.D0} * \sin(X(5))^{**2.D0} / (1.D0 - \text{nu}12 * \text{nu}21) + \\ & * 4.16667D-8 * E2 * \cos(X(5))^{**2.D0} * \sin(X(5))^{**2.D0} / (1.D0 - \text{nu}12 * \text{nu}21) - \\ & * 8.33333D-8 * E2 * \text{nu}12 * \cos(X(5))^{**2.D0} * \\ & * \sin(X(5))^{**2.D0} / (1.D0 - \text{nu}12 * \text{nu}21) + 4.16667D-8 * g12 * \sin(X(5))^{**4.D0} \end{aligned}$$

c

$$\begin{aligned} d663 = & -8.33333D-8 * g12 * \cos(X(6))^{**2.D0} * \sin(X(6))^{**2.D0} + \\ & * 4.16667D-8 * E1 * \cos(X(6))^{**2.D0} * \sin(X(6))^{**2.D0} / (1.D0 - \text{nu}12 * \text{nu}21) + \\ & * 4.16667D-8 * E2 * \cos(X(6))^{**2.D0} * \sin(X(6))^{**2.D0} / (1.D0 - \text{nu}12 * \text{nu}21) - \\ & * 8.33333D-8 * E2 * \text{nu}12 * \cos(X(6))^{**2.D0} * \\ & * \sin(X(6))^{**2.D0} / (1.D0 - \text{nu}12 * \text{nu}21) + 4.16667D-8 * g12 * \sin(X(6))^{**4.D0} - \\ & * 5.83333D-7 * g12 * \cos(X(7))^{**2.D0} * \sin(X(7))^{**2.D0} + \\ & * 2.91667D-7 * E1 * \cos(X(7))^{**2.D0} * \sin(X(7))^{**2.D0} / (1.D0 - \text{nu}12 * \text{nu}21) + \\ & * 2.91667D-7 * E2 * \cos(X(7))^{**2.D0} * \sin(X(7))^{**2.D0} / (1.D0 - \text{nu}12 * \text{nu}21) - \\ & * 5.83333D-7 * E2 * \text{nu}12 * \cos(X(7))^{**2.D0} * \\ & * \sin(X(7))^{**2.D0} / (1.D0 - \text{nu}12 * \text{nu}21) + 2.91667D-7 * g12 * \sin(X(7))^{**4.D0} - \\ & * 1.58333D-6 * g12 * \cos(X(8))^{**2.D0} * \sin(X(8))^{**2.D0} + \\ & * 7.91667D-7 * E1 * \cos(X(8))^{**2.D0} * \sin(X(8))^{**2.D0} / (1.D0 - \text{nu}12 * \text{nu}21) + \\ & * 7.91667D-7 * E2 * \cos(X(8))^{**2.D0} * \sin(X(8))^{**2.D0} / (1.D0 - \text{nu}12 * \text{nu}21) - \\ & * 1.58333D-6 * E2 * \text{nu}12 * \cos(X(8))^{**2.D0} * \\ & * \sin(X(8))^{**2.D0} / (1.D0 - \text{nu}12 * \text{nu}21) + 7.91667D-7 * g12 * \sin(X(8))^{**4.D0} - \\ & * 3.08333D-6 * g12 * \cos(X(9))^{**2.D0} * \sin(X(9))^{**2.D0} + \\ & * 1.54167D-6 * E1 * \cos(X(9))^{**2.D0} * \sin(X(9))^{**2.D0} / (1.D0 - \text{nu}12 * \text{nu}21) + \\ & * 1.54167D-6 * E2 * \cos(X(9))^{**2.D0} * \sin(X(9))^{**2.D0} / (1.D0 - \text{nu}12 * \text{nu}21) - \\ & * 3.08333D-6 * E2 * \text{nu}12 * \cos(X(9))^{**2.D0} * \\ & * \sin(X(9))^{**2.D0} / (1.D0 - \text{nu}12 * \text{nu}21) + 1.54167D-6 * g12 * \sin(X(9))^{**4.D0} \end{aligned}$$

c

$$d66 = d661 + d662 + d663$$

c

```

c   Calculate The Mass (mfree) And Stiffness (sfree) Matrices For The
c   Free Motion System
c
c       Mass Matrix
c
mfree(1,1) = 1.08845D0*rho
mfree(1,2) = 0.D0
mfree(1,3) = 2.76282D0*rho
mfree(1,4) = 0.D0
mfree(2,1) = mfree(1,2)
mfree(2,2) = 0.362874D0*rho
mfree(2,3) = 0.D0
mfree(2,4) = 0.921084D0*rho
mfree(3,1) = mfree(1,3)
mfree(3,2) = mfree(2,3)
mfree(3,3) = 7.20001D0*rho
mfree(3,4) = 0.D0
mfree(4,1) = mfree(1,4)
mfree(4,2) = mfree(2,4)
mfree(4,3) = mfree(3,4)
mfree(4,4) = 2.40038D0*rho

c
c       Stiffness Matrix
c
sfree(1,1) = 0.000880796902434194D0*d11
sfree(1,2) = -0.00856736D0*d16
sfree(1,3) = 0.001495287262745941D0*d11
sfree(1,4) = -0.0228463D0*d16
sfree(2,1) = sfree(1,2)
sfree(2,2) = 0.0002935989674780654D0*d11+0.205617D0*d66
sfree(2,3) = 0.02284630648400314D0*d16
sfree(2,4) = 0.0004984290875819803D0*d11+0.349066D0*d66
sfree(3,1) = sfree(1,3)
sfree(3,2) = sfree(2,3)
sfree(3,3) = 0.01409275043894711D0*d11
sfree(3,4) = 0.D0
sfree(4,1) = sfree(1,4)
sfree(4,2) = sfree(2,4)
sfree(4,3) = sfree(3,4)
sfree(4,4) = 0.004697583479649038D0*d11 + 0.822467D0*d66

c
c   Call a Subroutine Program Which Evaluates The Eigenvalues and
c   Eigenvectors For The Free Motion System
c
CALL DGVCRG (N, sfree, LDSF, mfree, LDMF, ALPHA, BETA, EVEC,

```

```

* LDEVEC)
c
DO 10 K=1,N
  IF (BETA(K) .NE. 0.0) THEN
    EVAL(K) = ALPHA(K)/BETA(K)
  ELSE
    EVAL(K) = AMACH(2)
  END IF
10 CONTINUE
c
A1(1) = EVEC(1,1)/(EVEC(1,1)**2.D0+EVEC(2,1)**2.D0+
* EVEC(3,1)**2.D0+EVEC(4,1)**2.D0)**.5D0
c
A1(2) = EVEC(2,1)/(EVEC(1,1)**2.D0+EVEC(2,1)**2.D0+
* EVEC(3,1)**2.D0+EVEC(4,1)**2.D0)**.5D0
c
A1(3) = EVEC(3,1)/(EVEC(1,1)**2.D0+EVEC(2,1)**2.D0+
* EVEC(3,1)**2.D0+EVEC(4,1)**2.D0)**.5D0
c
A1(4) = EVEC(4,1)/(EVEC(1,1)**2.D0+EVEC(2,1)**2.D0+
* EVEC(3,1)**2.D0+EVEC(4,1)**2.D0)**.5D0
c
A2(1) = EVEC(1,2)/(EVEC(1,2)**2.D0+EVEC(2,2)**2.D0+
* EVEC(3,2)**2.D0+EVEC(4,2)**2.D0)**.5D0
c
A2(2) = EVEC(2,2)/(EVEC(1,2)**2.D0+EVEC(2,2)**2.D0+
* EVEC(3,2)**2.D0+EVEC(4,2)**2.D0)**.5D0
c
A2(3) = EVEC(3,2)/(EVEC(1,2)**2.D0+EVEC(2,2)**2.D0+
* EVEC(3,2)**2.D0+EVEC(4,2)**2.D0)**.5D0
c
A2(4) = EVEC(4,2)/(EVEC(1,2)**2.D0+EVEC(2,2)**2.D0+
* EVEC(3,2)**2.D0+EVEC(4,2)**2.D0)**.5D0
c
A3(1) = EVEC(1,3)/(EVEC(1,3)**2.D0+EVEC(2,3)**2.D0+
* EVEC(3,3)**2.D0+EVEC(4,3)**2.D0)**.5D0
c
A3(2) = EVEC(2,3)/(EVEC(1,3)**2.D0+EVEC(2,3)**2.D0+
* EVEC(3,3)**2.D0+EVEC(4,3)**2.D0)**.5D0
c
A3(3) = EVEC(3,3)/(EVEC(1,3)**2.D0+EVEC(2,3)**2.D0+
* EVEC(3,3)**2.D0+EVEC(4,3)**2.D0)**.5D0
c
A3(4) = EVEC(4,3)/(EVEC(1,3)**2.D0+EVEC(2,3)**2.D0+
* EVEC(3,3)**2.D0+EVEC(4,3)**2.D0)**.5D0

```


c

$$A4(1) = \text{EVEC}(1,4)/(\text{EVEC}(1,4)**2.\text{D}0+\text{EVEC}(2,4)**2.\text{D}0+ \\ * \text{EVEC}(3,4)**2.\text{D}0+\text{EVEC}(4,4)**2.\text{D}0)**2.\text{D}0$$

c

$$A4(2) = \text{EVEC}(2,4)/(\text{EVEC}(1,4)**2.\text{D}0+\text{EVEC}(2,4)**2.\text{D}0+ \\ * \text{EVEC}(3,4)**2.\text{D}0+\text{EVEC}(4,4)**2.\text{D}0)**2.\text{D}0$$

c

$$A4(3) = \text{EVEC}(3,4)/(\text{EVEC}(1,4)**2.\text{D}0+\text{EVEC}(2,4)**2.\text{D}0+ \\ * \text{EVEC}(3,4)**2.\text{D}0+\text{EVEC}(4,4)**2.\text{D}0)**2.\text{D}0$$

c

$$A4(4) = \text{EVEC}(4,4)/(\text{EVEC}(1,4)**2.\text{D}0+\text{EVEC}(2,4)**2.\text{D}0+ \\ * \text{EVEC}(3,4)**2.\text{D}0+\text{EVEC}(4,4)**2.\text{D}0)**2.\text{D}0$$

c

Calculate The Mass And Stiffness Matrices For The Forced Motion
 System

c

c

c

Stiffness Matrix

c

$$\text{stiff}(1,1) = 0.000880796902434194\text{D}0*\text{A1}(1)**2.\text{D}0*\text{d11} + \\ * 0.0002935989674780654\text{D}0*\text{A1}(2)**2.\text{D}0*\text{d11} + \\ * 0.00299057452549188\text{D}0*\text{A1}(1)*\text{A1}(3)*\text{d11} + \\ * 0.01409275043894711\text{D}0*\text{A1}(3)**2.\text{D}0*\text{d11} + \\ \\ * 0.000996858175163961\text{D}0*\text{A1}(2)*\text{A1}(4)*\text{d11} + \\ * 0.004697583479649034\text{D}0*\text{A1}(4)**2.\text{D}0*\text{d11}-0.0171347\text{D}0*\text{A1}(1)*\text{A1}(2)* \\ * \text{d16}+0.04569261296800626\text{D}0*\text{A1}(2)*\text{A1}(3)*\text{d16}-0.0456926\text{D}0*\text{A1}(1)* \\ * \text{A1}(4)*\text{d16}+0.205617\text{D}0*\text{A1}(2)**2.\text{D}0*\text{d66} + 0.698132\text{D}0*\text{A1}(2)*\text{A1}(4)* \\ * \text{d66} +0.822467\text{D}0*\text{A1}(4)**2.\text{D}0*\text{d66}$$

c

$$\text{stiff}(1,2) = 0.000880796902434195\text{D}0*\text{A1}(1)*\text{A2}(1)*\text{d11} + \\ * 0.000293598967478065\text{D}0*\text{A1}(2)*\text{A2}(2)*\text{d11} + \\ * 0.00149528726274594\text{D}0*\text{A2}(1)*\text{A1}(3)*\text{d11} + \\ * 0.00149528726274594\text{D}0*\text{A1}(1)*\text{A2}(3)*\text{d11} + \\ * 0.01409275043894711\text{D}0*\text{A1}(3)*\text{A2}(3)*\text{d11} + \\ * 0.0004984290875819808\text{D}0*\text{A2}(2)*\text{A1}(4)*\text{d11} + \\ * 0.0004984290875819808\text{D}0*\text{A1}(2)*\text{A2}(4)*\text{d11} + \\ * 0.004697583479649042\text{D}0*\text{A1}(4)*\text{A2}(4)*\text{d11} - \\ * 0.00856736\text{D}0*\text{A2}(1)*\text{A1}(2)*\text{d16}-0.00856736\text{D}0*\text{A1}(1)*\text{A2}(2)*\text{d16} + \\ * 0.02284630648400313\text{D}0*\text{A2}(2)*\text{A1}(3)*\text{d16} + \\ * 0.02284630648400313\text{D}0*\text{A1}(2)*\text{A2}(3)*\text{d16} - \\ * 0.0228463\text{D}0*\text{A2}(1)*\text{A1}(4)*\text{d16} - 0.0228463\text{D}0*\text{A1}(1)*\text{A2}(4)*\text{d16} + \\ * 0.205617\text{D}0*\text{A1}(2)*\text{A2}(2)*\text{d66} + 0.349066\text{D}0*\text{A2}(2)*\text{A1}(4)*\text{d66} + \\ * 0.349066\text{D}0*\text{A1}(2)*\text{A2}(4)*\text{d66} + 0.822467\text{D}0*\text{A1}(4)*\text{A2}(4)*\text{d66}$$

c

$$\text{stiff}(1,3) = 0.000880796902434195\text{D}0*\text{A1}(1)*\text{A3}(1)*\text{d11} +$$

* 0.000293598967478065D0*A1(2)*A3(2)*d11 +
 * 0.00149528726274594D0*A3(1)*A1(3)*d11 +
 * 0.00149528726274594D0*A1(1)*A3(3)*d11 +
 * 0.01409275043894711D0*A1(3)*A3(3)*d11 +
 * 0.0004984290875819805D0*A3(2)*A1(4)*d11 +
 * 0.0004984290875819805D0*A1(2)*A3(4)*d11 +
 * 0.004697583479649042D0*A1(4)*A3(4)*d11 -
 * 0.00856736D0*A3(1)*A1(2)*d16-0.00856736D0*A1(1)*A3(2)*d16 +
 * 0.02284630648400313D0*A3(2)*A1(3)*d16 +
 * 0.02284630648400313D0*A1(2)*A3(3)*d16 -
 * 0.0228463D0*A3(1)*A1(4)*d16 - 0.0228463D0*A1(1)*A3(4)*d16 +
 * 0.205617D0*A1(2)*A3(2)*d66 + 0.349066D0*A3(2)*A1(4)*d66 +
 * 0.349066D0*A1(2)*A3(4)*d66 + 0.822467D0*A1(4)*A3(4)*d66

c

stiff(1,4) = 0.000880796902434195D0*A1(1)*A4(1)*d11 +
 * 0.000293598967478065D0*A1(2)*A4(2)*d11 +
 * 0.00149528726274594D0*A4(1)*A1(3)*d11 +
 * 0.00149528726274594D0*A1(1)*A4(3)*d11 +
 * 0.01409275043894711D0*A1(3)*A4(3)*d11 +
 * 0.0004984290875819805D0*A4(2)*A1(4)*d11 +
 * 0.0004984290875819805D0*A1(2)*A4(4)*d11 +
 * 0.004697583479649042D0*A1(4)*A4(4)*d11 -
 * 0.00856736D0*A4(1)*A1(2)*d16-0.00856736D0*A1(1)*A4(2)*d16 +
 * 0.02284630648400313D0*A4(2)*A1(3)*d16 +
 * 0.02284630648400313D0*A1(2)*A4(3)*d16 -
 * 0.0228463D0*A4(1)*A1(4)*d16-0.0228463D0*A1(1)*A4(4)*d16 +
 * 0.205617D0*A1(2)*A4(2)*d66 + 0.349066D0*A4(2)*A1(4)*d66 +
 * 0.349066D0*A1(2)*A4(4)*d66 + 0.822467D0*A1(4)*A4(4)*d66

c

stiff(2,1) = stiff(1,2)

c

stiff(2,2) = 0.000880796902434194D0*A2(1)**2.D0*d11 +
 * 0.0002935989674780654D0*A2(2)**2.D0*d11 +
 * 0.00299057452549188D0*A2(1)*A2(3)*d11 +
 * 0.01409275043894711D0*A2(3)**2.D0*d11 +
 * 0.000996858175163961D0*A2(2)*A2(4)*d11 +
 * 0.004697583479649034D0*A2(4)**2.D0*d11-0.0171347D0*A2(1)*A2(2)*
 * d16+0.04569261296800626D0*A2(2)*A2(3)*d16-0.0456926D0*A2(1)*
 * A2(4)*d16+0.205617D0*A2(2)**2.D0*d66 + 0.698132D0*A2(2)*A2(4)*
 * d66 +0.822467D0*A2(4)**2.D0*d66

c

stiff(2,3) = 0.000880796902434195D0*A2(1)*A3(1)*d11 +
 * 0.000293598967478065D0*A2(2)*A3(2)*d11 +
 * 0.00149528726274594D0*A3(1)*A2(3)*d11 +
 * 0.00149528726274594D0*A2(1)*A3(3)*d11 +

* 0.01409275043894711D0*A2(3)*A3(3)*d11 +
 * 0.0004984290875819805D0*A3(2)*A2(4)*d11 +
 * 0.0004984290875819805D0*A2(2)*A3(4)*d11 +
 * 0.004697583479649042D0*A2(4)*A3(4)*d11 -
 * 0.00856736D0*A3(1)*A2(2)*d16 - 0.00856736D0*A2(1)*A3(2)*d16 +
 * 0.02284630648400313D0*A3(2)*A2(3)*d16 +
 * 0.02284630648400313D0*A2(2)*A3(3)*d16 -
 * 0.0228463D0*A3(1)*A2(4)*d16 - 0.0228463D0*A2(1)*A3(4)*d16 +
 * 0.205617D0*A2(2)*A3(2)*d66 + 0.349066D0*A3(2)*A2(4)*d66 +
 * 0.349066D0*A2(2)*A3(4)*d66 + 0.822467D0*A2(4)*A3(4)*d66

c

stiff(2,4) = 0.000880796902434195D0*A2(1)*A4(1)*d11 +
 * 0.000293598967478065D0*A2(2)*A4(2)*d11 +
 * 0.00149528726274594D0*A4(1)*A2(3)*d11 +
 * 0.00149528726274594D0*A2(1)*A4(3)*d11 +
 * 0.01409275043894711D0*A2(3)*A4(3)*d11 +
 * 0.0004984290875819808D0*A4(2)*A2(4)*d11 +
 * 0.0004984290875819808D0*A2(2)*A4(4)*d11 +
 * 0.004697583479649042D0*A2(4)*A4(4)*d11 -
 * 0.00856736D0*A4(1)*A2(2)*d16 - 0.00856736D0*A2(1)*A4(2)*d16 +
 * 0.02284630648400313D0*A4(2)*A2(3)*d16 +
 * 0.02284630648400313D0*A2(2)*A4(3)*d16 -
 * 0.0228463D0*A4(1)*A2(4)*d16 - 0.0228463D0*A2(1)*A4(4)*d16 +
 * 0.205617D0*A2(2)*A4(2)*d66 + 0.349066D0*A4(2)*A2(4)*d66 +
 * 0.349066D0*A2(2)*A4(4)*d66 + 0.822467D0*A2(4)*A4(4)*d66

c

stiff(3,1) = stiff(1,3)

c

stiff(3,2) = stiff(2,3)

c

stiff(3,3) = 0.000880796902434194D0*A3(1)**2.D0*d11 +
 * 0.0002935989674780654D0*A3(2)**2.D0*d11 +
 * 0.00299057452549188D0*A3(1)*A3(3)*d11 +
 * 0.01409275043894711D0*A3(3)**2.D0*d11 +
 * 0.000996858175163961D0*A3(2)*A3(4)*d11 +
 * 0.004697583479649034D0*A3(4)**2.D0*d11-0.0171347D0*A3(1)*A3(2)*
 * d16+0.04569261296800626D0*A3(2)*A3(3)*d16-0.0456926D0*A3(1)*
 * A3(4)*d16+0.205617D0*A3(2)**2.D0*d66+0.698132D0*A3(2)*A3(4)*d66+
 * 0.822467D0*A3(4)**2.D0*d66

c

stiff(3,4) = 0.000880796902434195D0*A3(1)*A4(1)*d11 +
 * 0.000293598967478065D0*A3(2)*A4(2)*d11 +
 * 0.00149528726274594D0*A4(1)*A3(3)*d11 +
 * 0.00149528726274594D0*A3(1)*A4(3)*d11 +
 * 0.01409275043894711D0*A3(3)*A4(3)*d11 +

* 0.0004984290875819808D0*A4(2)*A3(4)*d11 +
 * 0.0004984290875819808D0*A3(2)*A4(4)*d11 +
 * 0.004697583479649042D0*A3(4)*A4(4)*d11 -
 * 0.00856736D0*A4(1)*A3(2)*d16 - 0.00856736D0*A3(1)*A4(2)*d16 +
 * 0.02284630648400313D0*A4(2)*A3(3)*d16 +
 * 0.02284630648400313D0*A3(2)*A4(3)*d16 -
 * 0.0228463D0*A4(1)*A3(4)*d16 - 0.0228463D0*A3(1)*A4(4)*d16 +
 * 0.205617D0*A3(2)*A4(2)*d66 + 0.349066D0*A4(2)*A3(4)*d66 +
 * 0.349066D0*A3(2)*A4(4)*d66 + 0.822467D0*A3(4)*A4(4)*d66

c

stiff(4,1) = stiff(1,4)

c

stiff(4,2) = stiff(2,4)

c

stiff(4,3) = stiff(3,4)

c

stiff(4,4) = 0.000880796902434194D0*A4(1)**2.D0*d11 +
 * 0.0002935989674780654D0*A4(2)**2.D0*d11 +
 * 0.00299057452549188D0*A4(1)*A4(3)*d11 +
 * 0.01409275043894711D0*A4(3)**2.D0*d11 +
 * 0.000996858175163961D0*A4(2)*A4(4)*d11 +
 * 0.004697583479649034D0*A4(4)**2.D0*d11-0.0171347D0*A4(1)*A4(2)*
 * d16+0.04569261296800626D0*A4(2)*A4(3)*d16-0.0456926D0*A4(1)*
 * A4(4)*d16+0.205617D0*A4(2)**2.D0*d66+0.698132D0*A4(2)*A4(4)*d66+
 * 0.822467*A4(4)**2.D0*d66

c

c Mass Matrix

c

mass(1,1) = 1.08845D0*A1(1)**2.D0*rho+0.362874D0*A1(2)**2.D0*rho+
 * 5.52564D0*A1(1)*A1(3)*rho + 7.20001D0*A1(3)**2.D0*rho +
 * 1.84217D0*A1(2)*A1(4)*rho + 2.40038D0*A1(4)**2.D0*rho

c

mass(1,2) = 1.08845D0*A1(1)*A2(1)*rho+0.362874D0*A1(2)*A2(2)*rho+
 * 2.76282D0*A2(1)*A1(3)*rho + 2.76282D0*A1(1)*A2(3)*rho +
 * 7.20001D0*A1(3)*A2(3)*rho + 0.921084D0*A2(2)*A1(4)*rho +
 * 0.921084D0*A1(2)*A2(4)*rho + 2.40038D0*A1(4)*A2(4)*rho

c

mass(1,3) = 1.08845D0*A1(1)*A3(1)*rho+0.362874D0*A1(2)*A3(2)*rho+
 * 2.76282D0*A3(1)*A1(3)*rho + 2.76282D0*A1(1)*A3(3)*rho +
 * 7.20001D0*A1(3)*A3(3)*rho + 0.921084D0*A3(2)*A1(4)*rho +
 * 0.921084D0*A1(2)*A3(4)*rho + 2.40038D0*A1(4)*A3(4)*rho

c

mass(1,4) = 1.08845D0*A1(1)*A4(1)*rho+0.362874D0*A1(2)*A4(2)*rho+
 * 2.76282D0*A4(1)*A1(3)*rho + 2.76282D0*A1(1)*A4(3)*rho +
 * 7.20001D0*A1(3)*A4(3)*rho + 0.921084D0*A4(2)*A1(4)*rho +

```

      * 0.921084D0*A1(2)*A4(4)*rho + 2.40038D0*A1(4)*A4(4)*rho
c
      mass(2,1) = mass(1,2)
c
      mass(2,2) = 1.08845D0*A2(1)**2.D0*rho+0.362874D0*A2(2)**2.D0*rho+
      * 5.52564D0*A2(1)*A2(3)*rho + 7.20001D0*A2(3)**2.D0*rho +
      * 1.84217D0*A2(2)*A2(4)*rho + 2.40038D0*A2(4)**2.D0*rho
c
      mass(2,3) = 1.08845D0*A2(1)*A3(1)*rho+0.362874D0*A2(2)*A3(2)*rho+
      * 2.76282D0*A3(1)*A2(3)*rho + 2.76282D0*A2(1)*A3(3)*rho +
      * 7.20001D0*A2(3)*A3(3)*rho + 0.921084D0*A3(2)*A2(4)*rho +
      * 0.921084D0*A2(2)*A3(4)*rho + 2.40038D0*A2(4)*A3(4)*rho
c
      mass(2,4) = 1.08845D0*A2(1)*A4(1)*rho+0.362874D0*A2(2)*A4(2)*rho+
      * 2.76282D0*A4(1)*A2(3)*rho + 2.76282D0*A2(1)*A4(3)*rho +
      * 7.20001D0*A2(3)*A4(3)*rho + 0.921084D0*A4(2)*A2(4)*rho +
      * 0.921084D0*A2(2)*A4(4)*rho + 2.40038D0*A2(4)*A4(4)*rho
c
      mass(3,1) = mass(1,3)
c
      mass(3,2) = mass(2,3)
c
      mass(3,3) = 1.08845D0*A3(1)**2.D0*rho+0.362874D0*A3(2)**2.D0*rho+
      * 5.52564D0*A3(1)*A3(3)*rho + 7.20001D0*A3(3)**2.D0*rho +
      * 1.84217D0*A3(2)*A3(4)*rho + 2.40038D0*A3(4)**2.D0*rho
c
      mass(3,4) = 1.08845D0*A3(1)*A4(1)*rho+0.362874D0*A3(2)*A4(2)*rho+
      * 2.76282D0*A4(1)*A3(3)*rho + 2.76282D0*A3(1)*A4(3)*rho +
      * 7.20001D0*A3(3)*A4(3)*rho + 0.921084D0*A4(2)*A3(4)*rho +
      * 0.921084D0*A3(2)*A4(4)*rho + 2.40038D0*A3(4)*A4(4)*rho
c
      mass(4,1) = mass(1,4)
c
      mass(4,2) = mass(2,4)
c
      mass(4,3) = mass(3,4)
c
      mass(4,4) = 1.08845D0*A4(1)**2.D0*rho+0.362874D0*A4(2)**2.D0*rho+
      * 5.52564D0*A4(1)*A4(3)*rho + 7.20001D0*A4(3)**2.D0*rho +
      * 1.84217D0*A4(2)*A4(4)*rho + 2.40038D0*A4(4)**2.D0*rho
c
c      Call a Subroutine Program Which Evaluates The Eigenvalues and
c      Eigenvectors For The Free Motion System
c
      CALL DGVCRG (N, stiff, LDS, mass, LDM, ALPHA1, BETA1, EVEC1,

```

```

      * LDEVEC)
c
      DO 100 K=1,N
        IF (BETA1(K) .NE. 0.0) THEN
          EVAL1(K) = ALPHA1(K)/BETA1(K)
        ELSE
          EVAL1(K) = AMACH(2)
        END IF
100  CONTINUE
c
c    Formulate The Open And Closed Loop State-Space Equations
c
c      Formulate The Inverse Of the Mass Matrix
c
c      CALL DLINRG (N, mass, LDM, invmas, LDMINV)
c
c      Multiply The Inverse Of the Mass Matrix By The Stiffness
c
c      CALL DMRRRR (NRIM, NCIM, invmas, LDMINV, NRS, NCS, stiff, LDS,
* NRT, NCT, TEMP, LDT)
c
      TEMP1(1,1) = KD*(0.0654498D0*A1(1)*Sin(0.0654498D0*X(11)) +
* 0.1309D0*A1(3)*Sin(0.1309D0*X(11)))
c
      TEMP1(2,1) = KD*(0.0654498D0*A2(1)*Sin(0.0654498D0*X(11)) +
* 0.1309D0*A2(3)*Sin(0.1309D0*X(11)))
c
      TEMP1(3,1) = KD*(0.0654498D0*A3(1)*Sin(0.0654498D0*X(11)) +
* 0.1309D0*A3(3)*Sin(0.1309D0*X(11)))
c
      TEMP1(4,1) = KD*(0.0654498D0*A4(1)*Sin(0.0654498D0*X(11)) +
* 0.1309D0*A4(3)*Sin(0.1309D0*X(11)))
c
      TEMP1(1,2) = KD*(0.0654498D0*A1(1)*Sin(0.0654498D0*X(12)) +
* 0.1309D0*A1(3)*Sin(0.1309D0*X(12)))
c
      TEMP1(2,2) = KD*(0.0654498D0*A2(1)*Sin(0.0654498D0*X(12)) +
* 0.1309D0*A2(3)*Sin(0.1309D0*X(12)))
c
      TEMP1(3,2) = KD*(0.0654498D0*A3(1)*Sin(0.0654498D0*X(12)) +
* 0.1309D0*A3(3)*Sin(0.1309D0*X(12)))
c
      TEMP1(4,2) = KD*(0.0654498D0*A4(1)*Sin(0.0654498D0*X(12)) +
* 0.1309D0*A4(3)*Sin(0.1309D0*X(12)))
c

```

```
CALL DMRRRR (NRIM, NCIM, invmas, LDMINV, NRT1, NCT1, TEMP1, LDT1,
* NRT2, NCT2, TEMP2, LDT2)
```

c

```
TEMP3(1,1) = -0.5D0*A1(2) + 0.5D0*A1(2)*Cos(0.0654498D0*xd) -
* 0.5D0*A1(4) + 0.5D0*A1(4)*Cos(0.1309D0*xd)
```

c

```
TEMP3(2,1) = -0.5D0*A2(2) + 0.5D0*A2(2)*Cos(0.0654498D0*xd) -
* 0.5D0*A2(4) + 0.5D0*A2(4)*Cos(0.1309D0*xd)
```

c

```
TEMP3(3,1) = -0.5D0*A3(2) + 0.5D0*A3(2)*Cos(0.0654498D0*xd) -
* 0.5D0*A3(4) + 0.5D0*A3(4)*Cos(0.1309D0*xd)
```

c

```
TEMP3(4,1) = -0.5D0*A4(2) + 0.5D0*A4(2)*Cos(0.0654498D0*xd) -
* 0.5D0*A4(4) + 0.5D0*A4(4)*Cos(0.1309D0*xd)
```

c

```
CALL DMRRRR (NRIM, NCIM, invmas, LDMINV, NRT3, NCT3, TEMP3, LDT3,
* NRT4, NCT4, TEMP4, LDT4)
```

c

c Derive The State Space Matrices

c

c Asys Matrix

c

```
Asys(1,1) = 0.D0
Asys(1,2) = 0.D0
Asys(1,3) = 0.D0
Asys(1,4) = 0.0
Asys(1,5) = 1.D0
Asys(1,6) = 0.D0
Asys(1,7) = 0.D0
```

```
Asys(1,8) = 0.D0
Asys(2,1) = 0.D0
Asys(2,2) = 0.D0
Asys(2,3) = 0.D0
Asys(2,4) = 0.D0
Asys(2,5) = 0.D0
Asys(2,6) = 1.D0
Asys(2,7) = 0.D0
Asys(2,8) = 0.D0
Asys(3,1) = 0.D0
Asys(3,2) = 0.D0
Asys(3,3) = 0.D0
Asys(3,4) = 0.D0
Asys(3,5) = 0.D0
Asys(3,6) = 0.D0
Asys(3,7) = 1.D0
```

```

Asys(3,8) = 0.D0
Asys(4,1) = 0.D0
Asys(4,2) = 0.D0
Asys(4,3) = 0.D0
Asys(4,4) = 0.D0
Asys(4,5) = 0.D0
Asys(4,6) = 0.D0
Asys(4,7) = 0.D0
Asys(4,8) = 1.D0
Asys(5,1) = -TEMP(1,1)
Asys(5,2) = -TEMP(1,2)
Asys(5,3) = -TEMP(1,3)
Asys(5,4) = -TEMP(1,4)
Asys(5,5) = 0.D0
Asys(5,6) = 0.D0
Asys(5,7) = 0.D0
Asys(5,8) = 0.D0
Asys(6,1) = -TEMP(2,1)
Asys(6,2) = -TEMP(2,2)
Asys(6,3) = -TEMP(2,3)
Asys(6,4) = -TEMP(2,4)
Asys(6,5) = 0.D0
Asys(6,6) = 0.D0
Asys(6,7) = 0.D0
Asys(6,8) = 0.D0
Asys(7,1) = -TEMP(3,1)
Asys(7,2) = -TEMP(3,2)
Asys(7,3) = -TEMP(3,3)
Asys(7,4) = -TEMP(3,4)
Asys(7,5) = 0.D0

```

```

Asys(7,6) = 0.D0
Asys(7,7) = 0.D0
Asys(7,8) = 0.D0
Asys(8,1) = -TEMP(4,1)
Asys(8,2) = -TEMP(4,2)
Asys(8,3) = -TEMP(4,3)
Asys(8,4) = -TEMP(4,4)
Asys(8,5) = 0.D0
Asys(8,6) = 0.D0
Asys(8,7) = 0.D0
Asys(8,8) = 0.D0

```

c

c B1 Matrix

c

```

B1(1,1) = 0.D0

```



```

B1(1,2) = 0.D0
B1(2,1) = 0.D0
B1(2,2) = 0.D0
B1(3,1) = 0.D0
B1(3,2) = 0.D0
B1(4,1) = 0.D0
B1(4,2) = 0.D0
B1(5,1) = TEMP2(1,1)
B1(5,2) = TEMP2(1,2)
B1(6,1) = TEMP2(2,1)
B1(6,2) = TEMP2(2,2)
B1(7,1) = TEMP2(3,1)
B1(7,2) = TEMP2(3,2)
B1(8,1) = TEMP2(4,1)
B1(8,2) = TEMP2(4,2)

```

c

c Gain Matrix

c

```

GAIN(1,1) = X(13)
GAIN(1,2) = 0.D0
GAIN(2,1) = 0.D0
GAIN(2,2) = X(14)

```

c

c C Matrix

c

```

C(1,1) = 0.D0
C(1,2) = 0.D0
C(1,3) = 0.D0
C(1,4) = 0.D0
C(1,5) = -.025*KS*(0.0654498D0*A1(1)*Sin(0.0654498D0*(X(11) +
* Ls/2.D0)) + 0.1309D0*A1(3)*Sin(0.1309D0*(X(11) + Ls/2.D0)) -
* 0.0654498D0*A1(1)*Sin(0.0654498D0*(X(11) - Ls/2.D0)) -
* 0.1309D0*A1(3)*Sin(0.1309D0*(X(11) - Ls/2.D0)))
C(1,6) = -.025*KS*(0.0654498D0*A2(1)*Sin(0.0654498D0*(X(11) +
* Ls/2.D0)) + 0.1309D0*A2(3)*Sin(0.1309D0*(X(11) + Ls/2.D0)) -
* 0.0654498D0*A2(1)*Sin(0.0654498D0*(X(11) - Ls/2.D0)) -
* 0.1309D0*A2(3)*Sin(0.1309D0*(X(11) - Ls/2.D0)))
C(1,7) = -.025*KS*(0.0654498D0*A3(1)*Sin(0.0654498D0*(X(11) +
* Ls/2.D0)) + 0.1309D0*A3(3)*Sin(0.1309D0*(X(11) + Ls/2.D0)) -
* 0.0654498D0*A3(1)*Sin(0.0654498D0*(X(11) - Ls/2.D0)) -
* 0.1309D0*A3(3)*Sin(0.1309D0*(X(11) - Ls/2.D0)))
C(1,8) = -.025*KS*(0.0654498D0*A4(1)*Sin(0.0654498D0*(X(11) +
* Ls/2.D0)) + 0.1309D0*A4(3)*Sin(0.1309D0*(X(11) + Ls/2.D0)) -
* 0.0654498D0*A4(1)*Sin(0.0654498D0*(X(11) - Ls/2.D0)) -
* 0.1309D0*A4(3)*Sin(0.1309D0*(X(11) - Ls/2.D0)))

```

```

C(2,1) = 0.D0
C(2,2) = 0.D0
C(2,3) = 0.D0
C(2,4) = 0.D0
C(2,5)= -.025*KS*(0.0654498D0*A1(1)*Sin(0.0654498D0*(X(12) +
* Ls/2.D0)) + 0.1309D0*A1(3)*Sin(0.1309D0*(X(12) + Ls/2.D0)) -
* 0.0654498D0*A1(1)*Sin(0.0654498D0*(X(12) - Ls/2.D0)) -
* 0.1309D0*A1(3)*Sin(0.1309D0*(X(12) - Ls/2.D0)))
C(2,6)= -.025*KS*(0.0654498D0*A2(1)*Sin(0.0654498D0*(X(12) +
* Ls/2.D0)) + 0.1309D0*A2(3)*Sin(0.1309D0*(X(12) + Ls/2.D0)) -
* 0.0654498D0*A2(1)*Sin(0.0654498D0*(X(12) - Ls/2.D0)) -
* 0.1309D0*A2(3)*Sin(0.1309D0*(X(12) - Ls/2.D0)))
C(2,7)= -.025*KS*(0.0654498D0*A3(1)*Sin(0.0654498D0*(X(12) +
* Ls/2.D0)) + 0.1309D0*A3(3)*Sin(0.1309D0*(X(12) + Ls/2.D0)) -
* 0.0654498D0*A3(1)*Sin(0.0654498D0*(X(12) - Ls/2.D0)) -
* 0.1309D0*A3(3)*Sin(0.1309D0*(X(12) - Ls/2.D0)))
C(2,8)= -.025*KS*(0.0654498D0*A4(1)*Sin(0.0654498D0*(X(12) +
* Ls/2.D0)) + 0.1309D0*A4(3)*Sin(0.1309D0*(X(12) + Ls/2.D0)) -
* 0.0654498D0*A4(1)*Sin(0.0654498D0*(X(12) - Ls/2.D0)) -
* 0.1309D0*A4(3)*Sin(0.1309D0*(X(12) - Ls/2.D0)))
c
c   H Matrix
c
H(1,1) = 0.D0
H(2,1) = 0.D0
H(3,1) = 0.D0
H(4,1) = 0.D0
H(5,1) = TEMP4(1,1)
H(6,1) = TEMP4(2,1)
H(7,1) = TEMP4(3,1)
H(8,1) = TEMP4(4,1)
c
c   Closed Loop Matrix
c
CALL DMRRRR (NRG, NCG, GAIN, LDG, NRC, NCC, C, LDC, NRT5, NCT5,
* TEMP5, LDT5)
c
CALL DMRRRR (NRB1, NCB1, B1, LDB1, NRT5, NCT5, TEMP5, LDT5,
* NRT6, NCT6, TEMP6, LDT6)
c
A(1,1) = Asys(1,1) - TEMP6(1,1)
A(1,2) = Asys(1,2) - TEMP6(1,2)
A(1,3) = Asys(1,3) - TEMP6(1,3)
A(1,4) = Asys(1,4) - TEMP6(1,4)
A(1,5) = Asys(1,5) - TEMP6(1,5)

```

$A(1,6) = Asys(1,6) - TEMP6(1,6)$
 $A(1,7) = Asys(1,7) - TEMP6(1,7)$
 $A(1,8) = Asys(1,8) - TEMP6(1,8)$
 $A(2,1) = Asys(2,1) - TEMP6(2,1)$
 $A(2,2) = Asys(2,2) - TEMP6(2,2)$
 $A(2,3) = Asys(2,3) - TEMP6(2,3)$
 $A(2,4) = Asys(2,4) - TEMP6(2,4)$
 $A(2,5) = Asys(2,5) - TEMP6(2,5)$
 $A(2,6) = Asys(2,6) - TEMP6(2,6)$
 $A(2,7) = Asys(2,7) - TEMP6(2,7)$
 $A(2,8) = Asys(2,8) - TEMP6(2,8)$
 $A(3,1) = Asys(3,1) - TEMP6(3,1)$
 $A(3,2) = Asys(3,2) - TEMP6(3,2)$
 $A(3,3) = Asys(3,3) - TEMP6(3,3)$
 $A(3,4) = Asys(3,4) - TEMP6(3,4)$
 $A(3,5) = Asys(3,5) - TEMP6(3,5)$
 $A(3,6) = Asys(3,6) - TEMP6(3,6)$
 $A(3,7) = Asys(3,7) - TEMP6(3,7)$
 $A(3,8) = Asys(3,8) - TEMP6(3,8)$
 $A(4,1) = Asys(4,1) - TEMP6(4,1)$
 $A(4,2) = Asys(4,2) - TEMP6(4,2)$
 $A(4,3) = Asys(4,3) - TEMP6(4,3)$
 $A(4,4) = Asys(4,4) - TEMP6(4,4)$
 $A(4,5) = Asys(4,5) - TEMP6(4,5)$
 $A(4,6) = Asys(4,6) - TEMP6(4,6)$
 $A(4,7) = Asys(4,7) - TEMP6(4,7)$
 $A(4,8) = Asys(4,8) - TEMP6(4,8)$
 $A(5,1) = Asys(5,1) - TEMP6(5,1)$
 $A(5,2) = Asys(5,2) - TEMP6(5,2)$
 $A(5,3) = Asys(5,3) - TEMP6(5,3)$
 $A(5,4) = Asys(5,4) - TEMP6(5,4)$
 $A(5,5) = Asys(5,5) - TEMP6(5,5)$
 $A(5,6) = Asys(5,6) - TEMP6(5,6)$

 $A(5,7) = Asys(5,7) - TEMP6(5,7)$
 $A(5,8) = Asys(5,8) - TEMP6(5,8)$
 $A(6,1) = Asys(6,1) - TEMP6(6,1)$
 $A(6,2) = Asys(6,2) - TEMP6(6,2)$
 $A(6,3) = Asys(6,3) - TEMP6(6,3)$
 $A(6,4) = Asys(6,4) - TEMP6(6,4)$
 $A(6,5) = Asys(6,5) - TEMP6(6,5)$
 $A(6,6) = Asys(6,6) - TEMP6(6,6)$
 $A(6,7) = Asys(6,7) - TEMP6(6,7)$
 $A(6,8) = Asys(6,8) - TEMP6(6,8)$
 $A(7,1) = Asys(7,1) - TEMP6(7,1)$
 $A(7,2) = Asys(7,2) - TEMP6(7,2)$

```

A(7,3) = Asys(7,3) - TEMP6(7,3)
A(7,4) = Asys(7,4) - TEMP6(7,4)
A(7,5) = Asys(7,5) - TEMP6(7,5)
A(7,6) = Asys(7,6) - TEMP6(7,6)
A(7,7) = Asys(7,7) - TEMP6(7,7)
A(7,8) = Asys(7,8) - TEMP6(7,8)
A(8,1) = Asys(8,1) - TEMP6(8,1)
A(8,2) = Asys(8,2) - TEMP6(8,2)
A(8,3) = Asys(8,3) - TEMP6(8,3)
A(8,4) = Asys(8,4) - TEMP6(8,4)
A(8,5) = Asys(8,5) - TEMP6(8,5)
A(8,6) = Asys(8,6) - TEMP6(8,6)
A(8,7) = Asys(8,7) - TEMP6(8,7)
A(8,8) = Asys(8,8) - TEMP6(8,8)
c
c   Form the Constant Term in the Lyap Equation
c
c   CALL DMRRRR (NRH, NCH, H, LDH, NRD, NCD, D, LDD, NRH, NCH,
* TEMP7, LDH)
c
c   CALL DMXYTF (NRH, NCH, TEMP7, LDH, NRH, NCH, H, LDH, NRB,
* NCB, B, LDB)
c
c   Calculate the Lyap Equation
c
c   Call lyap(A, B, NA, IROW, NDIM)
c
c   Calculate the Performance Index
c
W1(1,1) = A1(1) + A1(2) + 2.D0*A1(3) + 2.D0*A1(4)
W1(1,2) = A2(1) + A2(2) + 2.D0*A2(3) + 2.D0*A2(4)
W1(1,3) = A3(1) + A3(2) + 2.D0*A3(3) + 2.D0*A3(4)
W1(1,4) = A4(1) + A4(2) + 2.D0*A4(3) + 2.D0*A4(4)
W1(1,5) = 0.D0

W1(1,6) = 0.D0
W1(1,7) = 0.D0
W1(1,8) = 0.D0
c
W2(1,1) = A1(1) + 2.D0*A1(3)
W2(1,2) = A2(1) + 2.D0*A2(3)
W2(1,3) = A3(1) + 2.D0*A3(3)
W2(1,4) = A4(1) + 2.D0*A4(3)
W2(1,5) = 0.D0
W2(1,6) = 0.D0
W2(1,7) = 0.D0

```

```

W2(1,8) = 0.D0
c
W3(1,1) = W1(1,1) - W2(1,1)
W3(1,2) = W1(1,2) - W2(1,2)
W3(1,3) = W1(1,3) - W2(1,3)
W3(1,4) = W1(1,4) - W2(1,4)
W3(1,5) = W1(1,5) - W2(1,5)
W3(1,6) = W1(1,6) - W2(1,6)
W3(1,7) = W1(1,7) - W2(1,7)
W3(1,8) = W1(1,8) - W2(1,8)
c
CALL DMRRRR (NRW3, NCW3, W3, LDW3, NRB, NCB, B, LDB,
* NRT8, NCT8, TEMP8, LDT8)
c
CALL DMXYTF (NRT8, NCT8, TEMP8, LDT8, NRW3, NCW3, W3, LDW3,
* NRT9, NCT9, TEMP9, LDT9)
c
CALL DMRRRR (NRW2, NCW2, W2, LDW2, NRB, NCB, B, LDB,
* NRT11, NCT11, TEMP11, LDT11)
c
CALL DMXYTF (NRT11, NCT11, TEMP11, LDT11, NRW2, NCW2, W2,
* LDW2, NRT10, NCT10, TEMP10, LDT10)
c
OBJ = ZETA*TEMP9(1,1) + (1-ZETA)*TEMP10(1,1)
c
CALCULATE THE CONSTRAINTS
c
CALL DMRRRR (NRG, NCG, GAIN, LDG, NRC, NCC, C, LDC,
* NRT12, NCT12, TEMP12, LDT12)
c
CALL DMRRRR (NRT12, NCT12, TEMP12, LDT12, NRB, NCB, B, LDB,
* NRT13, NCT13, TEMP13, LDT13)
c
CALL DMXYTF (NRT13, NCT13, TEMP13, LDT13, NRC, NCC, C, LDC,
* NRT14, NCT14, TEMP14, LDT14)
c
CALL DMXYTF (NRT14, NCT14, TEMP14, LDT14, NRG, NCG, GAIN,
* LDG, NRT15, NCT15, TEMP15, LDT15)
c
G(1) = TEMP15(1,1)/160000.D0 - 1.D0
c
G(2) = TEMP15(2,2)/160000.D0 - 1.D0
c
end

```

This program which calculates the objective function and constraints also calls a subroutine which calculates the Lyapunov of the function. This subroutine is:

```

SUBROUTINE LYAP(A,B,NA,IROW,NDIM)
implicit double precision(a-h,o-z)
DOUBLE PRECISION A(NDIM,NDIM),B(NDIM,NDIM)
DOUBLE PRECISION AMAT(1200,1200),RHS(1200),X(20,20)
DOUBLE PRECISION WKAREA(10000)
INTEGER IROW(NDIM)
IA=1200
DO 1 I=1,NA*NA
    DO 1 J=1,NA*NA
        AMAT(I,J)=0.0D0
1  CONTINUE
NUN=0
DO 10 I=1,NA
DO 10 J=I,NA
    NUN=NUN+1
    RHS(NUN)=-B(I,J)
    NEQ=0
    DO 20 K=1,NA
    DO 20 L=K,NA
        NEQ=NEQ+1
        DO 30 M=1,NA
        DO 30 N=1,NA
            IF(K.EQ.M)THEN
                IF(I.EQ.N.AND.J.EQ.L)THEN
                    AMAT(NEQ,NUN)=AMAT(NEQ,NUN)+A(M,N)
                END IF
                IF(I.EQ.L.AND.J.EQ.N.AND.I.NE.J)THEN
                    AMAT(NEQ,NUN)=AMAT(NEQ,NUN)+A(M,N)
                END IF
            END IF
            IF(L.EQ.M)THEN
                IF(I.EQ.N.AND.J.EQ.K)THEN
                    AMAT(NEQ,NUN)=AMAT(NEQ,NUN)+A(M,N)
                END IF
                IF(I.EQ.K.AND.J.EQ.N.AND.I.NE.J)THEN
                    AMAT(NEQ,NUN)=AMAT(NEQ,NUN)+A(M,N)
                END IF
            END IF
        END IF
    END IF
30 CONTINUE
20 CONTINUE
10 CONTINUE
CALL LUDCMP(AMAT,NEQ,IA,IROW,D)
CALL LUBKSB(AMAT,NEQ,IA,IROW,RHS)

```

```

c  CALL LEQT1F(AMAT,1,NEQ,IA,RHS,0,WKAREA,IER)
    NEQ=0
    DO 31 I=1,NA
      DO 31 J=I,NA
        NEQ=NEQ+1
        B(I,J)=RHS(NEQ)
        B(J,I)=B(I,J)
31  CONTINUE
    RETURN
    END
    subroutine lubksb(a,n,np,indx,b)
    implicit double precision(a-h,o-z)
    double precision a(np,np),b(n)
    integer indx(np)
    ii=0
    do 12 i=1,n
      ll=indx(i)
      sum=b(ll)
      b(ll)=b(i)
      if (ii.ne.0)then
        do 11 j=ii,i-1
          sum=sum-a(i,j)*b(j)
11      continue
        else if (sum.ne.0.) then
          ii=i
        endif
      b(i)=sum
12  continue
    do 14 i=n,1,-1
      sum=b(i)
      if(i.lt.n)then
        do 13 j=i+1,n
          sum=sum-a(i,j)*b(j)
13      continue
        endif
      b(i)=sum/a(i,i)
14  continue
    return
    end
    subroutine ludcmp(a,n,np,indx,d)
    implicit double precision(a-h,o-z)
    parameter (nmax=500,tiny=1.0d-20)
    double precision a(np,np),vv(nmax)
    integer indx(np)
    d=1.
    do 12 i=1,n

```

```

    aamax=0.d0
    do 11 j=1,n
        if (abs(a(i,j)).gt.aamax) aamax=abs(a(i,j))
11    continue
        if (aamax.eq.0.d0) call exit(1)
        vv(i)=1./aamax
12    continue
        do 19 j=1,n
            if (j.gt.1) then
                do 14 i=1,j-1
                    sum=a(i,j)
                    if (i.gt.1)then
                        do 13 k=1,i-1
                            sum=sum-a(i,k)*a(k,j)
13                continue
                            a(i,j)=sum
                        endif
14                continue
            endif
            aamax=0.
            do 16 i=j,n
                sum=a(i,j)
                if (j.gt.1)then
                    do 15 k=1,j-1
                        sum=sum-a(i,k)*a(k,j)
15                continue
                        a(i,j)=sum
                    endif
                    dum=vv(i)*abs(sum)
                    if (dum.ge.aamax) then
                        imax=i
                        aamax=dum
                    endif
16                continue
                if (j.ne.imax)then
                    do 17 k=1,n
                        dum=a(imax,k)
                        a(imax,k)=a(j,k)
                        a(j,k)=dum
17                continue
                    d=-d
                    vv(imax)=vv(j)
                endif
                indx(j)=imax
                if(j.ne.n)then
                    if(a(j,j).eq.0.d0 )a(j,j)=tiny

```



```

        dum=1./a(j,j)
        do 18 i=j+1,n
            a(i,j)=a(i,j)*dum
18      continue
        endif
19    continue
    if(a(n,n).eq.0.d0) a(n,n)=tiny
    return
end
subroutine exit(iflag)
if (iflag .ne. 0) then
    print *, 'singular matrix.'
    stop
endif
return
end

```

Appendix C

This appendix contains the raw optimization data generated from the optimization program for each starting location.

Disturbance Force 1								
Starting Actuator Location 8/16								
Starting Gain Multiplier .00001								
	Start	Finish		Start	Finish		Start	Finish
ply angle	1.57079	1.03-1.56	ply angle	1.48352	.519-1.47	ply angle	1.39626	0.88-1.39
loc 1/loc 2	8/16	8, 19.2	loc 1/loc 2	8/16	7.45, 22.7	loc 1/loc 2	8/16	8, 22.7
gain 1/2	.00001	0, .0695	gain 1/2	.00001	.29, .12	gain 1/2	.00001	.56, .11
objective		4853.87	objective		467	objective		226
	Start	Finish		Start	Finish		Start	Finish
ply angle	1.30899	.78-1.3	ply angle	1.22173	.687-1.2	ply angle	1.13446	.286-1.12
loc 1/loc 2	8/16	7.57, 22.7	loc 1/loc 2	8/16	6.43, 22.7	loc 1/loc 2	8/16	6.88, 22.7
gain 1/2	.00001	.413, 1.2	gain 1/2	.00001	.34, .124	gain 1/2	.00001	.929, .127
objective		191	objective		171	objective		124
	Start	Finish		Start	Finish		Start	Finish
ply angle	1.04719	.42-1.04	ply angle	0.95993	.496-.953	ply angle	0.87266	.511-.867
loc 1/loc 2	8/16	7.29, 22.7	loc 1/loc 2	8/16	7.52, 22.7	loc 1/loc 2	8/16	7.7, 22.7
gain 1/2	.00001	1.1, .12	gain 1/2	.00001	1.25, .12	gain 1/2	.00001	1.43, .11
objective		138.4	objective		152	objective		158.8
	Start	Finish		Start	Finish		Start	Finish
ply angle	0.78539	.54-.78	ply angle	0.69813	.592-.696	ply angle	0.61086	.476-.61
loc 1/loc 2	8/16	7.6, 22.7	loc 1/loc 2	8/16	6.7, 22.7	loc 1/loc 2	8/16	4.9, 22.7
gain 1/2	.00001	1.33, 1.14	gain 1/2	.00001	.933, .129	gain 1/2	.00001	.743, .14
objective		149.7	objective		130.5	objective		112.3
	Start	Finish		Start	Finish		Start	Finish

ply angle	0.52359	.423-.522	ply angle	0.43633	.365-.435	ply angle	0.34906	.34-.35
loc 1/loc 2	8/16	5.03, 22.7	loc 1/loc 2	8/16	4.9, 22.7	loc 1/loc 2	8/16	5.07, 22.7
gain 1/2	.00001	.644, .137	gain 1/2	.00001	.669, .138	gain 1/2	.00001	.676, .138
objective		115	objective		109.3	objective		106.7
	Start	Finish		Start	Finish		Start	Finish
ply angle	0.26179	.263-.366	ply angle	0.17453	.181-.59	ply angle	0.08726	.097-.298
loc 1/loc 2	8/16	5.24, 22.7	loc 1/loc 2	8/16	4.98, 22.7	loc 1/loc 2	8/16	6, 22.7
gain 1/2	.00001	.66, .137	gain 1/2	.00001	.50, .134	gain 1/2	.00001	1.06, .14
objective		106.3	objective		121.9	objective		93.4
Starting Gain Multiplier .0001								
	Start	Finish		Start	Finish		Start	Finish
ply angle	1.57079	.383-1.54	ply angle	1.48352	1.18-1.48	ply angle	1.39626	.878-1.4
loc 1/loc 2	8/16	8, 22.7	loc 1/loc 2	8/16	8, 20.6	loc 1/loc 2	8/16	5.48, 22.7
gain 1/2	.0001	.529, .113	gain 1/2	.0001	.0001, .87	gain 1/2	.0001	.78, .14
objective		192	objective		4664	objective		486
	Start	Finish		Start	Finish		Start	Finish
ply angle	1.30899	.56-1.3	ply angle	1.22173	.304-1.2	ply angle	1.13446	.691-1.13
loc 1/loc 2	8/16	5, 22.7	loc 1/loc 2	8/16	4.84, 22.7	loc 1/loc 2	8/16	5.76, 22.7
gain 1/2	.0001	.55, .135	gain 1/2	.0001	.73, .14	gain 1/2	.0001	1.1, .14
objective		138	objective		118.4	objective		183.5
	Start	Finish		Start	Finish		Start	Finish
ply angle	1.04719	.67-1.04	ply angle	0.95993	.644-.955	ply angle	0.87266	.611-.87
loc 1/loc 2	8/16	5.76, 22.7	loc 1/loc 2	8/16	5.77, 22.7	loc 1/loc 2	8/16	5.77, 22.7
gain 1/2	.0001	1.1, .14	gain 1/2	.0001	1.1, .14	gain 1/2	.0001	1.1, .14
objective		159	objective		141	objective		125
	Start	Finish		Start	Finish		Start	Finish
ply angle	0.78539	.586-.78	ply angle	0.69813	.24-.69	ply angle	0.61086	.28-.61
loc 1/loc 2	8/16	5.78, 22.7	loc 1/loc 2	8/16	6.01, 22.3	loc 1/loc 2	8/16	5.98, 22.3
gain 1/2	.0001	1.1, .14	gain 1/2	.0001	1.2, .134	gain 1/2	.0001	1.17, .135

objective		114.6	objective		90	objective		87.4
	Start	Finish		Start	Finish		Start	Finish
ply angle	0.52359	.44-.52	ply angle	0.43633	.319-.435	ply angle	0.34906	.329-.347
loc 1/loc 2	8/16	5.16, 22.7	loc 1/loc 2	8/16	5.65, 22.7	loc 1/loc 2	8/16	5.52, 22.7
gain 1/2	.0001	.82, .14	gain 1/2	.0001	1, .14	gain 1/2	.0001	.942, .14
objective		103	objective		86.7	objective		89.5
	Start	Finish		Start	Finish		Start	Finish
ply angle	0.26179	.262-.372	ply angle	0.17453	.15-.53	ply angle	0.08726	.0944-.53
loc 1/loc 2	8/16	5.49, 22.7	loc 1/loc 2	8/16	6.15, 22.7	loc 1/loc 2	8/16	6.6, 22.7
gain 1/2	.0001	.93, .14	gain 1/2	.0001	1.38, .143	gain 1/2	.0001	.22, .122
objective		89	objective		81.6	objective		160.5
Starting Gain Multiplier .001								
	Start	Finish		Start	Finish		Start	Finish
ply angle	1.57079	.5-1.51	ply angle	1.48352	.25-1.48	ply angle	1.39626	.552-1.39
loc 1/loc 2	8/16	8, 22.7	loc 1/loc 2	8/16	5.5, 22.7	loc 1/loc 2	8/16	7.21, 22.7
gain 1/2	.001	.42, .115	gain 1/2	.001	.575, .133	gain 1/2	.001	.45, .12
objective		276	objective		194	objective		186.5
	Start	Finish		Start	Finish		Start	Finish
ply angle	1.30899	.286-1.3	ply angle	1.22173	.31-1.21	ply angle	1.13446	.45-1.12
loc 1/loc 2	8/16	5.35, 22.7	loc 1/loc 2	8/16	4.3, 22.7	loc 1/loc 2	8/16	5.9, 22.7
gain 1/2	.001	.865, .14	gain 1/2	.001	.611, .14	gain 1/2	.001	1.17, .14
objective		105	objective		132	objective		92
	Start	Finish		Start	Finish		Start	Finish
ply angle	1.04719	.268-1.03	ply angle	0.95993	.329-.943	ply angle	0.87266	.3-.857
loc 1/loc 2	8/16	5.97, 22.7	loc 1/loc 2	8/16	6.2, 22.7	loc 1/loc 2	8/16	6.15, 22.7
gain 1/2	.001	1.22, .14	gain 1/2	.001	1.44, .14	gain 1/2	.001	1.37, .14
objective		85.5	objective		78.9	objective		78.6
	Start	Finish		Start	Finish		Start	Finish
ply angle	0.78539	.25-.77	ply angle	0.69813	.26-.68	ply angle	0.61086	.276-.597

loc 1/loc 2	8/16	6.15	loc 1/loc 2	8/16	6.37, 22.7	loc 1/loc 2	8/16	6.45, 22.7
gain 1/2	.001	1.37, .142	gain 1/2	.001	1.63, .143	gain 1/2	.001	1.76, .143
objective		80	objective		74.1	objective		72.9
	Start	Finish		Start	Finish		Start	Finish
ply angle	0.52359	.226-.52	ply angle	0.43633	.325-.436	ply angle	0.34906	.347-.365
loc 1/loc 2	8/16	6.34, 22.7	loc 1/loc 2	8/16	6.27, 22.7	loc 1/loc 2	8/16	6.3, 22.7
gain 1/2	.001	1.58, .142	gain 1/2	.001	1.5, .143	gain 1/2	.001	1.55, .143
objective		75.7	objective		76	objective		75.4
	Start	Finish		Start	Finish		Start	Finish
ply angle	0.26179	.25-.39	ply angle	0.17453	.176-.472	ply angle	0.08726	.089-.543
loc 1/loc 2	8/16	6.39, 22.7	loc 1/loc 2	8/16	6.02, 22.7	loc 1/loc 2	8/16	5.92, 22.7
gain 1/2	.001	1.66, .143	gain 1/2	.001	1.26, .143	gain 1/2	.001	1.19, .143
objective		73.7	objective		79.5	objective		83.9
Starting Gain Multiplier .01								
	Start	Finish		Start	Finish		Start	Finish
ply angle	1.57079	1.24-1.43	ply angle	1.48352	.195-1.48	ply angle	1.39626	.28-1.39
loc 1/loc 2	8/16	7.94, 19.6	loc 1/loc 2	8/16	7.95, 22.7	loc 1/loc 2	8/16	5.29, 22.7
gain 1/2	.01	0, .075	gain 1/2	.01	0, .12	gain 1/2	.01	.852, .14
objective		16979.8	objective		451.8	objective		106
	Start	Finish		Start	Finish		Start	Finish
ply angle	1.30899	.338-1.3	ply angle	1.22173	.28-1.21	ply angle	1.13446	.3-1.12
loc 1/loc 2	8/16	5.22, 22.7	loc 1/loc 2	8/16	5.38, 22.6	loc 1/loc 2	8/16	5.79, 22.7
gain 1/2	.01	.84, .14	gain 1/2	.01	.878, .139	gain 1/2	.01	1.10, .142
objective		106.8	objective		98	objective		88
	Start	Finish		Start	Finish		Start	Finish
ply angle	1.04719	.374-1.03	ply angle	0.95993	.29-.926	ply angle	0.87266	.33-.845
loc 1/loc 2	8/16	5.77, 22.7	loc 1/loc 2	8/16	6.5, 22.7	loc 1/loc 2	8/16	6.38, 22.7
gain 1/2	.01	1.09, .142	gain 1/2	.01	1.84, .143	gain 1/2	.01	1.67, .143
objective		88.9	objective		72.7	objective		74.6

	Start	Finish		Start	Finish		Start	Finish
ply angle	0.78539	.31-.76	ply angle	0.69813	.27-.68	ply angle	0.61086	.347-.581
loc 1/loc 2	8/16	6.48, 22.7	loc 1/loc 2	8/16	6.45, 22.7	loc 1/loc 2	8/16	6.74, 22.7
gain 1/2	.01	1.82, .143	gain 1/2	.01	1.75, .143	gain 1/2	.01	2.46, .143
objective		72.7	objective		73.6	objective		68.4
	Start	Finish		Start	Finish		Start	Finish
ply angle	0.52359	.33-.52	ply angle	0.43633	.314-.431	ply angle	0.34906	.318-.347
loc 1/loc 2	8/16	6.42, 22.7	loc 1/loc 2	8/16	6.71, 22.7	loc 1/loc 2	8/16	6.6, 22.7
gain 1/2	.01	1.72, .143	gain 1/2	.01	2.33, .143	gain 1/2	.01	2.03, .143
objective		73.4	objective		68.7	objective		70.8
	Start	Finish		Start	Finish		Start	Finish
ply angle	0.26179	.259-.347	ply angle	0.17453	.18-.344	ply angle	0.08726	.0935-.47
loc 1/loc 2	8/16	6.67, 22.7	loc 1/loc 2	8/16	6.55, 22.7	loc 1/loc 2	8/16	6.1, 22.7
gain 1/2	.01	2.22, .143	gain 1/2	.01	1.93, .143	gain 1/2	.01	1.33, .143
objective		69.6	objective		71.9	objective		78.5
Starting Gain Multiplier .1								
	Start	Finish		Start	Finish		Start	Finish
ply angle	1.57079	.866-1.55	ply angle	1.48352	.353-1.48	ply angle	1.39626	.349-1.39
loc 1/loc 2	8/16	8.8, 17.3	loc 1/loc 2	8/16	8.07, 17.5	loc 1/loc 2	8/16	8.12, 17.5
gain 1/2	.1	.18, 0	gain 1/2	.1	.436, 0	gain 1/2	.1	.40, 0
objective		15899	objective		2660.1	objective		2802
	Start	Finish		Start	Finish		Start	Finish
ply angle	1.30899	.355-1.30	ply angle	1.22173	.351-1.2	ply angle	1.13446	.30-1.1
loc 1/loc 2	8/16	8.1, 17.5	loc 1/loc 2	8/16	6.4, 22.7	loc 1/loc 2	8/16	6.39, 22.7
gain 1/2	.1	.421, 0	gain 1/2	.1	1.69, .142	gain 1/2	.1	1.66, .143
objective		2791	objective		76.2	objective		75.4
	Start	Finish		Start	Finish		Start	Finish
ply angle	1.04719	.327-1.03	ply angle	0.95993	.326-.894	ply angle	0.87266	.33-.793
loc 1/loc 2	8/16	7.95, 17.5	loc 1/loc 2	8/16	6.87, 22.7	loc 1/loc 2	8/16	6.94, 22.7

gain 1/2	.1	.54, 0	gain 1/2	.1	2.99, .143	gain 1/2	.1	3.35, .143
objective		2149	objective		66.88	objective		65.7
	Start	Finish		Start	Finish		Start	Finish
ply angle	0.78539	.33-.686	ply angle	0.69813	.33-.68	ply angle	0.61086	.33-.597
loc 1/loc 2	8/16	7.1, 22.7	loc 1/loc 2	8/16	8, 17.5	loc 1/loc 2	8/16	8, 17.5
gain 1/2	.1	4.46, .143	gain 1/2	.1	.5, 0	gain 1/2	.1	.483, 0
objective		63.8	objective		2038	objective		2027
	Start	Finish		Start	Finish		Start	Finish
ply angle	0.52359	.33-.52	ply angle	0.43633	.343-.433	ply angle	0.34906	.345-.347
loc 1/loc 2	8/16	8.04, 17.5	loc 1/loc 2	8/16	8.14, 17.5	loc 1/loc 2	8/16	8.46, 17.6
gain 1/2	.1	.454, 0	gain 1/2	.1	.392, 0	gain 1/2	.1	.267, 0
objective		2016	objective		2021	objective		2079
	Start	Finish		Start	Finish		Start	Finish
ply angle	0.26179	.264-.34	ply angle	0.17453	.18-.36	ply angle	0.08726	.1-.354
loc 1/loc 2	8/16	8.29, 17.6	loc 1/loc 2	8/16	8.21, 17.6	loc 1/loc 2	8/16	6.56, 22.7
gain 1/2	.1	.326, 0	gain 1/2	.1	.363, 0	gain 1/2	.1	1.96, .143
objective		2049	objective		2046	objective		71.22
Starting Gain Multiplier 1								
	Start	Finish		Start	Finish		Start	Finish
ply angle	1.57079	1.38-1.4	ply angle	1.48352	.378-1.48	ply angle	1.39626	.346-1.39
loc 1/loc 2	8/16	5.55, 22.7	loc 1/loc 2	8/16	.561, 22.7	loc 1/loc 2	8/16	6.09, 22.7
gain 1/2	1	.947, .141	gain 1/2	1	1, .141	gain 1/2	1	1.32, .143
objective		16699	objective		103	objective		94.2
	Start	Finish		Start	Finish		Start	Finish
ply angle	1.30899	.321-1.29	ply angle	1.22173	.34-1.16	ply angle	1.13446	.352-1
loc 1/loc 2	8/16	6.53, 22.7	loc 1/loc 2	8/16	7.05, 22.7	loc 1/loc 2	8/16	7.15, 22.7
gain 1/2	1	1.91, .143	gain 1/2	1	4.25, .142	gain 1/2	1	5.83, .143
objective		74.8	objective		64.6	objective		62.7
	Start	Finish		Start	Finish		Start	Finish

ply angle	1.04719	.35-.74	ply angle	0.95993	.352-.669	ply angle	0.87266	.351-.565
loc 1/loc 2	8/16	7.24, 22.7	loc 1/loc 2	8/16	7.24, 22.7	loc 1/loc 2	8/16	7.24, 22.7
gain 1/2	1	8.24, .141	gain 1/2	1	8.02, .142	gain 1/2	1	8.07, .142
objective		61.9	objective		61.9	objective		61.8
	Start	Finish		Start	Finish		Start	Finish
ply angle	0.78539	.349-.591	ply angle	0.69813	.352-.494	ply angle	0.61086	.351-.45
loc 1/loc 2	8/16	7.19, 22.7	loc 1/loc 2	8/16	7.22, 22.7	loc 1/loc 2	8/16	7.22, 22.7
gain 1/2	1	6.57, .143	gain 1/2	1	7.58, .142	gain 1/2	1	7.47, .142
objective		61.9	objective		61.76	objective		61.9
	Start	Finish		Start	Finish		Start	Finish
ply angle	0.52359	.338-.426	ply angle	0.43633	.436-.444	ply angle	0.34906	.339-.352
loc 1/loc 2	8/16	7.22, 22.7	loc 1/loc 2	8/16	7.77, 22.7	loc 1/loc 2	8/16	7.22, 22.7
gain 1/2	1	7.36, .142	gain 1/2	1	.8, 0	gain 1/2	1	7.43, .142
objective		61.9	objective		2142	objective		61.8
	Start	Finish		Start	Finish		Start	Finish
ply angle	0.26179	.32-.353	ply angle	0.17453	.267-.356	ply angle	0.08726	-1.57-.35
loc 1/loc 2	8/16	7.24, 22.7	loc 1/loc 2	8/16	7.21, 22.7	loc 1/loc 2	8/16	7.13, 22.7
gain 1/2	1	7.93, .142	gain 1/2	1	7.03, .142	gain 1/2	1	5.28, .142
objective		61.65	objective		62	objective		63.4
Starting Gain Multiplier 10								
	Start	Finish		Start	Finish		Start	Finish
ply angle	1.57079	1.4	ply angle	1.48352	.344-1.48	ply angle	1.39626	.372-1.39
loc 1/loc 2	8/16	7.39, 22.7	loc 1/loc 2	8/16	7.08, 22.7	loc 1/loc 2	8/16	7.24, 22.7
gain 1/2	10	8.86, .12	gain 1/2	10	4.8, .143	gain 1/2	10	8.81, .142
objective		26875	objective		81.9	objective		83.3
	Start	Finish		Start	Finish		Start	Finish
ply angle	1.30899	.349-1.32	ply angle	1.22173	.333-1.21	ply angle	1.13446	.35-1.1
loc 1/loc 2	8/16	7.25, 22.7	loc 1/loc 2	8/16	7.24, 22.7	loc 1/loc 2	8/16	7.24, 22.7
gain 1/2	10	8.46, .142	gain 1/2	10	8.47, .142	gain 1/2	10	8.33, .142

objective		66.2	objective		66.45	objective		66
	Start	Finish		Start	Finish		Start	Finish
ply angle	1.04719	.34-1.0	ply angle	0.95993	.33-.93	ply angle	0.87266	.35-.85
loc 1/loc 2	8/16	7.24, 22.7	loc 1/loc 2	8/16	7.24, 22.7	loc 1/loc 2	8/16	7.23, 22.7
gain 1/2	10	8.23, .142	gain 1/2	10	8.2, .142	gain 1/2	10	8.17, .142
objective		65	objective		64.2	objective		63.6
	Start	Finish		Start	Finish		Start	Finish
ply angle	0.78539	.351-.761	ply angle	0.69813	.354-.679	ply angle	0.61086	.31-.6
loc 1/loc 2	8/16	7.24, 22.7	loc 1/loc 2	8/16	7.24, 22.7	loc 1/loc 2	8/16	7.25, 22.7
gain 1/2	10	8.18, .142	gain 1/2	10	8.21, .142	gain 1/2	10	8.4, .142
objective		63.1	objective		62.7	objective		62.45
	Start	Finish		Start	Finish		Start	Finish
ply angle	0.52359	.364-.517	ply angle	0.43633	.33-.435	ply angle	0.34906	.348-.36
loc 1/loc 2	8/16	7.23, 22.7	loc 1/loc 2	8/16	7.25, 22.7	loc 1/loc 2	8/16	7.23, 22.7
gain 1/2	10	7.95, .142	gain 1/2	10	8.46, .142	gain 1/2	10	7.93, .142
objective		62.2	objective		61.8	objective		61.5
	Start	Finish		Start	Finish		Start	Finish
ply angle	0.26179	.263-.33	ply angle	0.17453	.183-.387	ply angle	0.08726	.288-.356
loc 1/loc 2	8/16	7.46, 22.7	loc 1/loc 2	8/16	7.21, 22.7	loc 1/loc 2	8/16	7.24, 22.7
gain 1/2	10	7.67, 0	gain 1/2	10	7.12, .142	gain 1/2	10	8.09, .142
objective		3059	objective		62.3	objective		61.67

Vita

Capt Douglas DeHart was born 22 Jan 1963 in Oak Park, Illinois. He graduated from James B. Conant High School and then went to the University of Wisconsin at Madison on a four - year ROTC Scholarship. In 1985, he graduated from the University of Wisconsin at Madison with a B.S. in Engineering Mechanics and was commissioned a 2nd Lt in the Air Force. He then received an education delay from AFIT/CI to obtain a Master's Degree. In Dec. 1986, Capt DeHart graduated from the University of Wisconsin at Madison with a M.S. in Engineering Mechanics emphasizing in Aerospace Engineering. He entered active duty in 1987 at Edwards AFB, California and was assigned to the Rocket Propulsion Laboratory as a Space Systems Technology Project Analyst. During his stay at Edwards AFB, the laboratory changed its name and expanded its mission. It became the Air Force Astronautics Laboratory and became the Air Force's main laboratory in space structure research. At the Astronautics Laboratory, Capt DeHart managed both contracts and conducted research in the area of smart structures or embedded sensors and actuators. Based upon his research at the Astronautics Laboratory, he applied for and was accepted for the PhD program at the Air Force Institute of Technology in April 1990. He started his studies in October 1994 and in April 1994, he left AFIT and was assigned to the Air Force Phillips Laboratory, one of the new Air Force "super" laboratories. While finishing up his research, Capt DeHart also manage contracts in the area of multi-functional structures which is the integration of the satellite housekeeping functions into the load bearing structural shear panels which make up the spacecraft bus. Currently, he is the branch chief of the Applied Composite Branch. He is in charge of 12 engineers and 3 technicians. They conduct research and manage contracts to promote the use of composite materials in both spacecraft and launch vehicles.

REPORT DOCUMENTATION PAGE			Form Approved OMB No. 0704-0188	
Public reporting burden for this collection of information is estimated to average 1 hour per response, including the time for reviewing instructions, searching existing data sources, gathering and maintaining the data needed, and completing and reviewing the collection of information. Send comments regarding this burden estimate or any other aspect of this collection of information, including suggestions for reducing this burden, to Washington Headquarters Services, Directorate for Information Operations and Reports, 1215 Jefferson Davis Highway, Suite 1204, Arlington, VA 22202-4302, and to the Office of Management and Budget, Paperwork Reduction Project (0704-0188), Washington, DC 20503.				
1. AGENCY USE ONLY (Leave blank)	2. REPORT DATE Jun-1996	3. REPORT TYPE AND DATES COVERED Doctoral-Dissertation		
4. TITLE AND SUBTITLE SIMULTANEOUS COMPOSITE TAILORING AND BENDING CONTROL OPTIMIZATION FOR DAMPING THE TORSIONAL VIBRATION OF A PLATE		5. FUNDING NUMBERS		
6. AUTHOR(S) Douglas W. DeHart, Capt, USAF				
7. PERFORMING ORGANIZATION NAME(S) AND ADDRESS(ES) Air Force Institute of Technology 2750 P. Street WPAFB, OH 45433-6583		8. PERFORMING ORGANIZATION REPORT NUMBER AFIT/DS/ENY/96-8		
9. SPONSORING / MONITORING AGENCY NAME(S) AND ADDRESS(ES) Dr. Alok Das 3550 Aberdeen Avenue SE Kirtland AFB, NM 87117-5776		10. SPONSORING / MONITORING AGENCY REPORT NUMBER		
11. SUPPLEMENTARY NOTES				
12a. DISTRIBUTION / AVAILABILITY STATEMENT Approved for Public Release; Distribution Unlimited		12b. DISTRIBUTION CODE		
13. ABSTRACT (Maximum 200 words) A method for structural and control optimization for torsional vibration of a composite plate was developed. This research included the effects of using composite tailoring to promote the coupling of the twisting-bending mode to enhance the damping system. The plate was modeled by classical lamination plate theory using a linear elastic strain-displacement theory. This theory was then incorporated into a performance index that minimizes torsional and bending motion at the tip of the plate due to a torsional force at the tip. This performance index and constraints were incorporated into an optimization subroutine which then produced an optimal design. This optimal plate was fabricated and tested with a torsional load to decide the validity of the theory in improving damping. A comparison was made between the results of the theory and the experimental results of testing the optimized plate and a baseline plate made up of a quasi-isotropic lay-up. The frequencies of the experimental and the theoretical results were within 15% of each other. Also the damping factor for the 1st torsional and 2nd torsional modes of vibration increased significantly for the optimized plate versus the baseline plate which verifies the basic premise of the theory.				
14. SUBJECT TERMS Composite tailoring, Structural Optimization, Control Optimization, Bending-Torsional Coupling			15. NUMBER OF PAGES 149	
			16. PRICE CODE	
17. SECURITY CLASSIFICATION OF REPORT UNCLASSIFIED	18. SECURITY CLASSIFICATION OF THIS PAGE UNCLASSIFIED	19. SECURITY CLASSIFICATION OF ABSTRACT UNCLASSIFIED	20. LIMITATION OF ABSTRACT UL	